PASSIVE AND MIXED-CONVECTIVE COOLING OF VERTICAL STACKS OF HEAT-GENERATING BODIES IN A SQUARE CAVITY WITH OPENINGS

BY

OSCAR A. RAMIREZ-IRAHETA

A Thesis
Presented to the Faculty of Graduate Studies
In Partial Fulfilment of the Requirements for the Degree of

MASTER OF SCIENCE

Department of Mechanical and Manufacturing Engineering
University of Manitoba
Winnipeg, Manitoba

THE UNIVERSITY OF MANITOBA

FACULTY OF GRADUATE STUDIES

*****

COPYRIGHT PERMISSION

Passive and Mixed-Convective Cooling of Vertical Stacks of Heat-Generating Bodies in a Square Cavity with Openings

BY

Oscar A. Ramirez-Iraheta

A Thesis/Practicum submitted to the Faculty of Graduate Studies of The University of Manitoba in partial fulfillment of the requirement of the degree

Of

MASTER OF SCIENCE

ABSTRACT

A numerical investigation was conducted on the laminar fluid flow and heat transfer in a two dimensional cavity with one inlet opening and one outlet opening enclosing stacks of heat generating bodies. A two-dimensional domain was used to simulate a valve hall found in the Dorsey converter station owned and operated by Manitoba Hydro. The Navier-Stokes equations and energy equations were solved using the Computational Fluid Dynamics (CFD) code CFX-TASCflow. The computer code uses a finite volume method of solution and is based on a finite element approach for representing the geometry. The computed effects on the velocity and temperature distributions caused by the number of towers, the position of the tower within the cavity, the size of tower, the coolant mass flow rate, and the location of inlet and outlet ports were studied. To present the results in a generalized format, dimensionless parameters were derived and isotherm plots and velocity vector plots based on the results are shown.

Three different geometries were studied: Geometry 1 was a single tower formed by four blocks. Twenty-six different cases were solved for Geometry 1. Six different locations of the stack within the domain were studied. As well, passive convection and mixed convection were studied. Different locations of the inlet and outlet ports were examined. Twenty cases were solved for geometry 2 which was a single tower formed by nine blocks. Two different positions of the tower in the cavity were examined. Passive convection was studied for the two positions and two different inlet mass flow rates were examined corresponding to Re_o = 100 and 225. Again, different positions of the inlet and outlet ports were studied. Geometry 3 had three towers each formed by nine blocks. Passive convection and mixed convection were examined. The location of inlet and outlet ports was the main focus for geometry 3. Air was used as the coolant (Pr = 0.7) for all cases.

It was found that the location of the tower has a significant impact on the velocity and temperature distribution in the domain and especially on the tower. The tower location that provided the lowest maximum temperature was the location that maximized the air

flowing around and in between the channels formed by the blocks. This only became evident once the cases were run and compared.

The influence of the inlet mass flow rate was also examined in the study. In most cases, increased flow rates resulted in higher velocities, and consequently, improved cooling characteristics. However, there were cases were passive convection provided better cooling than mixed convection. Again, this would not have been known or predicted without numerical modeling in TASCflow.

ACKNOWLEDGEMENTS

The author would first like to thank God for His help through the writing of the Thesis and the Masters program. The author would also like to thank Dr. H. M. Soliman, Dr. S. Ormiston and Mr. H. Jhinger for their help and advice through the Master's program and the Thesis. The author is also grateful for the financial assistance provided by Manitoba Hydro, NSERC and the Department of Mechanical and Manufacturing Engineering. The author would also like to thank his family for their support through the Masters program and Ms. Cindy Arias for her help and advice in the preparation of the Thesis.

TABLE OF CONTENTS

ABSTRACT ii

ACKNOWLEDGEMENTS iv

TABLE OF CONTENTS v

LIST OF FIGURES vii

LIST OF TABLES xii

NOMENCLATURE xiii

CHAPTER 1 INTRODUCTION 1

CHAPTER 2 LITERATURE REVIEW 8

CHAPTER 3 MODEL DESCRIPTION 14

3.1 Domain 14

3.2 Assumptions 16

3.3 Conservation Equations 16

3.4 Boundary Conditions 19

3.5 Geometries Studied 20

CHAPTER 4 NUMERICAL SOLUTION METHOD 22

4.1 Introduction 22

4.2 CFX-TASCflow 22

4.3 CFX-TASCgrid 22

CHAPTER 5 VALIDATION TESTS 28

5.1 Introduction 28

5.2 Grid Independence 28

5.2.1 Geometry 1 (N = 4 and M = 1) 28

5.2.2 Geometry 2 (N = 9 and M = 1) 34

5.2.3 Geometry 3 (N = 9 and M = 3) 37

CHAPTER 6 RESULTS AND DISCUSSION 40

6.1 Introduction 40

6.2 Geometry 1 40

6.2.1 Effect of the Tower Location Within the Domain 43

6.2.2 Passive versus Mixed Convection Cooling 46

6.2.3 Effect of the Location of Inlet and Outlet Ports 49
6.3 Geometry 2 52
6.3.1 Effect of the Tower Location Within the Domain 54
6.3.2 Passive versus Mixed Convection Cooling 81
6.3.3 Effect of the Location of Inlet and Outlet Ports 87
6.4 Geometry 3 88
CHAPTER 7 SUMMARY, CONCLUSIONS AND RECOMMENDATIONS 100
7.1 Summary 100
7.2 Conclusions 100
7.2.1 Geometry 1 100
7.2.2 Geometry 2 101
7.2.3 Geometry 3 102
7.3 Recommendations 102
REFERENCES 103

LIST OF FIGURES

Figure 1.1: Elevation view of a valve hall (dimensions are in metres).....2

Figure 1.2: Plan view of a valve hall (dimensions are in metres).....3

Figure 1.3: Side View of a valve hall (dimensions in metres).....4

Figure 1.4: Schematic diagram of a thyristor module (dimensions in metres).....5

Figure 1.5: Schematic diagram of the cooling water circuit used for each of the valve groups.....5

Figure 2.1: Forced Convection cooling domain for Bejan et al. (1995).....8

Figure 2.2: Natural Convection cooling domain for Bejan et al. (1995).....8

Figure 2.3: Schematic diagram of the experimental obstacle apparatus for Young and Vafai (1999).....10

Figure 2.4: Schematic of obstacles on substrate for Hung (2001).....10

Figure 2.5: Array of two-dimensional rectangular blocks for Mufuta and Van de Bulck (2001).....11

Figure 2.6: Schematic view of the calculation domain for Shuja et al. (2000).....12

Figure 2.7: Domain for Shuja et al. (2001).....13

Figure 3.1: Generic description of the domain.....15

Figure 3.2: Boundary conditions.....19

Figure 4.1: Regions for Geometry 1.....23

Figure 4.2: Regions for Geometry 2.....24

Figure 4.3: Regions for Geometry 3.....26

Figure 5. 1: Values of dimensionles parameter *s* around a block.....28

Figure 5.2: Temperature distribution around block 1.....29

Figure 5.3: Temperature distribution around block 2.....30

Figure 5.4: Temperature distribution around block 3.....31

Figure 5.5: Temperature distribution around block 4.....31

Figure 5.6: Node distribution for Geometry 1.....33

Figure 5.7: Temperature comparison between the G3 and G4 grids at constant Y=0.89..35

Figure 5.8: Node distribution for Geometry 2.....36

Figure 5.9: Temperature comparison at line Y = 0.89.....38

Figure 5.10: Node distribution for Geometry 3.....39

Figure 6.1: Geometry 1.....41

Figure 6.2: Velocity vectors for case 16, position 4 with inlet B-0.5, outlet T-0.5, and Re_o= 100 44

Figure 6.3: Temperature distribution in the stack for case 16, position 4 with inlet B-0.5, outlet T-0.5, and Re_o = 100 45

Figure 6.4: Velocity vectors for case 24, position 5 with inlet B-0.5, and outlet T-0.5, and Re_o = 100 46

Figure 6.5: Temperature distribution in the stack for case 24, position 5 with inlet B-0.5, outlet T-0.5, and Re_o = 100 47

Figure 6.6: Case 6, passive cooling (Re_o = 22.8) for position 2, inlet L-0.05, and outlet R-0.95 47

Figure 6.7: Case 9, mixed convection cooling (Re_o = 100) for position 2, inlet L-0.05, and outlet R-0.95 48

Figure 6.8: Case 17, mixed convection cooling (Re_o = 100) for stack position 4, inlet L – 0.05, and outlet R – 0.95 50

Figure 6.9: Case 21, mixed convection cooling (Re_o = 100) for stack position 4, inlet L – 0.24, and outlet R – 0.24 50

Figure 6.10: Temperature distribution in the stack for case 17, position 4 with inlet L-0.05, Outlet R-0.05, and Re_o = 100 51

Figure 6.11: Temperature distribution on the stack for case 21, position 4 with inlet L – 0.24, Outlet R – 0.24, and Re_o = 100 51

Figure 6.12: Geometry 2.....52

Figure 6.13: Case 13, mixed convection cooling ($Re_o = 100$) for $a_9 = 0.4$, inlet B – 0. 5, and outlet T – 0. 5.....54

Figure 6.14: Case 11, mixed convection cooling ($Re_o = 100$) for $a_9 = 0.1$, inlet B – 0. 5, and outlet T – 0. 5.....57

Figure 6.15: Temperature contours for case 3, mixed convection ($Re_o = 100$), inlet B-0.5, and outlet T-0.5 57

Figure 6.16: Temperature contour for case 11, mixed convection (Re_o=100), inlet B-0.5 and oulet T-0.5.....58

Figure 6.17: Case 6, mixed convection cooling ($Re_o = 225$) for $a_9 = 0.4$, inlet B-0.5 and outlet T-0.5.....59

Figure 6.18: Case 16, mixed convection cooling ($Re_o = 225$) for $a_9 = 0.1$, inlet B-0.5 and outlet T-0.5.....60

Figure 6.19: Temperature contours for case 6, mixed convection ($Re_o = 225$), inlet B-0.5 and outlet T – 0.5.....62

Figure 6.20: Temperature contours for case 16, mixed convection ($Re_o = 225$), inlet B - 0.5 and outlet T - 0.5.....63.

Figure 6.21: Case 4, mixed convection cooling ($Re_o = 100$) for $a_9 = 0.4$, inlet L – 0.05 and outlet R – 0.95.....64

Figure 6.22: Case 15, mixed convection cooling ($Re_o = 100$) for $a_9 = 0.1$, inlet L-0.05 and outlet R-0.95.....65

Figure 6.23: Percentage of inlet mass flow rate flowing through each channel for case 4 and case 15.....66

Figure 6.24: Temperature contours for case 4, mixed convection ($Re_o = 100$), inlet L-0.05 and outlet R -0.95.....67

Figure 6.25: Temperature contours for case 15, mixed convection ($Re_o = 100$), inlet L - 0.05 and outlet R -0.95.....68

Figure 6.26: Case 7, mixed convection cooling ($Re_o = 225$) for $a_9 = 0.4$, inlet L-0.05 and outlet R-0.95.....69

Figure 6.27: Case 17, mixed convection cooling ($Re_o = 225$) for $a_9 = 0.1$, inlet L-0.05 and outlet R-0.95 70

Figure 6.28: Percentage of inlet mass flow rate flowing through each channel for case 7 and case 17 71

Figure 6.29: Temperature contours for mixed convection ($Re_o = 225$), inlet L - 0.05 and outlet R - 0.95 72

Figure 6.30: Temperature contours for case 17, mixed convection (Reo = 225), inlet L - 0.05 and outlet R - 0.95 73

Figure 6.31: Case 5, mixed convection cooling ($Re_o = 100$) for $a_9 = 0.4$, inlet at L-0.5 and outlet at R-0.5 74

Figure 6.32: Case 13, mixed convection cooling ($Re_o = 100$) for $a_9 = 0.1$, inlet at L-0.5 and outlet at R-0.5 75

Figure 6.33: Case 20, mixed convection cooling ($Re_o = 100$) for $a_9 = 0.7$, inlet L-0.5 and outlet R – 0.5 75

Figure 6.34: Percentage of inlet mass flow rate flowing through each channel for cases 5, 13 and 20 77

Figure 6.35: Temperature contours for case 5, mixed convection ($Re_o = 100$), inlet L-0.5 and outlet R-0.5 78

Figure 6.36: Temperature contours for case 13, mixed convection (Re_o=100), inlet L-0.5 and outlet R-0.5 79

Figure 6.37: Temperature contours for case 20, mixed convection ($Re_o = 100$), inlet L-0.5 and outlet R-0.5 80

Figure 6.38: Case 9, passive convection cooling ($Re_o = 12.78$) for $a_9 = 0.1$, inlet L-0.05 and outlet R-0.5 81

Figure 6.39: Case 14, mixed convection Cooling ($Re_o = 100$) for $a_9 = 0.1$, inlet L-0.05 and outlet R-0.5 82

Figure 6.40: Case 18, mixed convection Cooling ($Re_o = 225$) for $a_9 = 0.1$, inlet L-0.05 and outlet R-0.5 82

Figure 6.41: Temperature contours for case 9, passive convection ($Re_o = 12.78$), inlet L- 0.05 and outlet R - 0.5 84

Figure 6.42: Temperature contours for case 14, mixed convection (Re_o = 100), inlet L - 0.05 and outlet R - 0.5.....85

Figure 6.43: Temperature contours for case 18, mixed convection (Re_o = 225), inlet L - 0.05 and outlet R - 0.5.....86

Figure 6.44: Percentage of mass flow rate flowing through each channel for case 9, 14 and 18.....87

Figure 6.45: Geometry 3 90

Figure 6.46: Case 5, mixed convection cooling (Re_o = 100), inlet L - 0.05 and outlet R - 0.95.....91

Figure 6.47: Temperature contours for case 5, mixed convection (Re_o = 100), inlet L-0.05 and outlet R-0.95.....92

Figure 6.48: Case 2, mixed convection cooling (Re_o = 100), inlet B - 0.5 and outlet T - 0.5.....93

Figure 6.49: Temperature contours for case 2, mixed convection (Re_o=100), inlet B-0.5 and outlet T-0.5 94

Figure 6.50: Case 4, mixed convection cooling (Reo = 100), inlet L -0.05 and outlet R - 0.5.....95

Figure 6.51: Temperature contours for case 4, mixed convection (Re_o = 100), inlet L-0.05 and outlet R-0.5 96

Figure 6.52: Case 8, mixed convection cooling (Re_o = 100), inlet L-0.5 and outlet R-0.5.....97

Figure 6.53: Temperature contours for case 8, mixed convection (Re_o = 100), inlet L-0.5 and outlet R-0.5 98

LIST OF TABLES

Table 4.1: Size of regions for Geometry 1 in non-dimensional form.....24

Table 4.2: Size of regions for geometry 2 in non-dimensional form.....25

Table 4.3: Size of regions in Y direction for Geometry 3 in non-dimensional form 26

Table 5.1: Number of nodes for the grids used in Geometry 2.....34

Table 5.2: Maximum temperature computed by the four grids for Geometry 2.....34

Table 5.3: Grid sizes for geometry 3.....37

Table 5.4: Maximum θ and its deviation between grids.....37

Table 6.1: Summary of stack positions for geometry 1.....40

Table 6.2: Results from Geometry 1.....42

Table 6.3: Maximum and average temperatures corresponding to different stack positions 43

Table 6.4: Results from Geometry 2.....53

Table 6.5: Results from Geometry 3 89

NOMENCLATURE

a_1	defines inlet size
a_2	defines location of inlet
a_3	defines outlet size
a_4	defines location of outlet
a_5	defines horizontal space between towers
a_6	defines vertical height of block
a_7	defines horizontal width of block
a_8	defines vertical space between blocks
a_9	defines horizontal distance from right wall to tower
a_{10}	defines vertical distance from top wall to tower
Cp	specific heat [J/kg·K]
g	gravitational acceleration [m/s^2]
Gr	Grashof number defined by Eq. (3.21)
k	thermal conductivity [W/m·K]
L	length of domain [m]
M	number of towers
N	number of blocks
P	Pressure [Pa]
Pr	Prandtl number defined by Eq. (3.19)
q''	heat flux [W/m^2]
Re	Reynolds number defined by Eq. (3.20)
s	dimensionless perimeter of block measured counterclockwise from bottom left corner
T	Temperature [°C]
u	velocity component in the x direction [m/s]
U	dimensionless velocity component in the x direction defined by Eq. (3.15)
v	velocity component in the y direction [m/s]
V	dimensionless velocity component in the y direction defined by Eq. (3.16)
x	coordinate along width of domain [m]

X dimensionless coordinate along width of domain

Y coordinate along height of domain [m]

Y dimensionless coordinate along height of domain

Greek Symbols

β coefficient of expansion [1/K]

θ dimensionless temperature defined by Eq. (3.18)

μ dynamic viscosity [N·s/m^2]

ρ density [kg/m^3]

υ kinematic viscosity [m^2/s]

Subscripts

$_o$ inlet

Chapter 1
INTRODUCTION

The current study deals with how the temperature distribution is affected by the air movement around towers of heat generating blocks that are stacked one on top of each other. The study is of relevance to Manitoba Hydro for possible upgrades to an actual DC/AC electric converter station. The thesis provides discussions of the situations that provided effective cooling of the towers. This is also the basis for a future three-dimensional study. Other applications where this study might be of relevance are in dealing with electronic packages, transformers, and spent nuclear fuel cooling.

In all previous investigations, the electronic packages were simulated by heat generating bodies of different shapes (depending on the application), and the objective was to find the arrangement of these heat-generating bodies that gives the highest heat transfer rate for a given temperature level or the lowest temperature level for a given rate of heat dissipation. But none of these studies could be used to effectively predict or understand the temperature distribution in the vertical stacks used in DC/AC converter towers.

The present study covers in detail the geometry that is relevant to the thyristor valve towers enclosed in the valve halls of DC/AC converter stations. The Dorsey converter station is located near the town of Rosser, Manitoba, about 26 kilometres northwest of the City of Winnipeg. Over 70 per cent of the electricity produced in Manitoba is transmitted through Manitoba Hydro's Dorsey Converter Station. The electric current is transmitted to the Dorsey converter station from the generating stations in the north via two high voltage direct current (HVDC) transmission lines: Bipole 1 and Bipole 2. The converter station is the southern terminus for the utility's high voltage direct current (HVDC) transmission lines. The alternating current converted at Dorsey supplies Manitoba's southern power system as well as the interconnecting power systems that link the province to Saskatchewan, Ontario and the United States. Each bipole consists of the same major components: the HVDC switchyard, converter buildings, valve halls, synchronous condensers, converter transformer area, and 230-kV switchyard.

The converter buildings house the valve halls, the control room, mechanical and electrical services as well as the maintenance facilities. Each valve hall contains 12 converter valves which turn on and off in a controlled sequence to convert the DC to AC. The elevation view of a valve hall is shown in Figure 1.1, the plan view is shown in Figure 1.2 and the side view is shown in Figure 1.3. The valve hall is 23.1 m x 15.2 m in floor area as seen in Figure 1.2, and 12.4 m in height as shown in Figure 1.1.

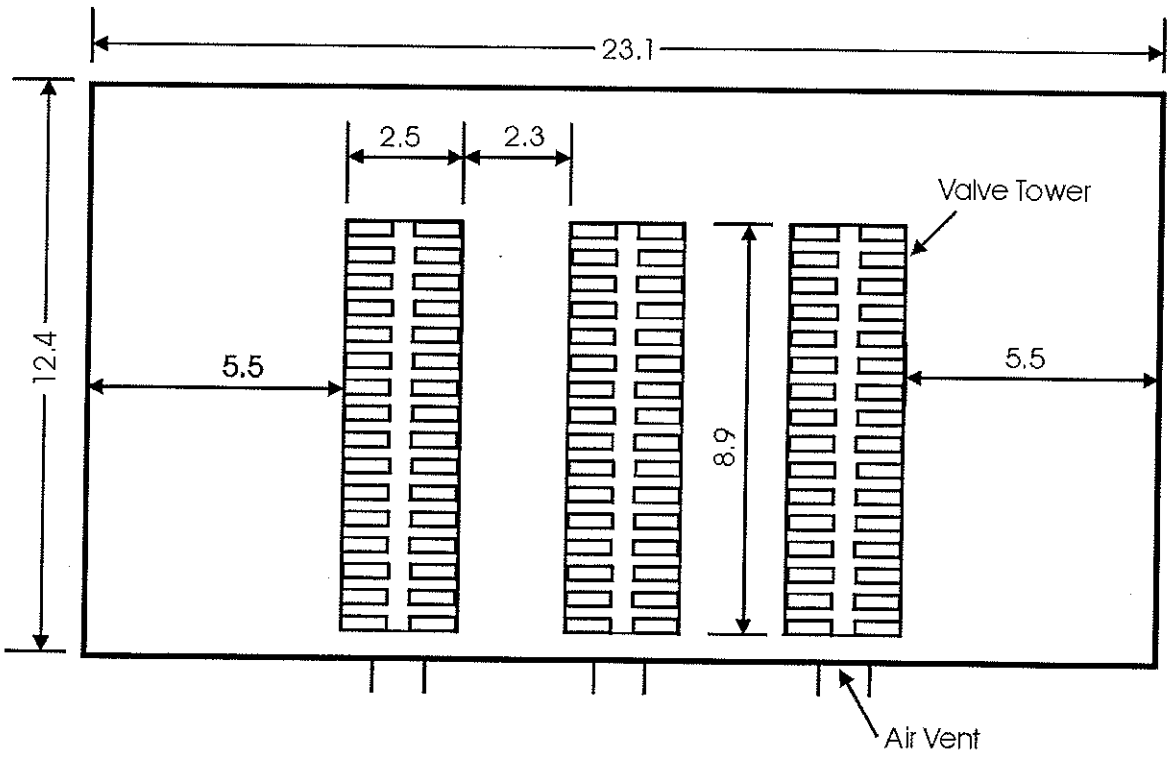

Figure 1.1: Elevation view of a valve hall (dimensions are in metres)

The converter valves are arranged in the form of three towers inside the valve halls, as shown in Figure 1.1. The towers are 8.9 m in height and 2.5 x 3.5 m in cross section. Sixteen tiers consisting of four thyristor modules and two reactor modules form each tower. A schematic of a thyristor module is shown in Figure 1.4; it is in the form of a block with optical inputs at one end to control the switching.

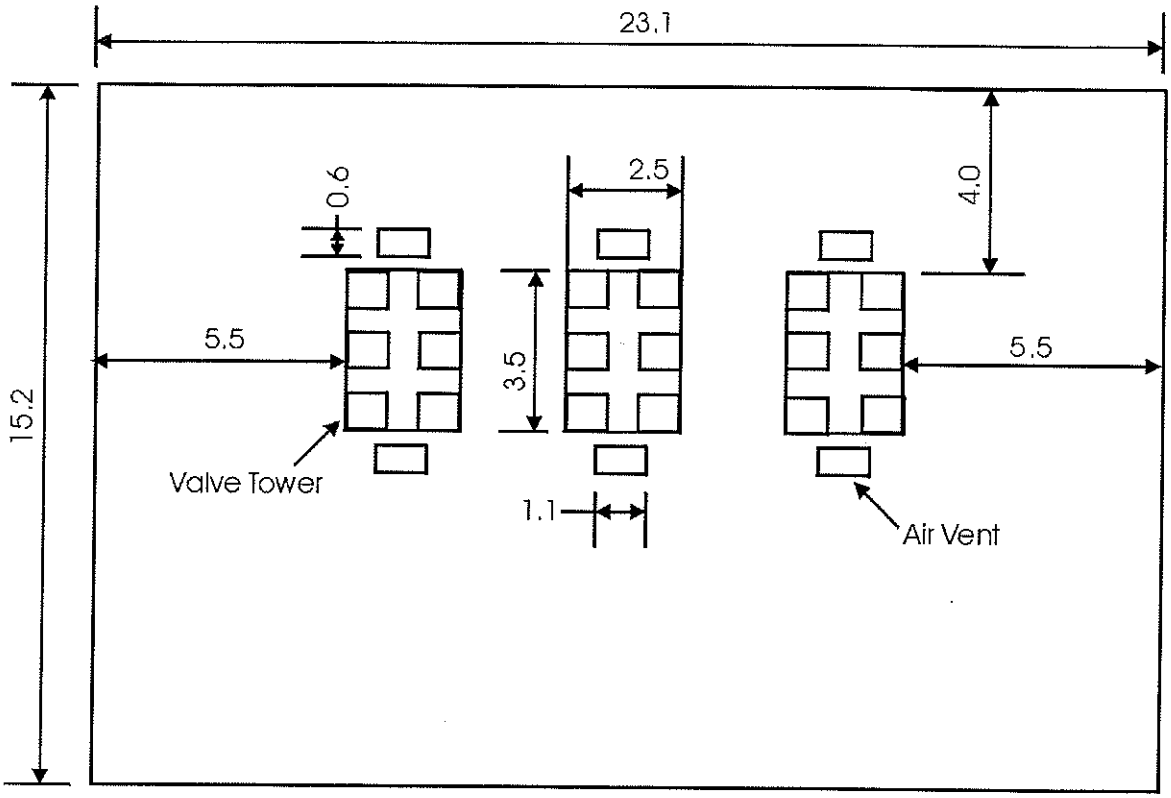

Figure 1.2: Plan view of a valve hall (dimensions are in metres)

A large amount of heat is generated within the converter valves due to electrical power losses. This heat is removed by a combination of a water cooling system and an air conditioning system. Figure 1.5 shows a schematic diagram of the cooling water circuit used for each of the valve halls. Deionized water pumped through the water cooling system removes approximately 90% of the heat generated from the thyristors. The heat acquired by the deionized water is then transferred to a glycol-water mixture in three shell and tube heat exchangers. The water cooling system was designed to be capable of removing 2.1MW of heat.

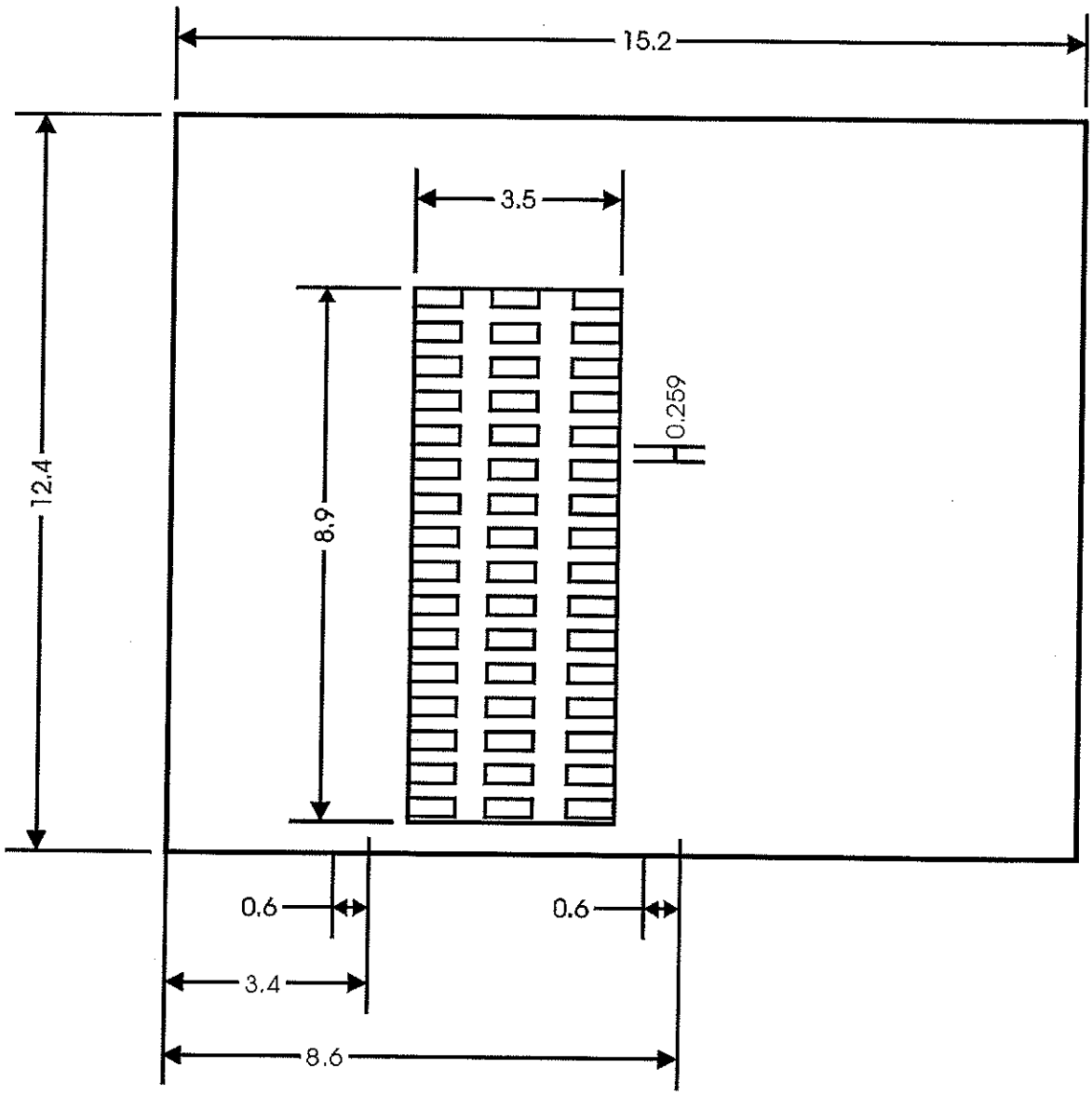

Figure 1.3: Side view of a valve hall (dimensions in metres)

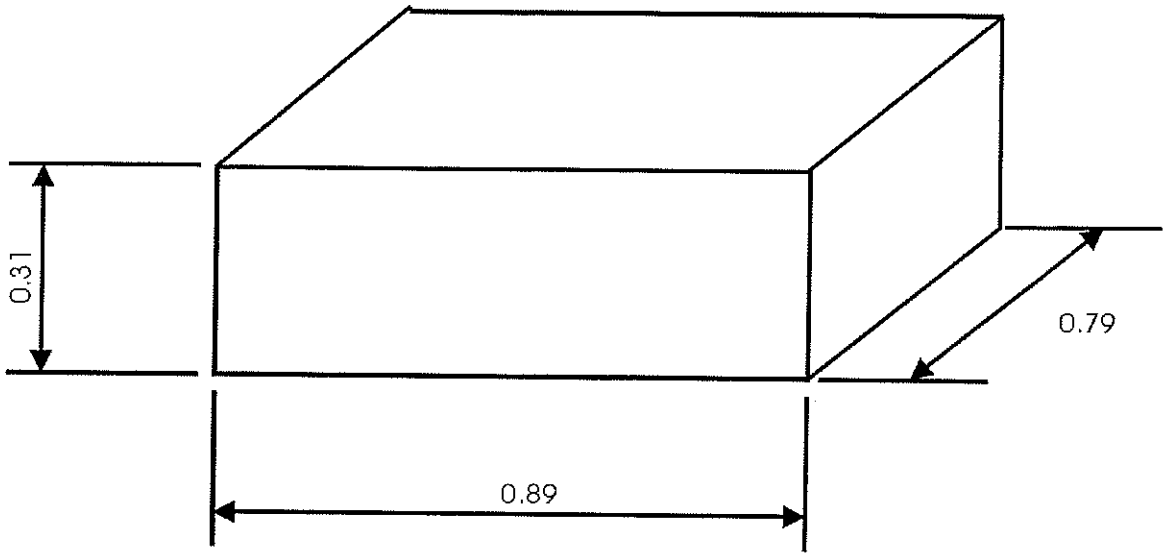

Figure 1.4: Schematic diagram of a thyristor module (dimensions in metres)

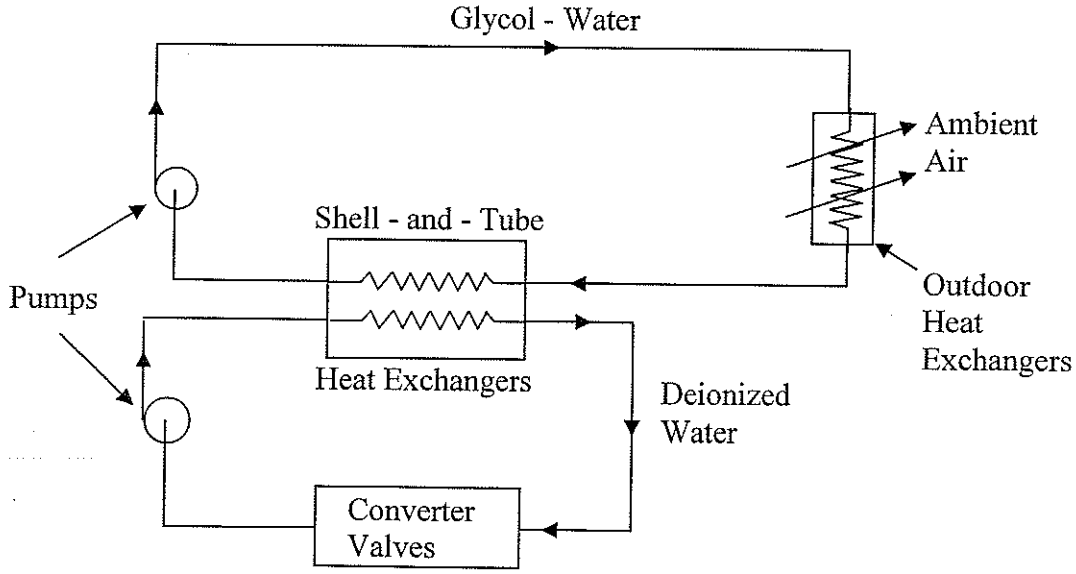

Figure 1.5: Schematic diagram of the cooling water circuit used for each of the valve groups

The remaining 10% of heat is dissipated into the air in the valve hall where it is removed by an air conditioning system that has a constant volumetric flow rate of 6.6 m^3/s. The air is introduced into the valve hall through six grills in the floor as seen in Figure 1.2. The return air is drawn from the highest point in the valve hall. The design requirements specify that the environmental temperature of the valve hall be maintained between 5°C and 40°C. Currently, there are no provisions for forced circulation of the air within the valve hall.

The optimum design of the air cooling system requires an evaluation of the airflow rate, location of the heat generating bodies within the cavity, and the location of the inlet and outlet openings in the cavity walls. For this purpose fundamental knowledge of the velocity and temperature distributions within the cavity is necessary. The aim of the project is to study the effects of the various parameters on the velocity and temperature distribution in order to obtain the most effective air cooling system design. However, from the start, modelling the entire three-dimensional domain was thought to be a large undertaking for the scope of one master's thesis. Therefore, this thesis will consider a two-dimensional geometry and thus lay the foundation for a future three-dimensional study that will provide guidelines for Manitoba Hydro.

The goal of this work is to model a case similar to the valve hall and gain knowledge of the velocity and temperature distribution that are the result of changes in the inlet flow rate, location of the bodies in the domain and the location of the inlet and outlets. Consequently, the valve hall was simulated as two-dimensional for the purposes of the study. A generic description was created and is shown in Figure 3.1. From this generic description, three domains were created and studied. The first domain (Geometry 1) was a single tower with four blocks. For this domain, the tower of four blocks was moved to 6 different positions. Both passive cooling and mixed convection cooling were studied. Different inlet and outlet positions were also studied. The second domain (Geometry 2) was a single tower formed by nine blocks. Two positions are investigated for Geometry 2. Three different inlet flow rates were examined: one for passive cooling and two for

mixed convection cooling. Again, different inlet and outlet positions were studied. The third domain (Geometry 3) was created with three towers of nine blocks each positioned side by side. For this domain passive and mixed convection cooling were studied; as well as different inlet and outlet positions. The results from the three domains are presented in Chapter 6.

CHAPTER 2

LITERATURE REVIEW

Bejan et al. (1995) studied how to cool a stack of parallel, heat generating boards when the flow is impeded by electromagnetic screens placed upstream and downstream of the stack. Both forced and natural convection were studied in the paper. The resultant domain studied for forced convection is shown in Figure 2.1; the domain studied for Natural convection is shown in Figure 2.2.

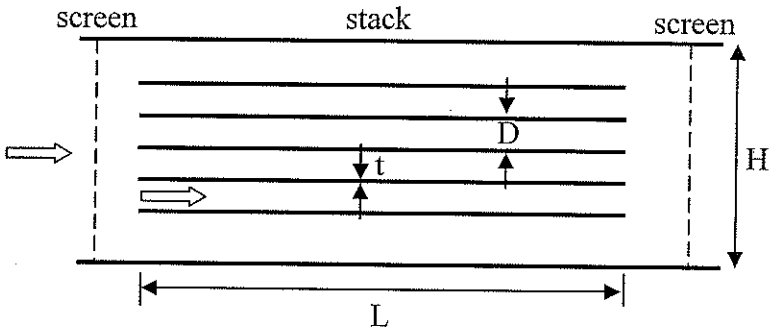

Figure 2.1: Forced convection cooling domain for Bejan et al. (1995)

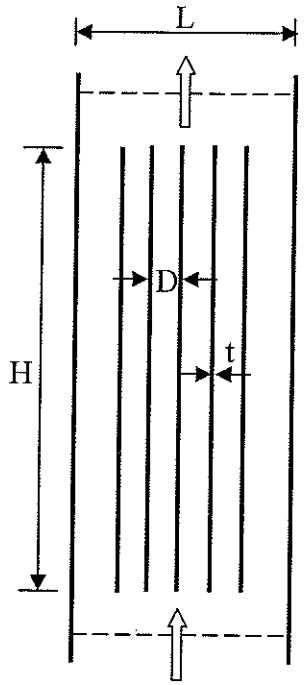

Figure 2.2: Natural Convection cooling domain for Bejan et al. (1995)

The flow through the spaces between the parallel plates was assumed laminar. Four separate designs were considered in the study. The first was forced convection cooling of a stack with board-to-board spacing selected to minimize the stack-coolant thermal resistance. The second was forced convection cooling of a stack with fixed board-to-board spacing. The third was natural convection cooling of a vertical stack with spacing selected to minimize the overall thermal resistance, and the fourth design was natural convection cooling of a vertical stack with fixed spacing. Thermal design optimization was the goal of the study. It was found that a single dimensionless group controls the effect of the screen. This dimensionless group was identified for each design; forced versus natural convection, high versus low screen Reynolds number. The results were reported for the design of screens made of wire meshes, or perforated plate with square (sharp) edges.

Fowler et al. (1997) performed experimental and numerical studies to find the optimal geometric arrangement of staggered and parallel plates in a fixed volume with forced convection heat transfer. Their results showed experimentally and numerically that the geometric arrangement of staggered plates can be optimized for maximum heat transfer (maximum thermal conductance) when the optimization is subjected to an overall volume constraint. In addition, the theory of intersecting asymptotes (small spacing versus large spacing) showed that it is possible to anticipate the optimal spacing of staggered plates, and the associated thermal conductance maximum.

Young and Vafai (1999) performed an experimental and numerical investigation of the forced convective heat transfer of individual obstacles and arrays of multiple two-dimensional obstacles. A schematic of the experimental apparatus is shown in Figure 2.3. The effects of changes in the channel height, input heat power and airflow rate upon the mean Nusselt numbers and temperature differences were recorded for individual as well as an array of obstacles within the channel.

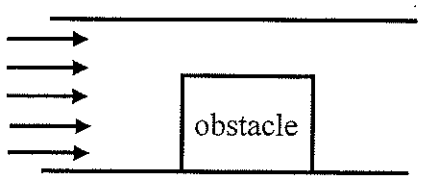

Figure 2.3: Schematic diagram of the experimental obstacle apparatus for Young and Vafai (1999)

As expected, low flow rates in the channel were found to significantly increase the temperature of the obstacle. The experimental results were found to be in good agreement with the results obtained numerically. A set of correlations for the arrays of channel mounted obstacles was given.

Hung (2001) numerically considered the cooling of obstacles attached to a substrate similar to electronic devices. The substrate with these obstacles was placed in a channel and it allowed fluid flow between upper and lower channels as seen in Figure 2.4.

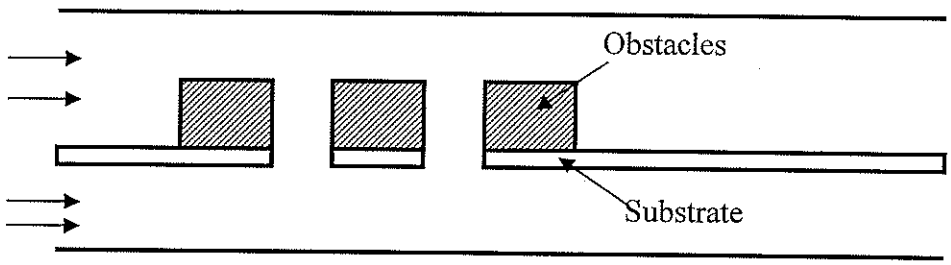

Figure 2.4: Schematic of obstacles on substrate for Hung (2001)

The results showed that high coolant flow rates did not necessarily produce higher heat transfer rates and that with appropriate geometric arrangements, passive cooling could give better results.

Dooher and Mills (2000) studied experimentally steady laminar natural convection of water about vertically stacked, two sided, horizontal heated plates. In their Experiments they varied the plate gap to plate half-width ratio while measuring the power input per plate, plate temperatures, and inlet and outlet bulk fluid temperatures. From the measurements the average Nusselt and Rayleigh numbers for each plate were correlated with a power law function.

Mufuta and Van de Bulck (2001) examined the distribution of mass flow due to natural convection around an array of two-dimensional rectangular blocks, as shown in Figure 2.5. They established conditions that would allow transversal flow and a correlation between the Rayleigh number and the maximum mass flow rate through the horizontal channel.

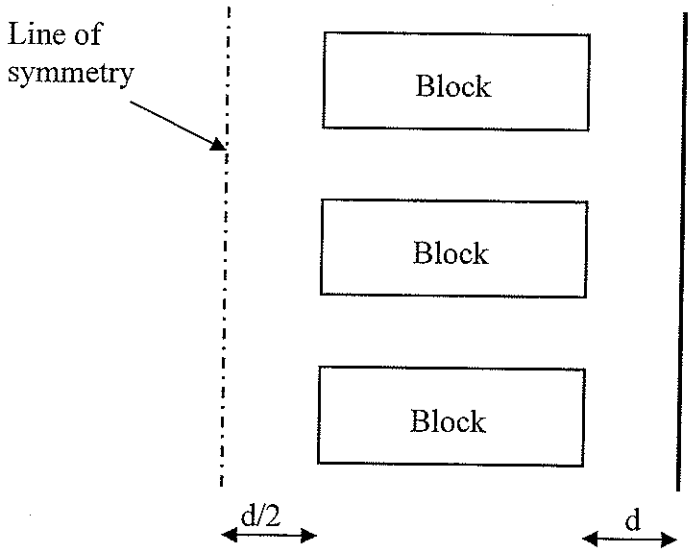

Figure 2.5: Array of two-dimensional rectangular blocks for Mufuta and Van de Bulck (2001)

Shuja et al. (2000) studied natural convection in a square cavity with a single, two dimensional, heat generating rectangular body. They studied the effect of the location of the body inside the cavity. Air or water was considered as the fluid in the cavity. The

cavity had two sides partially opened for an inlet and an outlet. The domain studied is shown in Figure 2.6.

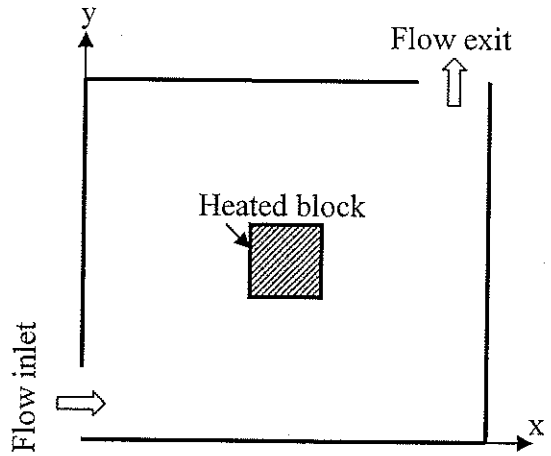

Figure 2.6: Schematic view of the calculation domain for Shuja et al. (2000)

The conclusions of the work were that the velocity in the vicinity of the solid body surfaces varied considerably with the location of the solid body within the cavity and that non-uniform cooling of the solid body occurred when the solid body was located in the bottom left and right corners of the cavity. The authors suggested that the non-uniform cooling may be the result of convection cooling of the two surfaces of the solid body facing the inlet and exit of the cavity.

Shuja et al. (2001) continued their previous work by studying natural convection in a square cavity but this time considering the effect of the aspect ratio of the heated block on the Nusselt number. The domain is shown in Figure 2.7. They concluded that fluid circulation cells developed within the cavity and the location of the circulation cells behind the solid body moved downwards as the aspect ratio reduced.

Dubovsky et al. (2002) considered experimentally and numerically the cooling of cylindrical bodies in an enclosed space with openings. They studied symmetric and asymmetric openings in the enclosure. They found that for a single cylinder the closer the cylinder was to the inlet port the lower the temperature; and that the temperature of any

cylinder in a three cylinder row is lower than that of a single cylinder placed at the same location.

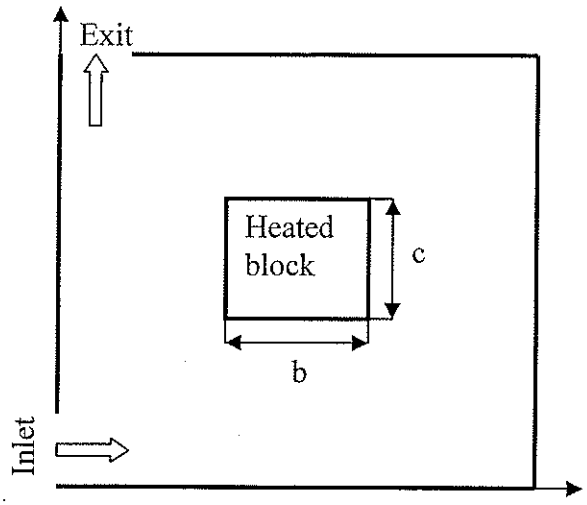

Figure 2.7: Domain for Shuja et al. (2001)

The literature review demonstrates the fact that most work previously published deals with optimization of spacing or optimization of arrangement between heat generating plates or blocks. The previous work does not encompass the case where the geometric spacing is fixed and the only variables are the mass flow rate and the inlet and outlet locations as in the case of the towers at the Dorsey converter station.

Chapter 3

MODEL DESCRIPTION

3.1 Domain

The valve hall shown in Figures 1.1 and 1.2 in Chapter 1 was simplified for the purposes of the study. The resultant domain can be described by the generic description shown in Figure 3.1. Figure 3.1 illustrates a two-dimensional square domain with dimensions (L x L), and two openings. There is an inlet opening at the bottom of the domain (a_1L) and its location is denoted by (a_2L). The location of this opening is not limited to the bottom of the domain and can be placed on the left-hand-side wall of the domain. The outlet (a_3L) is shown at the top of the domain and its centerline is located at a_4L from the left wall. The location of the outlet is not limited to the top of the domain and it can be placed at the right hand side of the domain. Within the domain there are M towers. The towers are formed by blocks stacked vertically on top of each other. The parameters a_6L, a_7L, a_8L and N define the size of the tower. The vertical height of the block is a_6L, the horizontal width of the block is a_7L and the vertical spacing between the blocks is a_8L. There are N blocks in each tower. The location of the tower relative to the right and top sides is defined by a_9L and $a_{10}L$. The distance between towers is a_5L. This generic description would permit the examination of how the number of towers, position of the tower, size of tower, inlet mass flow rate, and the location of inlet and outlet affect the flow structure and the temperature distribution in the domain.

Coordinates of x and y were assigned to directions in the horizontal and vertical directions in the domain, respectively. The coordinate z was assigned to the direction out of the page (not shown). Using Figure 3.1 for this investigation will not only give an understanding of the velocity and temperature distribution in the domain but will also give possible ideas to Manitoba Hydro for possible upgrades to the existing converter station. Along with the future work in three dimensions, it can be used to design the new converter station being proposed for Bipole 3.

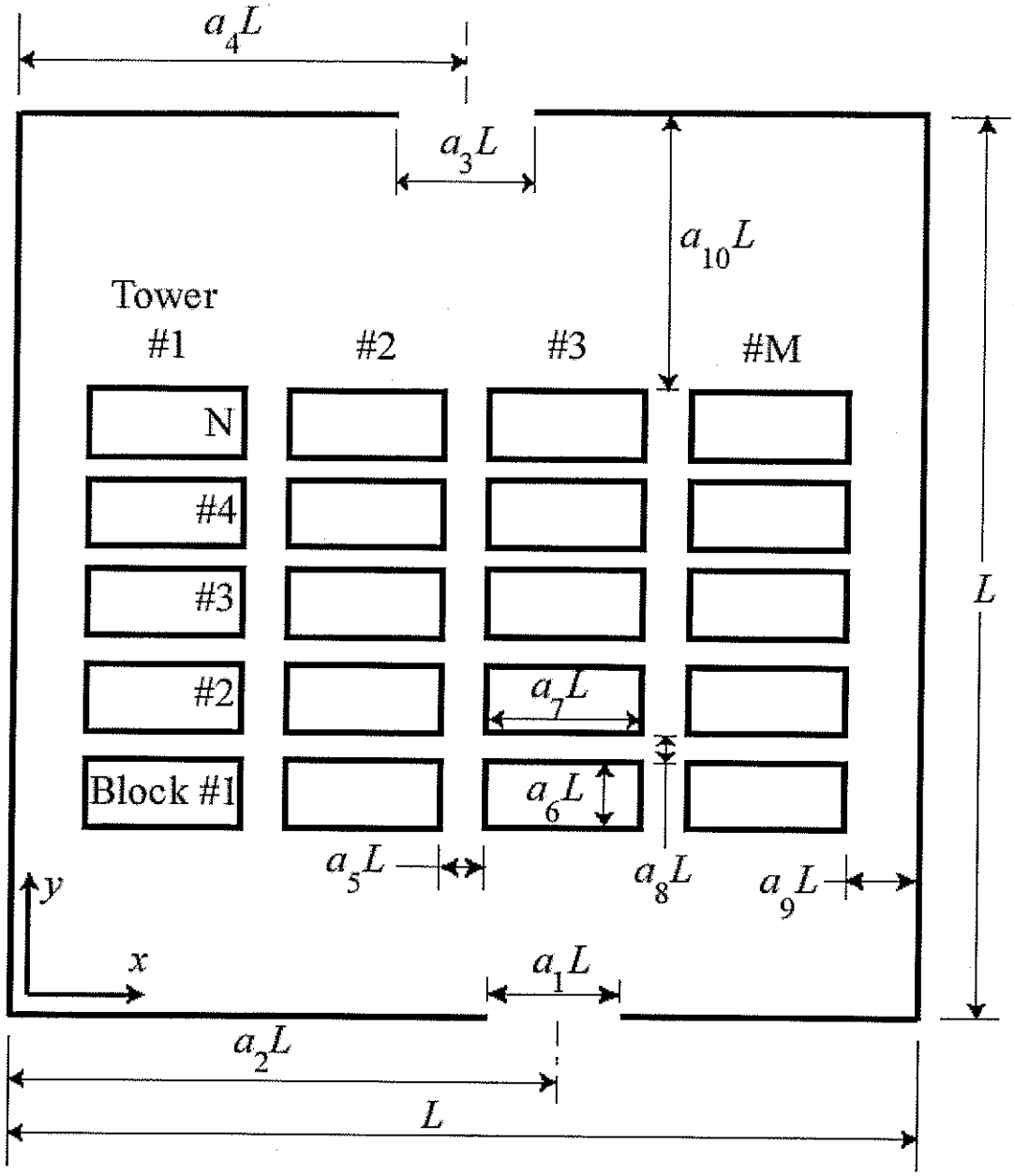

Figure 3.1: Generic description of the domain.

3.2 Assumptions

The following assumptions were made:

- Laminar flow
- Steady state with respect to time
- Two-dimensional analyses
- Newtonian fluid
- Constant properties
- Incompressible flow
- Negligible radiation
- Negligible viscous dissipation

For this two dimensional analysis the towers were assumed to be very long in the z direction, the towers were assumed to have no power surges and there were no outside effects on the walls such as radiation from the sun.

3.3 Conservation Equations

The governing equations considered are the conservation of mass, momentum and energy.

$$\frac{\partial u}{\partial x}+\frac{\partial v}{\partial y}=0 \qquad \textbf{(3. 1)}$$

$$\rho\left[u\frac{\partial u}{\partial x}+v\frac{\partial u}{\partial y}\right]=-\frac{\partial P}{\partial x}+\mu\left[\frac{\partial^2 u}{\partial x^2}+\frac{\partial^2 u}{\partial y^2}\right] \qquad \textbf{(3. 2)}$$

$$\rho\left[u\frac{\partial v}{\partial x}+v\frac{\partial v}{\partial y}\right]=-\frac{\partial P}{\partial y}+\mu\left[\frac{\partial^2 v}{\partial x^2}+\frac{\partial^2 v}{\partial y^2}\right]-\rho g \qquad \textbf{(3. 3)}$$

$$u\frac{\partial T}{\partial x}+v\frac{\partial T}{\partial y}=\frac{k}{\rho C_p}\left[\frac{\partial^2 T}{\partial x^2}+\frac{\partial^2 T}{\partial y^2}\right] \quad \textbf{(3. 4)}$$

Using the Boussinesq approximation

$$\rho g=+\rho_o\left[1-\beta\left(T-T_o\right)\right]g \quad \textbf{(3. 5)}$$

where ρ_o and T_o are the density and temperature at the inlet (20°C)

Also define,

$$P^*=P+\rho_o gy \quad \textbf{(3. 6)}$$

$$\frac{\partial P}{\partial x}=\frac{\partial P^*}{\partial x} \quad \textbf{(3. 7)}$$

$$\frac{\partial P}{\partial y}=\frac{\partial P^*}{\partial y}-\rho_o g \quad \textbf{(3. 8)}$$

The governing equations become

$$\frac{\partial u}{\partial x}+\frac{\partial v}{\partial y}=0 \quad \textbf{(3. 9)}$$

$$\rho\left[u\frac{\partial u}{\partial x}+v\frac{\partial u}{\partial y}\right]=-\frac{\partial P^*}{\partial x}+\mu\left[\frac{\partial^2 u}{\partial x^2}+\frac{\partial^2 u}{\partial y^2}\right] \quad \textbf{(3. 10)}$$

$$\rho\left[u\frac{\partial v}{\partial x}+v\frac{\partial v}{\partial y}\right]=-\frac{\partial P^*}{\partial y}+\mu\left[\frac{\partial^2 v}{\partial x^2}+\frac{\partial^2 v}{\partial y^2}\right]+\rho_o g\beta\left(T-T_o\right) \quad \textbf{(3. 11)}$$

$$u\frac{\partial T}{\partial x}+v\frac{\partial T}{\partial y}=\frac{k}{\rho C_p}\left[\frac{\partial^2 T}{\partial x^2}+\frac{\partial^2 T}{\partial y^2}\right] \quad \textbf{(3. 12)}$$

Introducing the following dimensionless groups

$$X = \frac{x}{L} \tag{3. 13}$$

$$Y = \frac{y}{L} \tag{3. 14}$$

$$U = \frac{u}{V_o} \tag{3. 15}$$

$$V = \frac{v}{V_o} \tag{3. 16}$$

$$P = \frac{P^*}{\frac{1}{2}\rho V_o^{\,2}} \tag{3. 17}$$

$$\theta = \frac{T - T_o}{q'' \frac{L}{k}} \tag{3. 18}$$

$$\mathrm{Pr} = \frac{\mu C_p}{k} \tag{3. 19}$$

$$\mathrm{Re}_o = \frac{a_1 \rho V_o L}{\mu} \tag{3. 20}$$

$$Gr = \frac{g\beta q'' L^4 NM}{k\upsilon^2} \tag{3. 21}$$

Where V_o is the velocity at the inlet and q″ is the heat flux

Substituting the above dimensionless groups into the governing equations we get

$$\frac{\partial U}{\partial X} + \frac{\partial V}{\partial Y} = 0 \tag{3. 22}$$

$$U\frac{\partial U}{\partial X} + V\frac{\partial U}{\partial Y} = -\frac{1}{2}\frac{\partial P^*}{\partial X} + \frac{a_1}{\mathrm{Re}_o}\left[\frac{\partial^2 U}{\partial X^2} + \frac{\partial^2 U}{\partial Y^2}\right] \tag{3. 23}$$

$$U\frac{\partial V}{\partial X}+V\frac{\partial V}{\partial Y}=-\frac{1}{2}\frac{\partial P^{*}}{\partial Y}+\frac{a_1}{\mathrm{Re}_o}\left[\frac{\partial^2 V}{\partial X^2}+\frac{\partial^2 V}{\partial Y^2}\right]+\frac{1}{NM}a_1^{\,2}\left(\frac{Gr}{\mathrm{Re}_o^{\,2}}\right)\theta \qquad \textbf{(3. 24)}$$

$$U\frac{\partial \theta}{\partial X}+V\frac{\partial \theta}{\partial Y}=\frac{a_1}{\mathrm{Re}_o\,\mathrm{Pr}}\left(\frac{\partial^2 \theta}{\partial X^2}+\frac{\partial^2 \theta}{\partial Y^2}\right) \qquad \textbf{(3. 25)}$$

3.4 Boundary Conditions

The boundary conditions applied to the geometries are as follows; they can also be viewed in Figure 3.2. All outer walls are adiabatic, uniform heat flux in the tower of q'' = 30.654[W/m^2] for all cases, uniform inlet velocity V_o for mixed convection and uniform inlet temperature T_o.

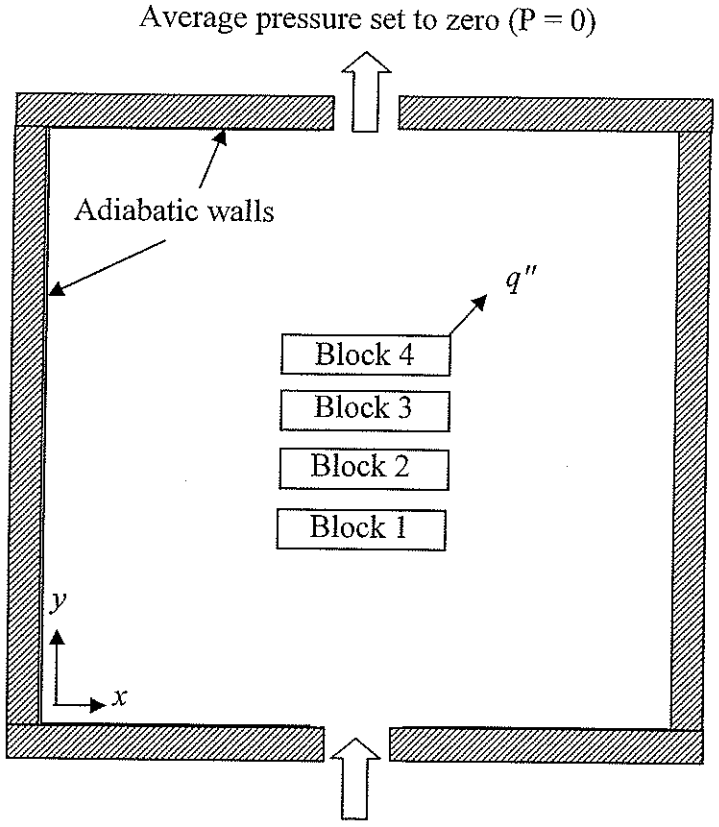

- Uniform inlet temperature
- Free Convection: Average inlet pressure set to zero (P= 0)
- Mixed Convection: Uniform Inlet velocity specified (Re_o = 100, 225)

Figure 3.2: Boundary conditions

To obtain results for natural convection and mixed convection different boundary conditions must be set. For natural convection, the incoming air is allowed to flow into the domain unaided. An average inlet pressure equal to zero was needed at the inlet boundary condition. For mixed convection a uniform inlet velocity was set at the specified velocity corresponding to the inlet Reynolds number.

An average pressure of zero was set for the outlet boundary condition for both natural convection and mixed convection.

Walls are insulated:

$$\frac{\partial \theta}{\partial X} = 0 \text{ at } X = 0 \text{ and } X = 1 \qquad \textbf{(3. 26)}$$

$$\frac{\partial \theta}{\partial Y} = 0 \text{ at } Y = 0 \text{ and } Y = 1 \qquad \textbf{(3. 27)}$$

Blocks:

$$\frac{\partial \theta}{\partial X} = -1 \text{ on the right face of a block} \qquad \textbf{(3. 28)}$$

$$\frac{\partial \theta}{\partial X} = 1 \text{ on the left face of a block} \qquad \textbf{(3. 29)}$$

$$\frac{\partial \theta}{\partial Y} = -1 \text{ on the top face of a block} \qquad \textbf{(3. 30)}$$

$$\frac{\partial \theta}{\partial Y} = 1 \text{ on the bottom face of a block} \qquad \textbf{(3. 31)}$$

3.5 Geometries studied

The coolant used in this study was air; therefore, Prandtl number was fixed at 0.7. Three geometries were derived from Figure 3.1. The size of the blocks in the towers defined by a_6, a_7, and a_8 were kept constant for the three geometries. The dimensions of the blocks were $a_6 = 0.06$, $a_7 = 0.2$, and $a_8 = 0.03$. The size of the openings, a_1 for the inlet and a_3 for the outlet, were kept constant at 0.1 for the three geometries. The values of a_2, inlet

port locator and a_4, outlet port locator, were varied in all three geometries to study the effect of their location on the velocity and temperature distribution. Geometry 1 corresponds to N = 4 and M = 1 (one tower), Gr = 1.0E+6. Six different locations of the tower within the domain were studied for Geometry 1, this was achieved by varying the values of a_9 and a_{10} and the values are shown later in Table 6.1. The inlet Reynolds number (Re_o) was varied to correspond to passive or one case of mixed convection cooling (Re_o = 100). Geometry 2 corresponds to N = 9 and M = 1, Gr = 2.25E+6. Two tower locations were studied for Geometry 2 these correspond to a_9 = 0.1 and 0.4. The value of a_{10} = 0.11 for all cases corresponding to Geometry 2. The value of Re_o was varied to correspond to passive or two cases of mixed convection cooling (Re_o = 100 and 225). Geometry 3 corresponds to N = 9 and M = 3 (three towers), Gr = 6.75E+6. For Geometry 3, one case of passive cooling was studied and the remainder of the cases corresponded to a Re_o = 100.

Chapter 4

NUMERICAL SOLUTION METHOD

4.1 Introduction

To obtain a numerical solution to the governing equations, the domain was subdivided into small control volumes by creating a computational grid. An iterative solution of the linearized algebraic equations was performed in dimensional form, from which the U, V, W, θ, and P solution fields at all nodal points in the fluid were obtained.

4.2 CFX-TASCflow

The numerical solver used in the study was CFX-TASCflow 2.11; it is distributed by AEA Technology. TASCflow uses a finite volume method of discretization (Patankar, 1980), but it is based on a finite element approach for representing the geometry. In the present work Cartesian velocity components were used on a structured, non-staggered grid. Each run was considered converged when the sum of the absolute dimensionless residuals of the discretized equations was less than 1.0×10^{-6}.

CFX-TASCflow has two user interfaces, a graphical user interface (GUI) and a command line user interface. The boundary conditions, material properties and solver parameters were defined using the command line user interface. The GUI was used only for post processing the results obtained from the solver.

4.3 CFX-TASCgrid

The grids were generated with CFX-TASCgrid also distributed by AEA Technology. To create the grid for Geometry 1, the domain had to be "built" by TASCgrid. The domain was made up of 63 blocks or regions as shown by the rectangles that make up Figure 4.1. The hatched regions in the figure represent the areas occupied by the blocks. The regions

were created with TASCgridg by defining the vertices of all 63 regions, the attachment of adjacent regions, and the number and spacing of nodes in all regions.

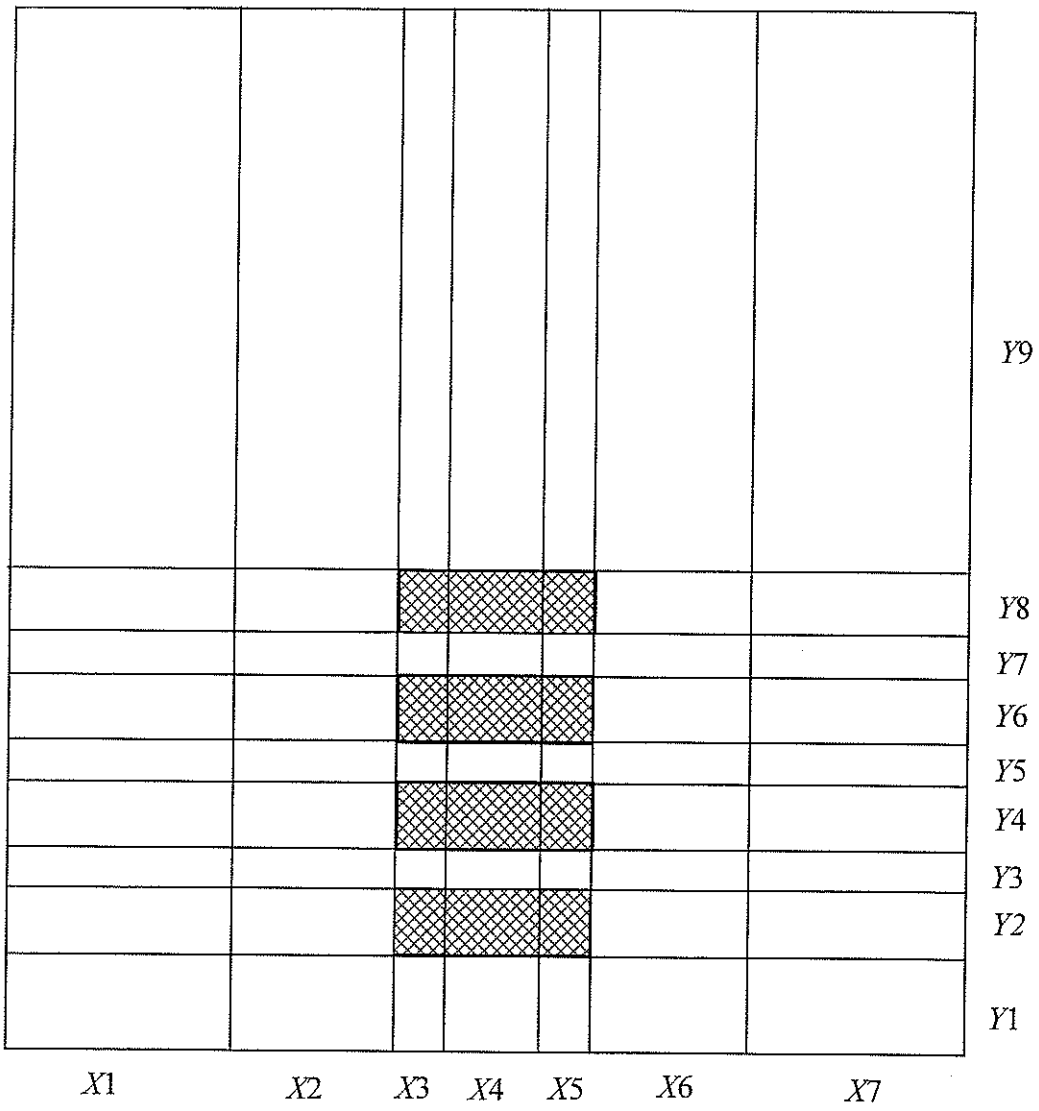

Figure 4.1: Regions for Geometry 1

The sizes of the regions for Geometry 1 are given in non-dimensional form in Table 4.1. Geometry 2 required the addition of more regions for a total of 133 regions and the result is shown in Figure 4.2. The sizes of the regions for Geometry 2 are given in Table 4.2.

Table 4.1: Size of regions for Geometry 1 in non-dimensional form

	X		Y		
	a_9=0.4	a_9=0.1	a_{10}=0.57	a_{10}=0.335	a_{10}=0.1
1	0.25	0.25	0.1	0.335	0.57
2	0.15	0.20	0.06	0.06	0.06
3	0.05	0.1	0.03	0.03	0.03
4	0.1	0.15	0.06	0.06	0.06
5	0.05	0.05	0.03	0.03	0.03
6	0.15	0.15	0.06	0.06	0.06
7	0.25	0.1	0.03	0.03	0.03
8			0.06	0.06	0.06
9			0.57	0.335	0.1

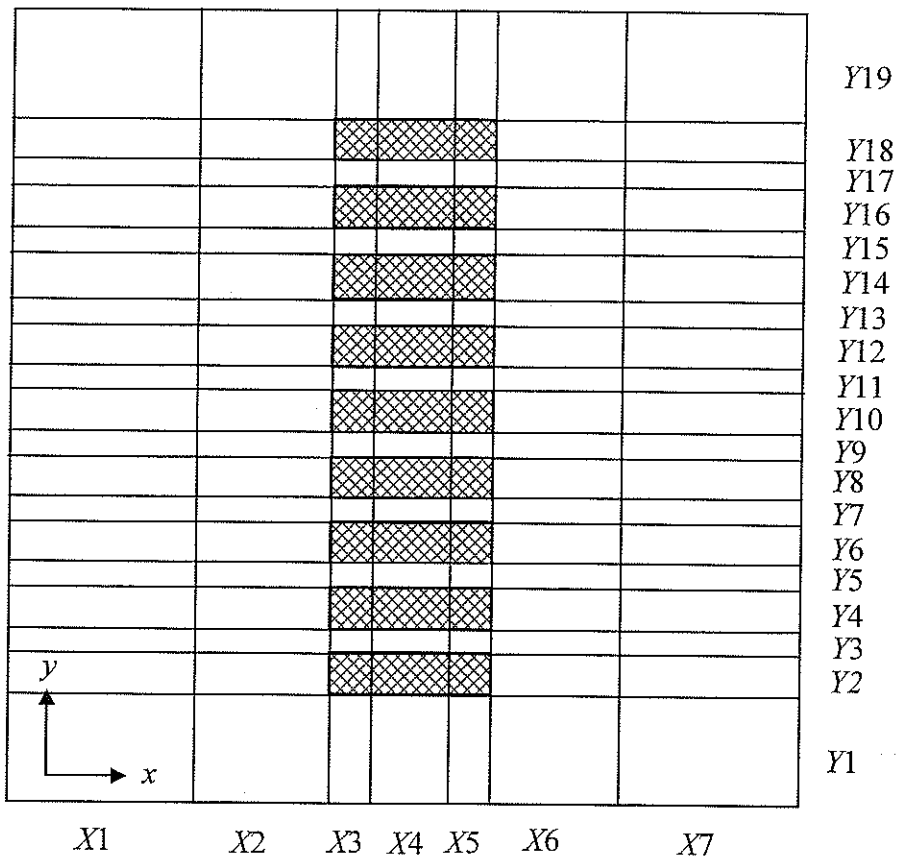

Figure 4.2: Regions for Geometry 2

Table 4.2: Size of regions for Geometry 2 in non-dimensional form

	X		Y
	a_9=0.4	a_9=0.1	
1	0.25	0.25	0.11
2	0.15	0.20	0.06
3	0.05	0.1	0.03
4	0.1	0.15	0.06
5	0.05	0.05	0.03
6	0.15	0.15	0.06
7	0.25	0.1	0.03
8			0.06
9			0.03
10			0.06
11			0.03
12			0.06
13			0.03
14			0.06
15			0.03
16			0.06
17			0.03
18			0.06
19			0.11

For Geometry 3 the size of the regions was only altered in the X direction while keeping the Y dimensions the same as Geometry 2. The regions for Geometry 3 are shown in Figure 4.3. The sizes of the regions in the X direction for Geometry 3 are given in Table 4.3. The following parameters were fixed for Geometry 3; $a_5 = 0.1$, $a_9 = 0.1$ and $a_{10} = 0.11$.

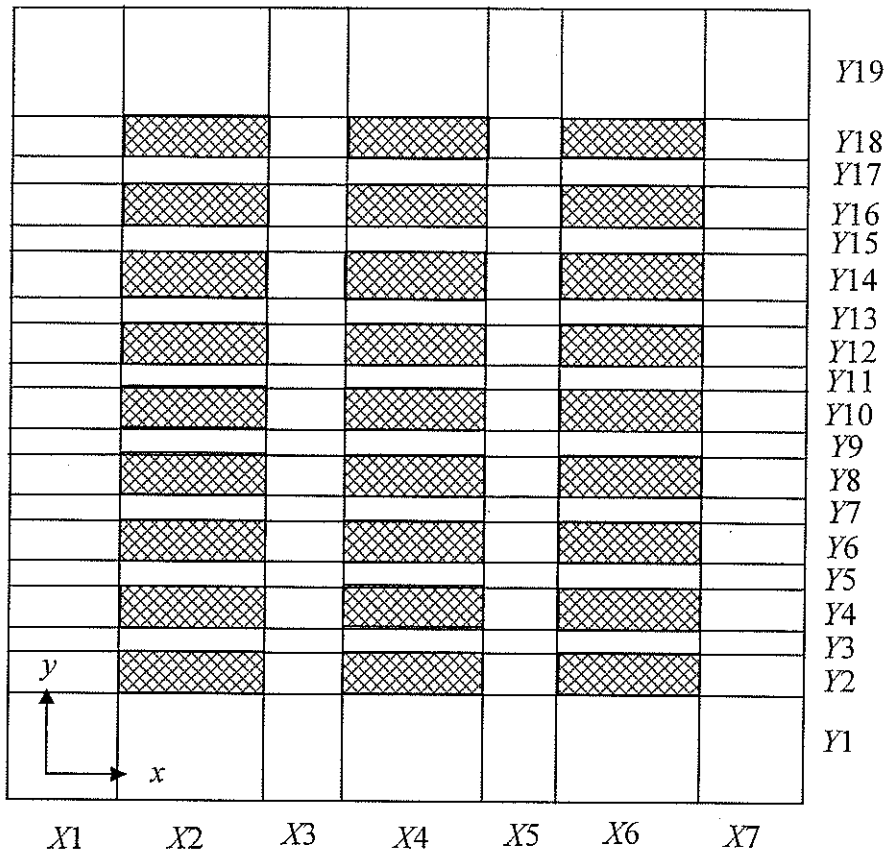

Figure 4.3: Regions for Geometry 3

Table 4.3: Size of regions in *X* direction for Geometry 3 in non-dimensional form

	X
1	0.1
2	0.2
3	0.1
4	0.2
5	0.1
6	0.2
7	0.1

The mesh was then created with the rest of the TASCgrid programs (TASCgridc, TASCgrids, and TASCgridi) this is discussed in detail in Chapter 5. The boundary conditions and initial guesses of all the fields were specified and the TASCflow numerical solver was invoked to produce results for the temperature, velocity and pressure of the case that was studied.

Chapter 5

VALIDATION TESTS

5.1 Introduction

To ensure that the results obtained from CFX-TASCflow were numerically accurate, the code was validated. The results were ensured to be grid independent, which means the solutions between two grids of differing resolutions have to be reasonably close. Grid independence was performed each time the geometry was changed. Therefore, grid independence tests are presented for Geometries 1, 2 and 3. In the following discussion, the nomenclature for the location of the inlet and outlet openings has the form POS – VAL. The part "POS", always has a letter L, B, T or R for left, bottom, top or right. The part "VAL", is the value of X or Y of the opening centerline.

5.2 Grid Independence

5.2.1 Geometry 1 (N=4 and M=1)

Three grids of varying nodal numbers were compared for one case to test for grid independence. The grid-independence results were done for the case of natural convection, position 1 (a_9 = 0.4 and a_{10} = 0.57), inlet centered at the bottom of the domain (B – 0.5) and the outlet centered at the top of the domain (T – 0.5). A coarse grid comprised of 47 nodes in the x direction and 56 nodes in the y direction (47 X 56), a medium grid containing 93 X 111 nodes and a fine grid containing 139 X 166 nodes were selected for the comparison. To compare the results, the temperature around the heat generating blocks was monitored. The temperatures were first written into separate result files containing the temperatures for the lower, right, top and left surfaces of each block. A FORTRAN program was then used to sort the temperatures in order as depicted in Figure 5.1. A dimensionless parameter s was used to indicate the location on the block as a fraction of the perimeter measured in a counter-clockwise direction starting from the lower left corner.

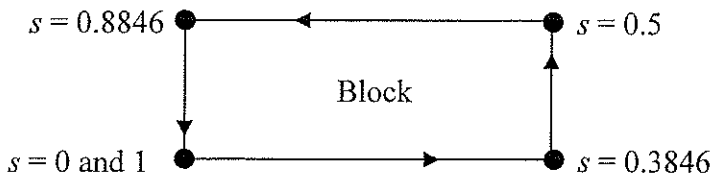

Figure 5.1: Values of dimensionless parameter s around a block

The procedure was done for each block in the tower. The output files containing the sorted temperature data were then compared for each grid. Grid independence was assumed when the refinement of the grid results in insignificant changes in the temperature around the blocks.

Figures 5.2 to 5.5 depict the temperature around each of the four blocks for the three grids; coarse, medium and fine.

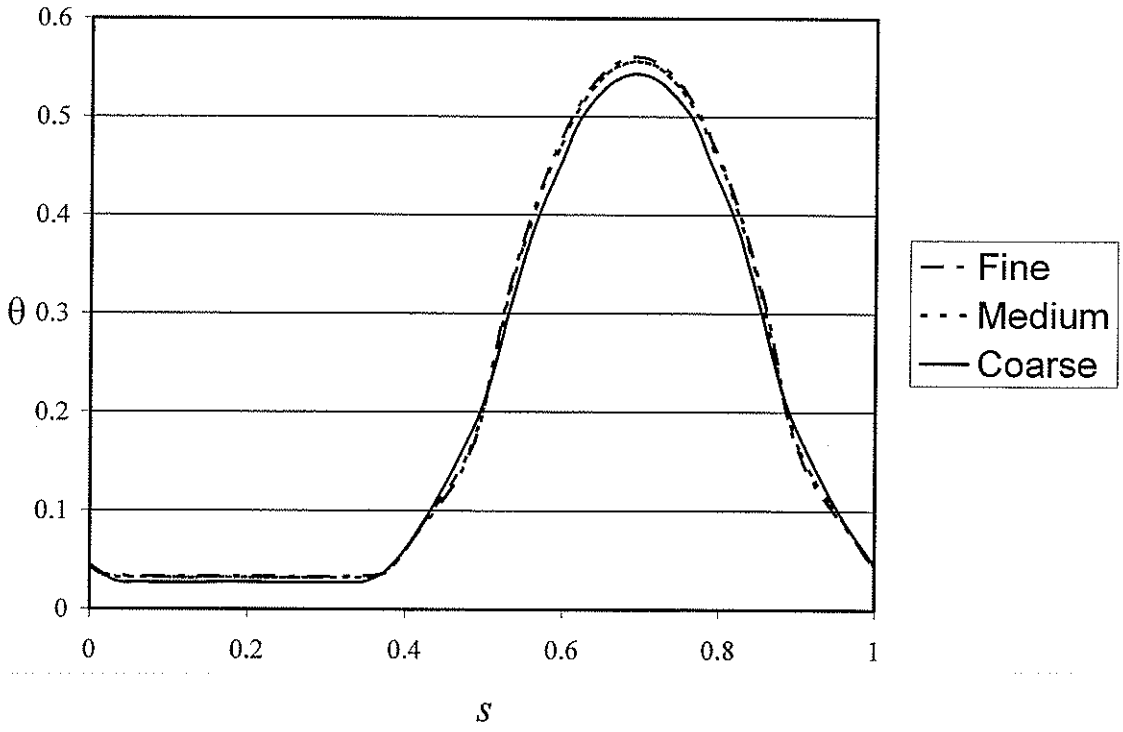

Figure 5.2: Temperature distribution around block 1

The temperature for the three grids around the first block is shown in Figure 5.2. Recalling from Figure 5.1 the bottom surface of the block is between $s = 0$ and 0.3846, this is where the incoming air is impacting the bottom surface of block one and therefore the bottom surface has a low temperature value. On the right surface of block one, $s =$ 0.3846 to 0.5, the temperature increases. The temperature increase is the result from the velocity of the flow around the block decreasing. At the top surface of the block, $s = 0.5$ to 0.8846, this is the area where the block reaches its maximum temperature. Note that the maximum temperature occurs at the middle of the top surface ($s = 0.6923$) meaning that the air inside the channel between the first block and the second block does not have a high velocity. Also, note that there is symmetry in the results of temperature for all the blocks. The portion of the curve between $s = 0.1923$ and 0.6923 is a mirror image of the curve between 0.6923 and 0.1923.

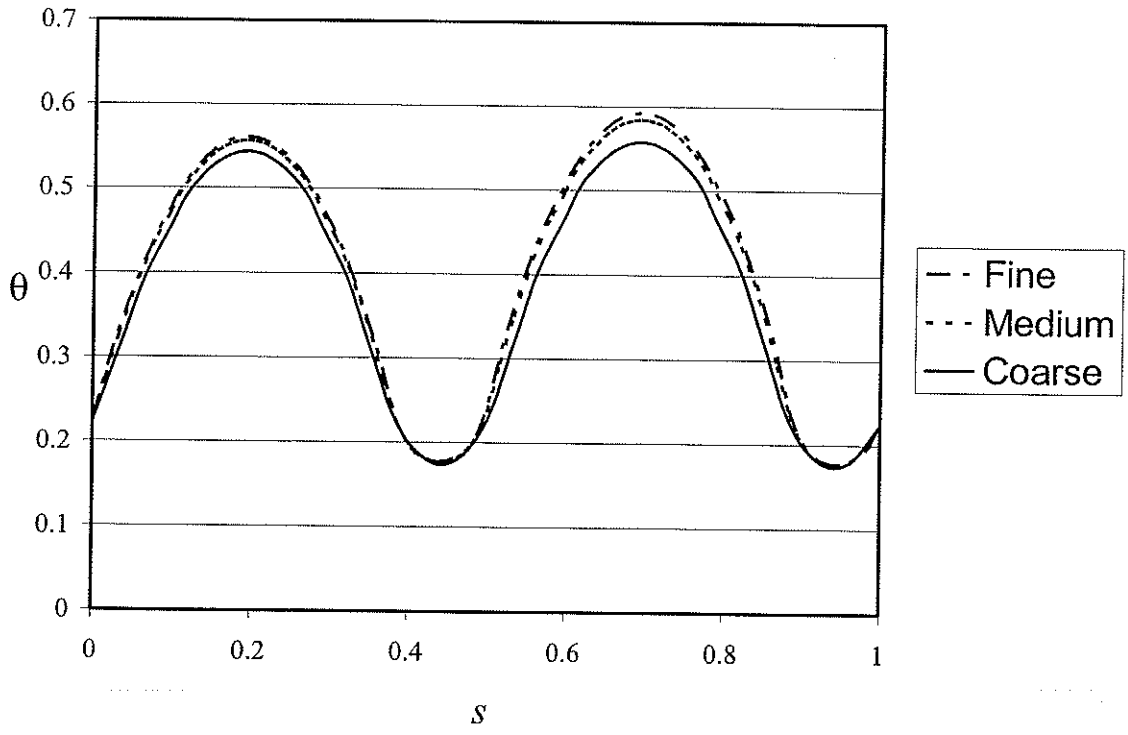

Figure 5.3: Temperature distribution around block 2

Figures 5.3 and 5.4 are very similar in the sense that both the bottom and top surfaces of blocks 2 and 3 are at an elevated temperature compared to the sides. The maximum temperature for block 2 occurs in the top part of the block at about $s = 0.695$. The temperatures in the lower and top surfaces of block 4 have increased in Figure 5.4.

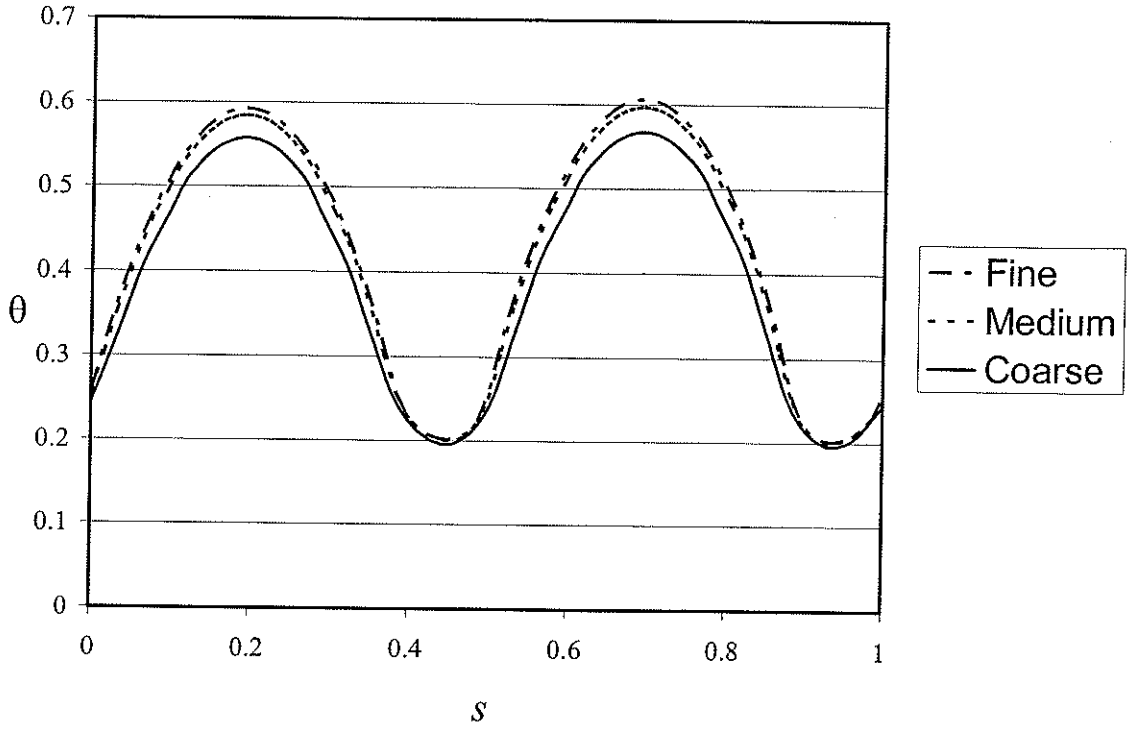

Figure 5.4: Temperature distribution around block 3

In Figure 5.5 the lower surface of the block is at an elevated temperature compared to the upper surface. The lower surface of block 4 is where the highest value of temperature occurs for the four blocks, the maximum temperature is about 0.6. The upper surface is at a substantially lower temperature and has a "peak" temperature, around 0.21.

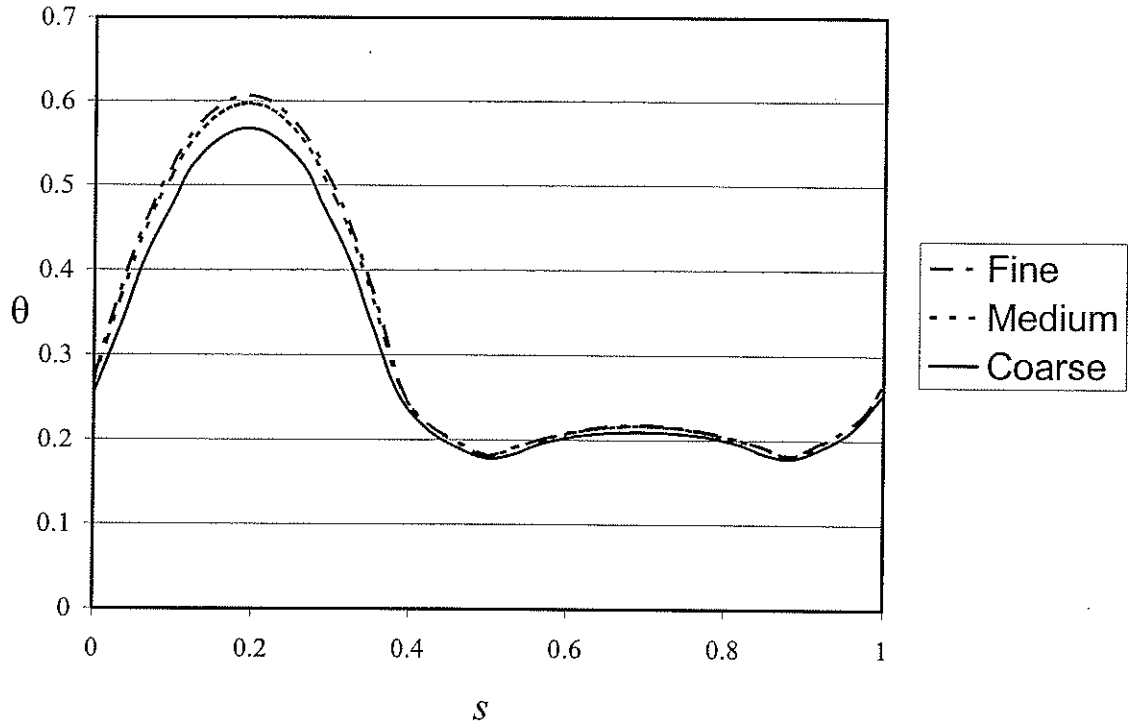

Figure 5.5: Temperature distribution around block 4

Note that in Figures 5.2 to 5.5, the medium and fine grid lines are close to each other and the differences in θ between the medium and fine grids were less than 4 %. Based on these results the medium grid was selected for the rest of the runs involving Geometry 1.

The node distribution in the medium grid (93 X 111) is shown in Figure 5.6 for the stack position corresponding to $a_9 = 0.4$ and $a_{10} = 0.57$. In the figure, the node number on the edge of each region is given in the x and y directions. From Figure 5.6, it can be seen that the grid is refined in the y direction between the blocks where the number of nodes in the y direction for the blocks equals 6 and the number of nodes between the blocks equals 12 nodes. In the x direction, the area designated for the inlet and outlet ports, when they are positioned on the bottom and the top (nodes 37-57), has 20 nodes. The resolution of nodes in the y direction corresponding to the tower (e.g., 11-71) remained constant for the different positions of the tower that were studied; however, the number of nodes surrounding the tower was increased or decreased accordingly to move the tower around the domain while keeping the total amount of nodes constant in the x and y directions.

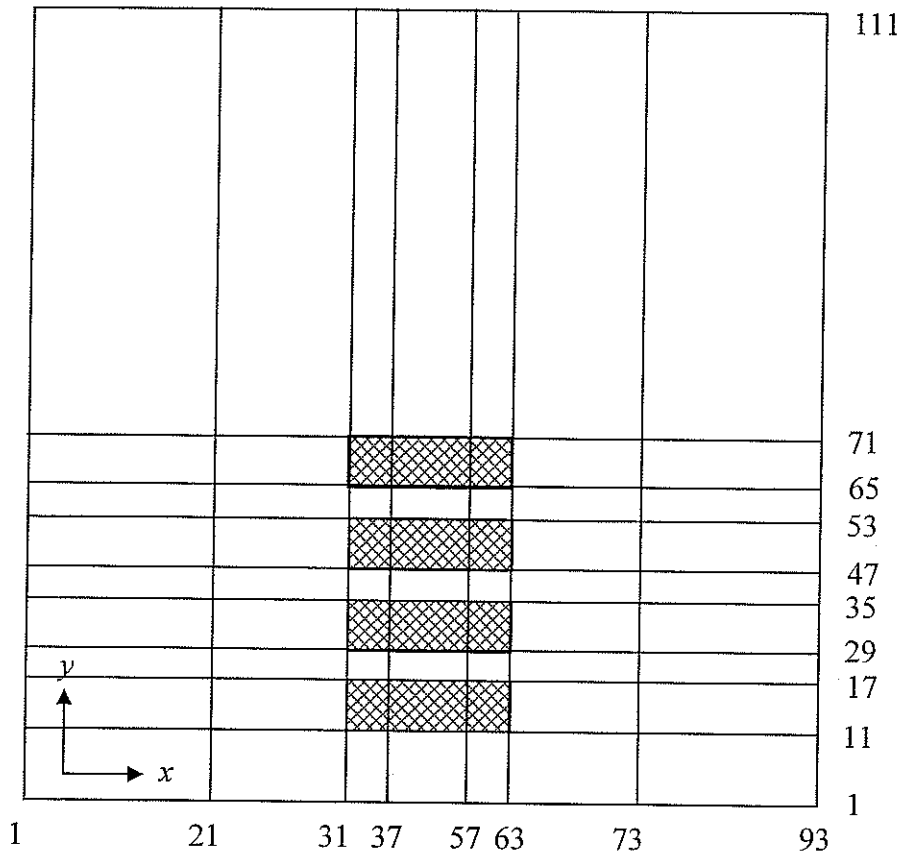

Figure 5.6: Node distribution for Geometry 1

5.2.2 Geometry 2 (N = 9 and M = 1)

For Geometry 2, grid independence was done on the case of forced convection (Re_o = 100) and inlet opening centered at the bottom of the domain (B – 0.5) and the outlet opening centered at the top of the domain (T – 0.5). Four grids were considered: G1, G2, G3 and G4. The grid definitions are shown in Table 5.1. For these tests the value of a_9 was fixed at 0.4.

Table 5.1: Number of nodes for the grids used in Geometry 2

	G1	G2	G3	G4
NX	93	185	277	369
NY	173	345	517	689

Table 5.2: Maximum temperature computed by the four grids for Geometry 2

	G1	G2	G3	G4
θ max	0.761	0.896	0.915	0.919

Deviation %	G1 vs G2	G2 vs G3	G3 vs G4
θ max	17.818	2.041	0.468

Grid independence was assessed by two tests. The first test involved monitoring the maximum temperature in the domain. As seen in Table 5.2, the change in the maximum temperature decreases as the grid is refined. The deviation defined for example as the difference between G2 and G1 divided by G1, decreases from 17.82% between G1 and G2 to 0.47% between G3 and G4 making the last two grids G3 and G4 the most accurate. The second test involved a comparison of the temperature along a line in the domain. A line of constant Y= 0.89 value was selected and the values of temperature were extracted along this line with TASCtool for each of the two grids G3 and G4. The temperature values are compared in Figure 5.7 and the deviation in θ between the two grids is less than 5.5%. Therefore, the lines appear one on top of the other in Figure 5.7.

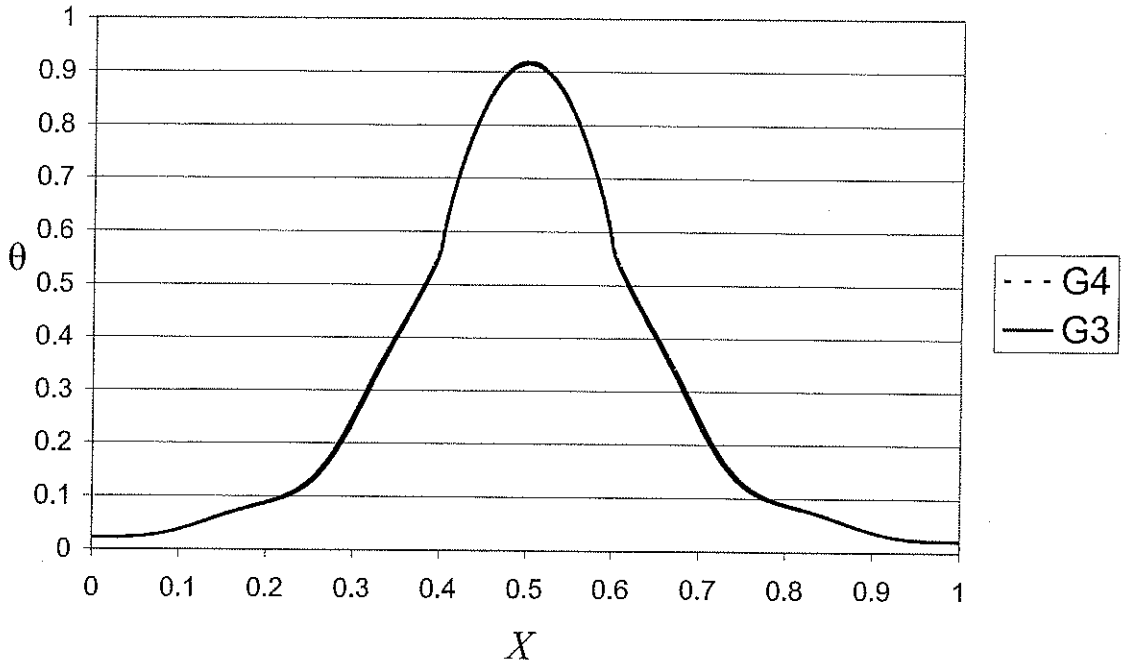

Figure 5.7: Temperature comparison between the G3 and G4 grids at constant $Y = 0.89$

The results in Table 5.2 and Figure 5.7 signify that the G3 grid having 277 nodes in the X direction and 517 nodes in the Y direction has values that are grid independent and this grid was used for all runs with Geometry 2. The node distribution in the grid can be seen in Figure 5.8.

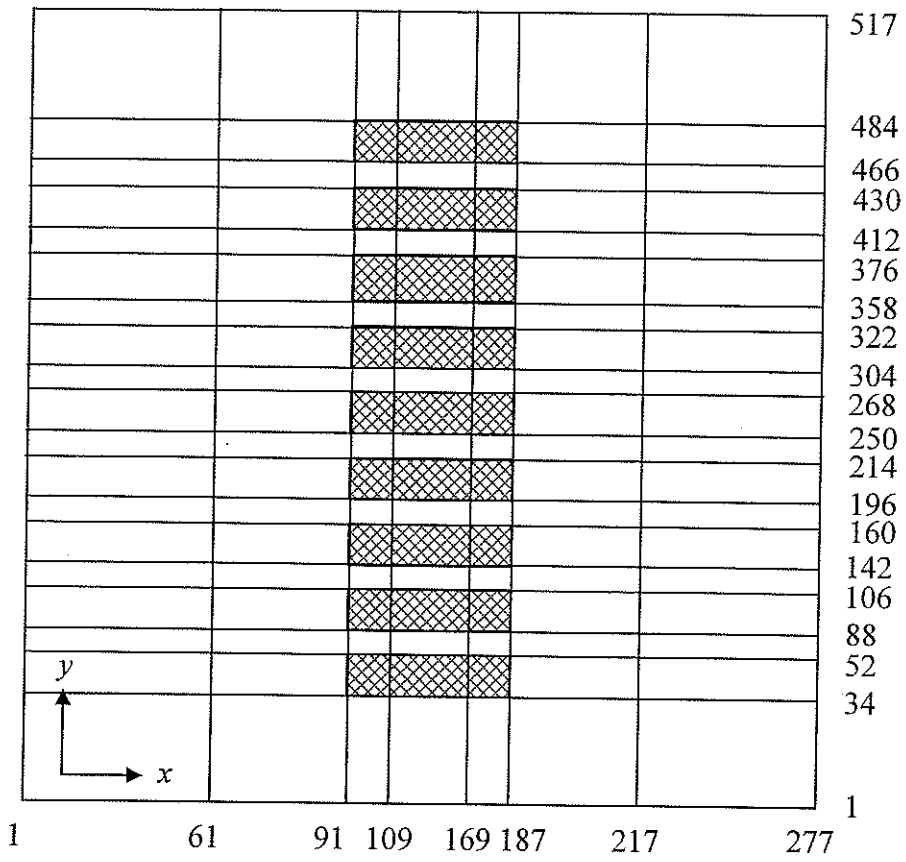

Figure 5.8: Node distribution for Geometry 2

5.2.3 Geometry 3 (N = 9, M =3)

Grid independence was performed for three different grid sizes. The grid independence tests were performed for forced convection (Re_o = 100), the inlet port at the left side of the domain (L – 0.05), and the outlet at the right side of the domain (R – 0.5). The three grids examined are found in Table 5.3. When examining the values of Table 5.3 we can see that the value of NY is constant at 517 nodes for the three grids studied. When the grid of geometry 2 was chosen in Section 5.2.2, the grid G3 was used because the resolution of both the X and Y directions was very similar to G4, which contained a lot more nodes and was detrimental to the speed of convergence. Yet, Geometry 3 has the same number of blocks in the Y direction (N = 9) but not in the X direction. The resolution of nodes in the Y direction was agreed to be of a sufficient resolution while maintaining the number of nodes at a relatively low number to have fast convergence. Therefore, only the nodes in the X direction are tested for grid independence.

Table 5.3: Grid sizes for Geometry 3

	Coarse	Medium	Fine
NX	101	201	401
NY	517	517	517

For each grid, the maximum temperature was obtained and is listed in Table 5.4.

Table 5.4: Maximum θ and its deviation between grids

Grid	θ_{max}	**Deviation (%)**
COARSE	0.784	0.912
MEDIUM	0.791	0.383
FINE	0.794	

The percent deviation between grids for the maximum temperature can also be found in Table 5.4. Between the medium and fine grid the deviation is 0.383%, and the deviation between the coarse and medium grid is less than one percent. A line of constant Y (Y = 0.89) was chosen to compare the temperature for the three grids. The location Y = 0.89

was chosen because the maximum temperature occurred along this line. The comparison can be seen in Figure 5.9.

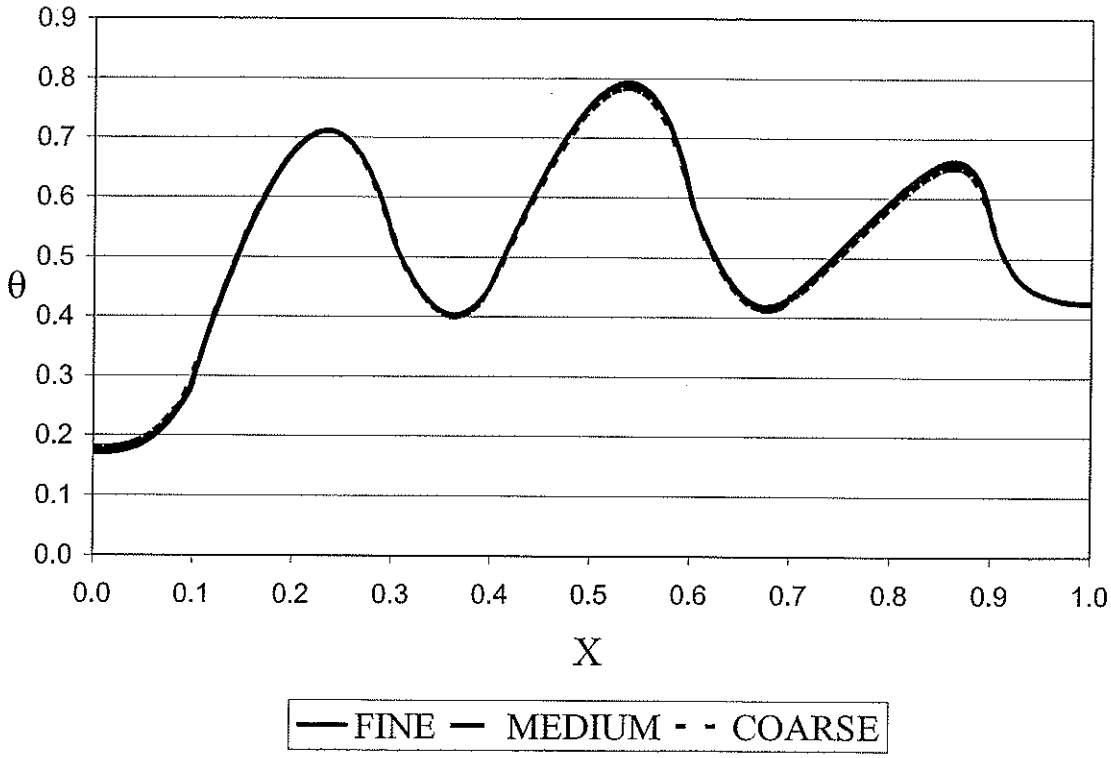

Figure 5.9: Temperature comparison at line $Y = 0.89$

From Figure 5.9, the percent deviation is highest between the coarse and medium grids. The percent deviation stays close to 1.0% in most results, with a maximum percent deviation of 2.02%. From the results in Table 5.4, it can be concluded that the deviation between the coarse grid and medium grid is significant. However, from the results in Figure 5.9, the maximum deviation is 2.88% but the average percent deviation of θ between the medium and fine grids is less than 0.9%. When including the values from Table 5.4, the medium grid compared to the fine grid gives reasonably close results. Therefore, the medium grid was chosen to obtain the results for all the cases. The node distribution is shown in Figure 5.10.

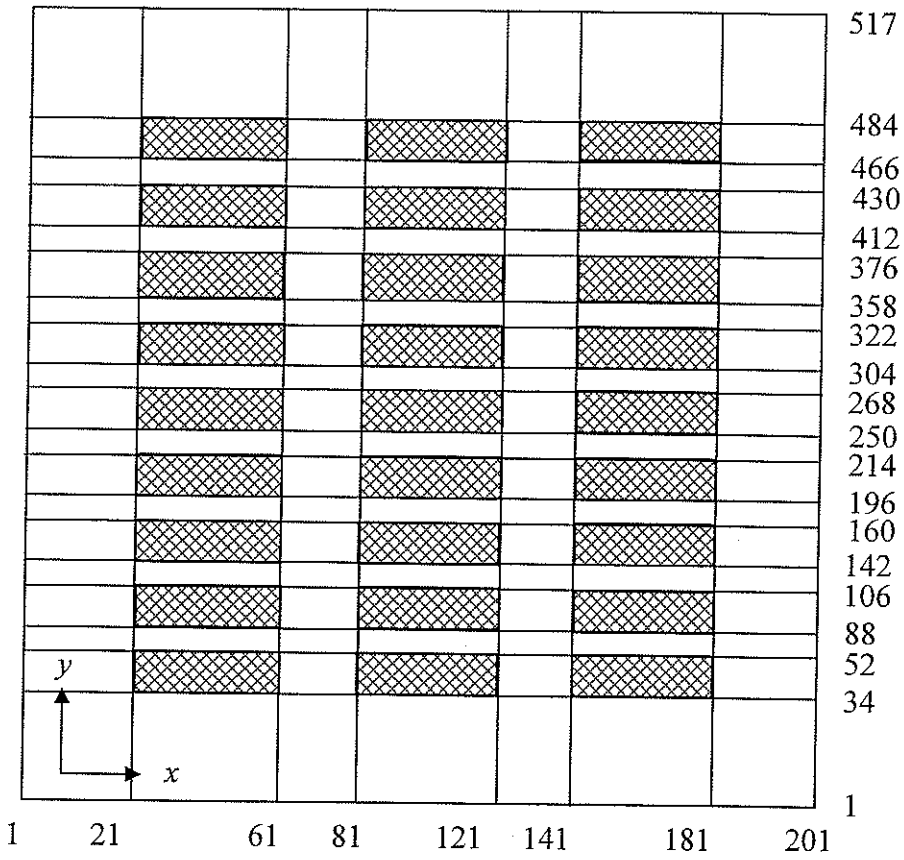

Figure 5.10: Node distribution for Geometry 3

Chapter 6

RESULTS AND DISCUSSION

6.1 Introduction

Three geometries were used based on the generic description (Figure 3.1) to study the effect of the number of towers, position of the tower, size of tower, inlet mass flow rate, and the location of inlet and outlet on the flow and temperature distributions. The first geometry studied was a single tower formed by four blocks (Figure 6.1); the second, a single tower formed by nine blocks (Figure 6.11) and the last, three towers each formed by nine blocks (Figure 6.43). For geometries 1 and 2, the location of tower, inlet mass flow rate and the inlet and outlet locations were examined. For geometry 3 the inlet mass flow rate and the inlet and outlet locations were examined.

6.2 Geometry 1

Geometry 1, shown in Figure 6.1, was the first studied. For this geometry there are four blocks forming a single tower. Referring to Figure 3.1, Geometry 1 corresponds to $a_1 = a_3 = 0.1$, $a_6 = 0.06$, $a_7 = 0.2$, $a_8 = 0.03$, M = 1, and N = 4. The parameter a_5 is irrelevant to this geometry. The variables studied in this geometry were the location of the tower, denoted by a_9 and a_{10}, the location of inlet and outlet denoted by a_2 and a_4, and the incoming mass flow rate.

Six tower positions were studied with Geometry 1. To obtain the six positions, the values of a_9 and a_{10} were changed for each position and are summarized in Table 6.1.

Table 6.1: Summary of stack positions for Geometry 1

	Position 1	Position 2	Position 3	Position 4	Position 5	Position 6
a_{10}	0.57	0.335	0.1	0.570	0.335	0.1
a_9	0.4	0.4	0.4	0.1	0.1	0.1

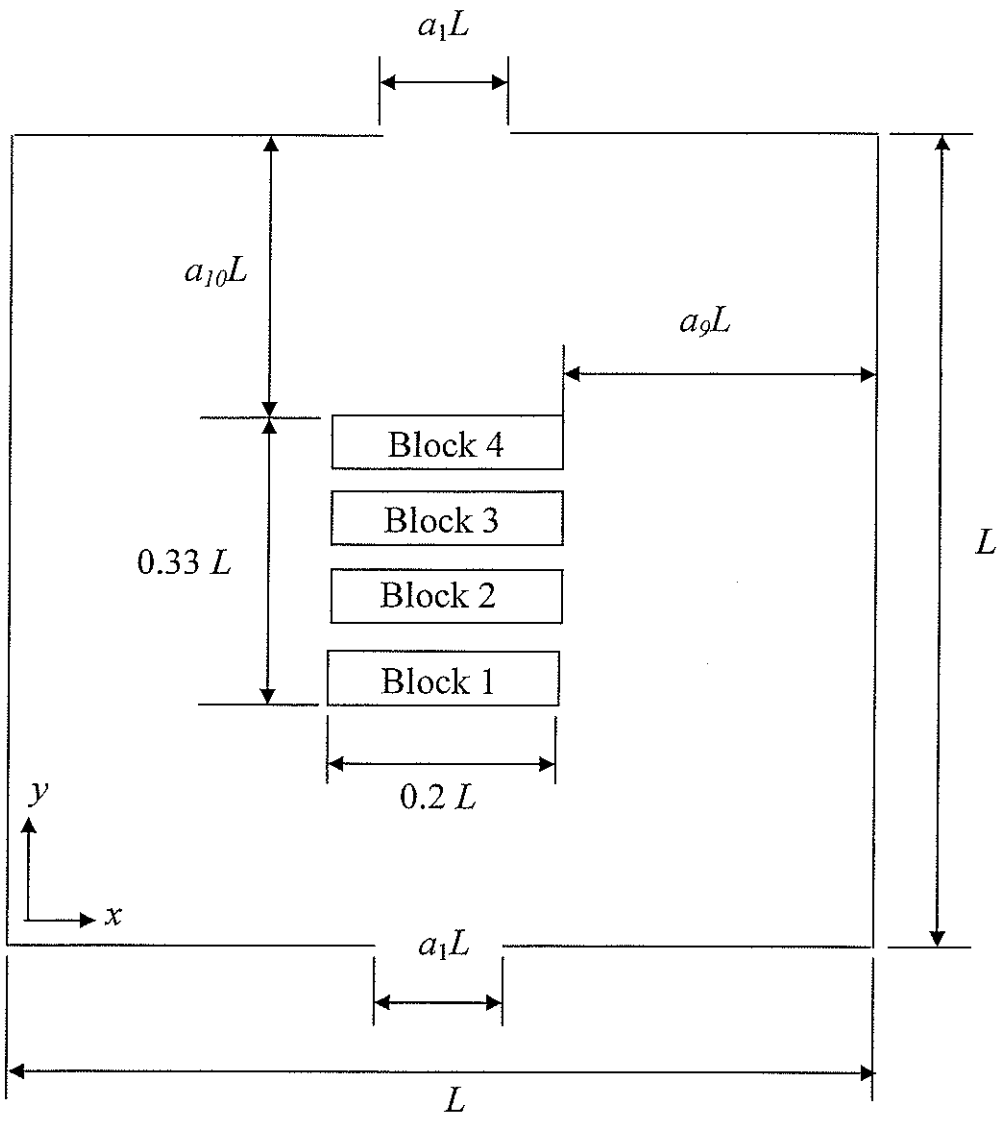

Figure 6.1: Geometry 1

In total, 26 cases were studied for Geometry 1 that will be discussed in subsections. These subsections study various effects. The first is the effect of the location of tower within the domain. The second is the effect of inlet mass flow rate with mixed convection versus natural convection. The third is the effect of the location of inlet and outlet openings. Velocity vector plots, temperature profiles around the blocks and temperature

contour plots are used to discuss the results. The values of the maximum temperature, the average temperature, and the percentage of inlet mass flow rate through all the gaps between blocks are summarized in Table 6.2 for all 26 cases. The column in Table 6.2 titled location indicates the location of the maximum temperature. The first letter signifies upper (U) or lower (L) surface. The second number indicates the block number and the last digits indicate the location along the surface of the block.

Table 6.2: Results from Geometry 1

Case	a_9	a_{10}	Re_o	Inlet	Outlet	θ_{max}	Location	θ_{avg}	% inlet mass flow
1	0.4	0.57	26.12	B - 0.5	T - 0.5	0.598	L4 - 0.5	0.334	0.00
2	0.4	0.57	23.61	L - 0.05	R - 0.95	0.579	L4 - 0.6	0.299	12.87
3	0.4	0.57	100	B - 0.5	T - 0.5	0.691	L4 - 0.5	0.357	0.00
4	0.4	0.57	100	L - 0.05	R - 0.95	0.491	L4 - 0.78	0.177	17.88
5	0.4	0.335	25.63	B - 0.5	T - 0.5	0.595	L4 - 0.5	0.328	0.00
6	0.4	0.335	22.8	L - 0.05	R - 0.95	0.601	L4 - 0.5	0.329	1.95
7	0.4	0.335	45.54	B - 0.5	T - 0.5	2.57	L4 - 0.5	1.367	0.00
8	0.4	0.335	100	B - 0.5	T - 0.5	0.657	L4 - 0.5	0.363	0.00
9	0.4	0.335	100	L - 0.05	R - 0.95	0.771	L4 - 0.47	0.477	0.42
10	0.4	0.335	100	L - 0.475	R - 0.475	0.234	L4 - 0.91	0.104	40.23
11	0.4	0.335	100	L - 0.596	R - 0.596	0.284	U1 - 0.91	0.114	37.94
12	0.4	0.1	16.86	B - 0.5	T - 0.5	0.618	L4 - 0.5	0.327	0.00
13	0.4	0.1	100	B - 0.5	T - 0.5	0.589	L2 - 0.5	0.291	0.00
14	0.1	0.57	24.88	B - 0.5	T - 0.5	0.565	L4 - 0.65	0.291	19.08
15	0.1	0.57	20.72	L - 0.05	R - 0.95	0.585	L4 - 0.6	0.313	15.21
16	0.1	0.57	100	B - 0.5	T - 0.5	0.694	L2 - 0.4	0.424	1.73
17	0.1	0.57	100	L - 0.05	R - 0.05	0.332	U3 - 0.7	0.114	26.34
18	0.1	0.57	100	L - 0.05	R - 0.24	0.22	U3 - 0.8	0.077	40.46
19	0.1	0.57	100	L - 0.05	R - 0.33	0.22	U3 - 0.8	0.08	37.83
20	0.1	0.57	100	L - 0.05	R - 0.95	0.288	L4 - 0.8	0.11	27.12
21	0.1	0.57	100	L - 0.24	R - 0.24	0.129	L4 - 0.8	0.057	56.55
22	0.1	0.57	100	L - 0.33	R - 0.33	0.187	L2 - 0.85	0.068	47.94
23	0.1	0.335	22.05	B - 0.5	T - 0.5	0.591	L4 - 0.55	0.316	8.28
24	0.1	0.335	100	B - 0.5	T - 0.5	0.551	L4 - 0.85	0.262	11.75
25	0.1	0.1	17.92	B - 0.5	T - 0.5	0.66	L4 - 0.5	0.371	3.71
26	0.1	0.1	100	B - 0.5	T - 0.5	0.73	L4 - 0.8	0.372	7.56

The left side of the block is indicated by 0 and the right side of the block is indicated by 1. Thus, U3 – 0.8 would indicate that the maximum temperature is on the upper surface of block 3 and the maximum temperature occurs at a location 80.0% along the upper surface of block 3 from left to right.

6.2.1 Effect of the Tower Location Within the Domain

Results were obtained for six different stack positions with mixed convection (Re_o =100), inlet port at B-0.5 and outlet port T-0.5. Location B-0.5 means the inlet is at the bottom wall of the cavity with a_2=0.5 and T-0.5 means that the outlet is at the top of the cavity with a_4=0.5. The maximum temperature in the stack and the spatial average temperature of the stack for the 6 different cases are shown in Table 6.3.

Table 6.3: Maximum and average temperatures corresponding to different stack positions

	Position 1	Position 2	Position 3	Position 4	Position 5	Position 6
θ_{max}	0.691	0.657	0.589	0.694	0.551	0.730
θ_{avg}	0.357	0.363	0.291	0.424	0.262	0.372

From Table 6.3, position 4 corresponds to the highest average temperature level in the stack (θ_{avg} = 0.424) while position 5 corresponds to the lowest average temperature level in the stack (θ_{avg} = 0.262).

The velocity vector plot for stack position 4, Figure 6.2, shows that most of the inlet flow bypasses to the left of the stack and exits at the top of the cavity with two counter-rotating zones created in the upper part of the cavity. There is a counter clockwise rotation to the left of the direct flow and a clockwise rotation to the right of the direct flow. The total mass flow rate flowing through the three channels separating the four blocks in the stack was calculated and found to be only 1.73% of the total inlet mass flow rate.

Figure 6.3 shows the temperature profile around the four blocks. The bottom surface of block 1 and the top surface of block 4 have the lowest temperature in the stack. All remaining six horizontal surfaces have significantly elevated temperatures, as shown in Figure 6.3. The average temperature in the stack is $\theta_{avg} = 0.424$ and the maximum is $\theta_{max} = 0.694$, which occurs on the bottom surface of block 2.

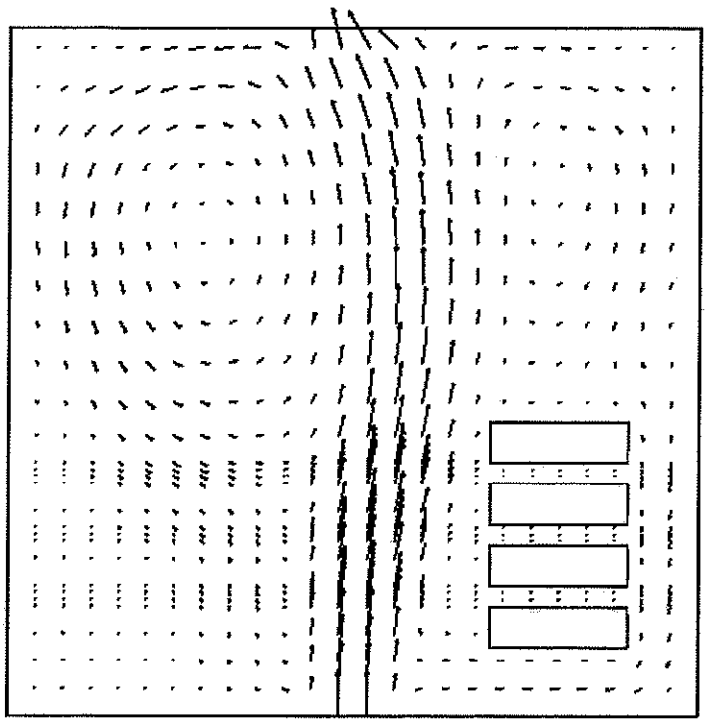

Figure 6.2: Velocity vectors for case 16, position 4 with inlet B-0.5, outlet T-0.5, and $Re_o = 100$

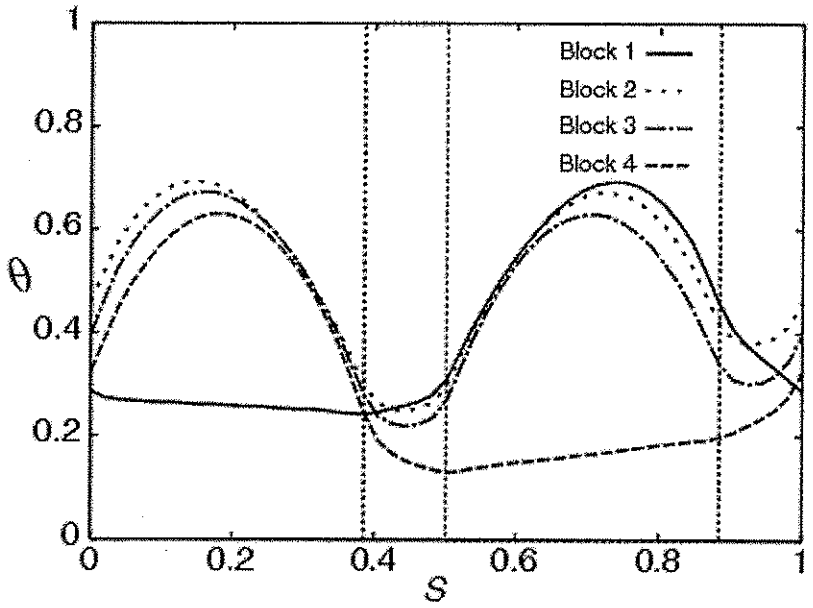

Figure 6.3: Temperature distribution in the stack for case 16, position 4 with inlet B-0.5, outlet T-0.5, and $Re_o = 100$

For stack position 5, the velocity vector plot, Figure 6.4, demonstrates a flow structure with three major re-circulation zones. One at the bottom right side of the inlet jet rotating clockwise, another above the tower rotating clockwise and the last on the top left side of the domain rotating counter-clockwise. There is more interaction between the air and the stack compared to what was seen earlier in Figure 6.2. The total mass flow rate flowing through the three channels between the blocks was 11.75% of the inlet mass flow rate (compared to 1.73% for position 4). The change in the flow structure and the increased flow near and through the stack has a significant impact on the magnitude and trend of the temperature variation on the stack; this can be seen from the comparison between Figures 6.3 and 6.5. The average temperature dropped notably to $\theta_{avg} = 0.262$ and the maximum to $\theta_{max} = 0.551$.

6.2.2 Passive Versus Mixed Convection Cooling

Increased flow rates result in higher velocities, higher heat transfer coefficients and consequently, improved cooling characteristics in most applications. This trend was investigated with the cases with four blocks. It was found that when comparing results of passive and mixed-convection cooling for the same stack position and the same inlet and outlet position, the increased flow rate improved the heat transfer which led to lower temperatures. However, the heat transfer deteriorated in other cases such as the comparison shown below related to Figures 6.6 and 6.7.

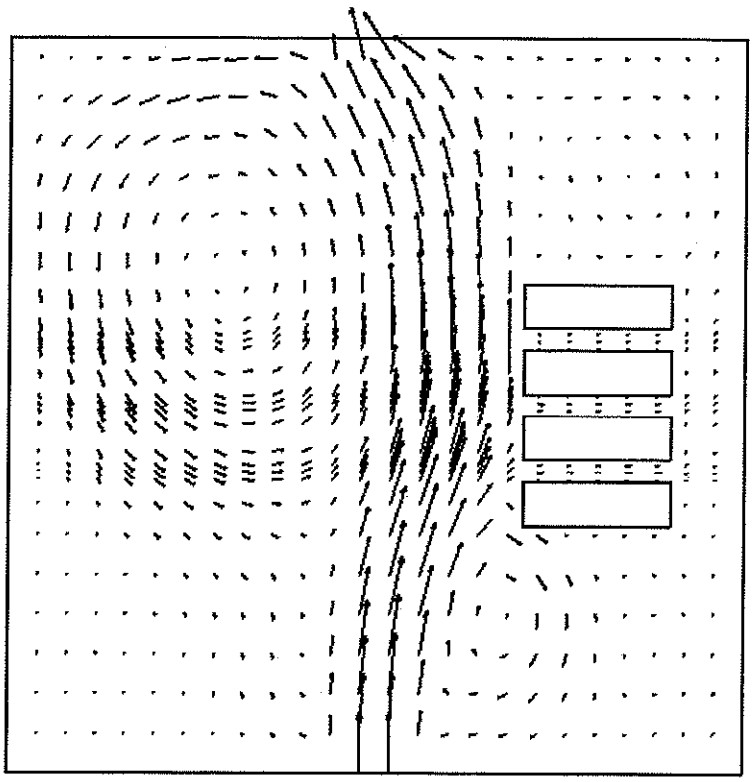

Figure 6.4: Velocity vectors for case 24,
position 5 with inlet B-0.5,
outlet T-0.5, and $Re_o = 100$

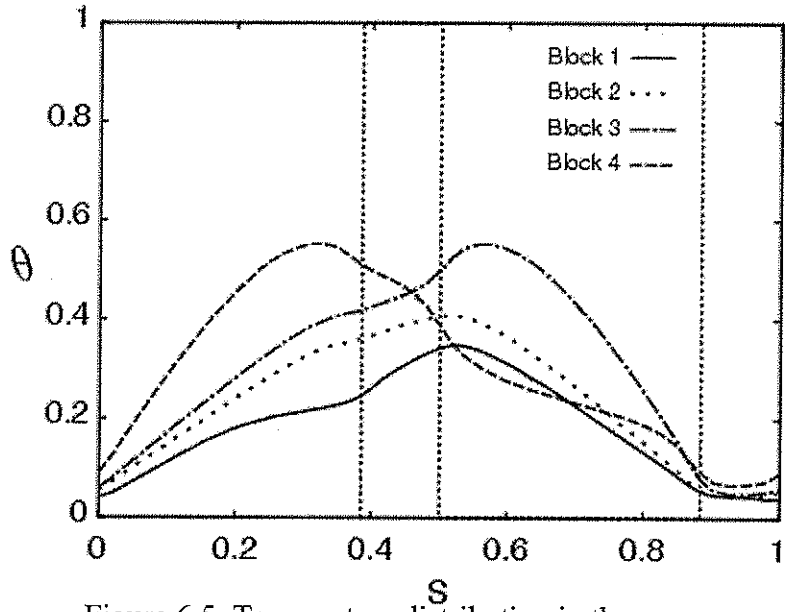

Figure 6.5: Temperature distribution in the stack for case 24, position 5 with inlet B-0.5, outlet T-0.5, and $Re_o = 100$

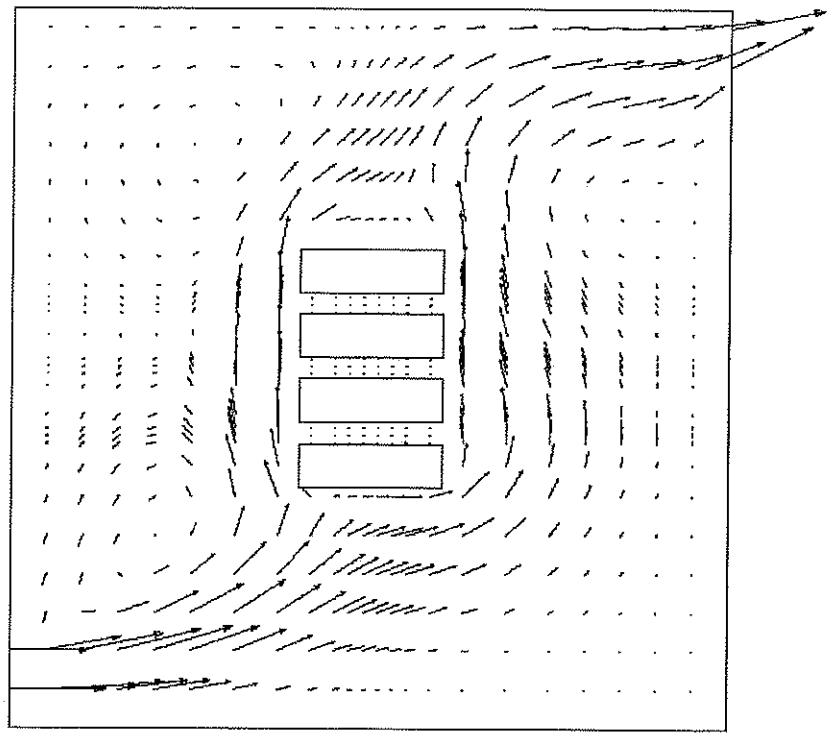

Figure 6.6: Passive cooling for case 6, $Re_o = 22.8$, position 2, inlet L-0.05, and outlet R-0.95

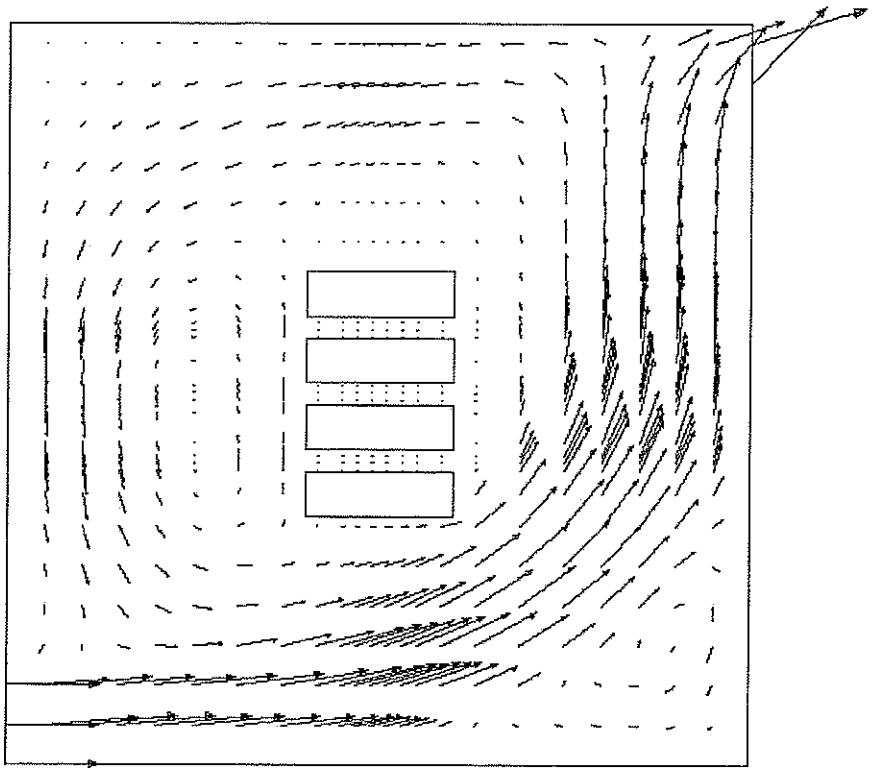

Figure 6.7: Case 9, mixed convection cooling
(Re_o = 100), position 2,
inlet L – 0.05, and outlet R – 0.95

The above velocity vector plots are for passive cooling (Figure 6.6) and mixed-convection cooling (Figure 6.7). For passive cooling there is significant air motion near and through the channels within the stack, while the incoming air in Figure 6.7 bypasses the stack, resulting in reduced velocities near and through the stack. The average stack temperature for passive and mixed-convection cooling were θ_{avg} = 0.330 and 0.479, respectively, and the maximum temperature for passive and mixed-convection cooling were θ_{max} = 0.604 and 0.775, respectively. The results demonstrate that a higher velocity does not necessarily provide higher cooling rates. In this case passive cooling provided a lower maximum temperature.

6.2.3 Effect of the Location of Inlet and Outlet Ports

An additional independent parameter is the location of the inlet and outlet ports. There is a significant importance of this parameter and this is demonstrated by comparing the cooling effectiveness in three cases corresponding to the same tower position (position 4), same inlet mass flow rate (Re_o = 100), but three different locations of the inlet and outlet ports. The velocity vectors are presented in Figures 6.2 (inlet B – 0.5, outlet T – 0.5), 6.8 (inlet L – 0.05, outlet R – 0.05) and 6.9 (inlet L – 0.24, outlet R – 0.24).

Visual examination of the velocity vectors leads to the conclusion that the minimum air movement through the stacks corresponds to Figure 6.2, while Figure 6.9 corresponds to the maximum air motion through the stacks. The total flow rate of air in the three channels within the stacks amounts to 1.73% of the total inlet flow rate in Figure 6.2, this percentage increases to 26.34% in Figure 6.8 and 56.56% in Figure 6.9.

The temperature level in the stack was found to decrease with the increase in air movement though the stack. The average stack temperatures were: θ_{avg} = 0.424 in Figure 6.2, θ_{avg} = 0.114 in Figure 6.8, and θ_{avg} = 0.0562 and Figure 6.9. The maximum stack temperatures were: θ_{max} = 0.694 in Figure 6.2, θ_{max} = 0.332 in Figure 6.8, and θ_{max} = 0.129 and Figure 6.9. Figures 6.10 and Figure 6.11 show the temperature distributions for the case of inlet L – 0.05, outlet R – 0.05 and inlet L – 0.24, outlet R – 0.24 respectively.

A large reduction in the temperature levels is observed when comparing Figure 6.11 to Figure 6.10. The importance of the location of the inlet and outlet ports is demonstrated as the same amount of mass flow rate can significantly reduce the average and maximum temperatures when the mass flow is introduced into the domain at different locations.

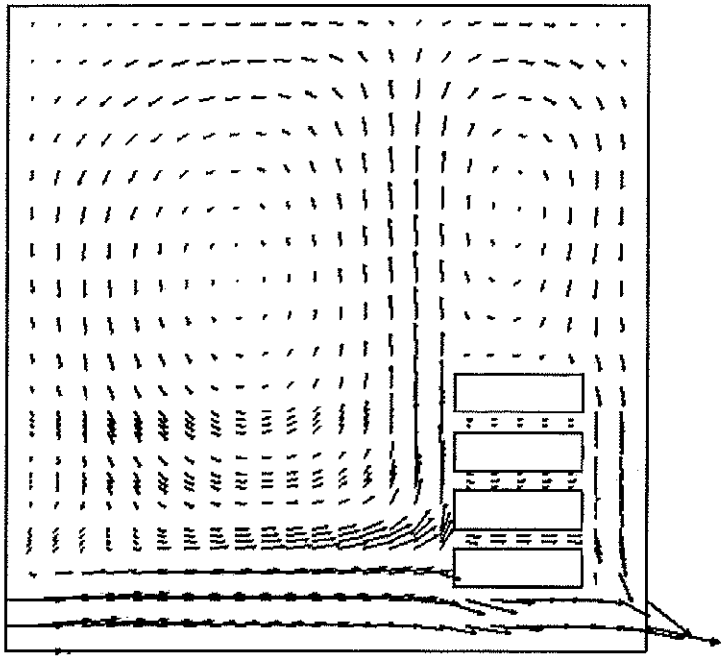

Figure 6.8: Case 17, mixed convection cooling (Re_o = 100), stack position 4, inlet L – 0.05, and outlet R – 0.05

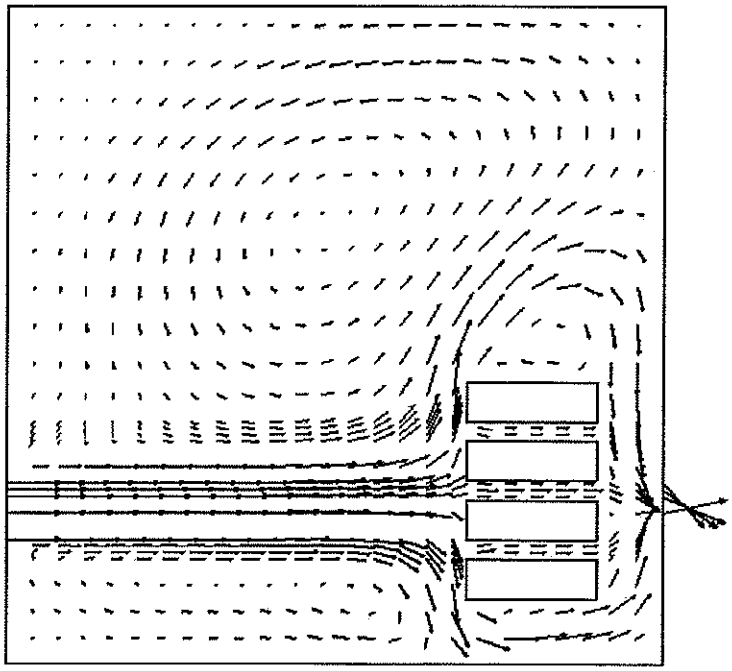

Figure 6.9: Case 21, mixed convection cooling (Re_o = 100), stack position 4, inlet L – 0.24, and outlet R – 0.24

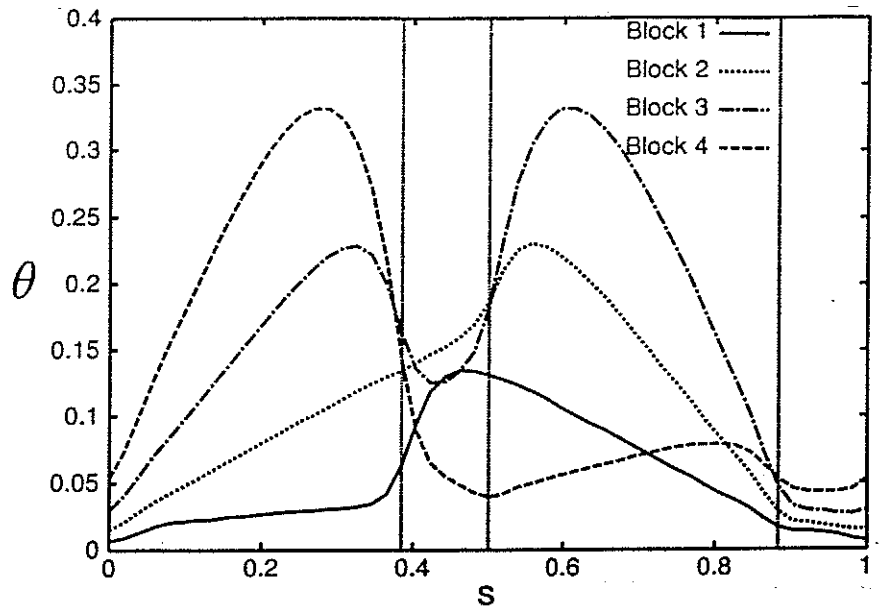

Figure 6.10: Temperature distribution in the stack for case 17, position 4, inlet L-0.05, Outlet R-0.05, and $Re_o = 100$

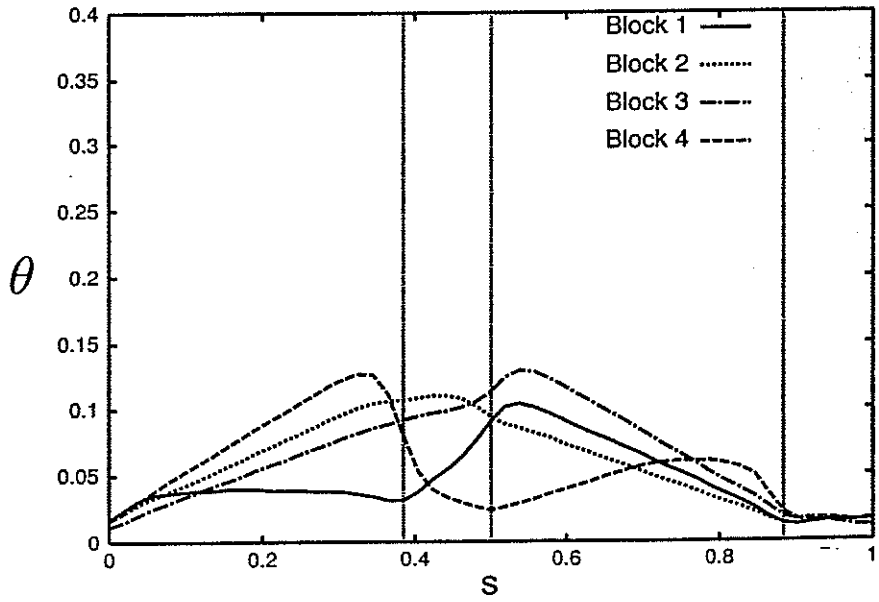

Figure 6.11: Temperature distribution on the stack for case 21, position 4, inlet L – 0.24, Outlet R – 0.24, and $Re_o = 100$

6.3 Geometry 2

A schematic diagram for Geometry 2 is shown in Figure 6.12. Referring to Figure 3.1, Geometry 2 corresponds to $a_1 = a_3 = 0.1$, $a_6 = 0.06$, $a_7 = 0.2$, and $a_8 = 0.03$, $a_{10} = 0.11$, M=1, and N=9. The parameter a_5 is irrelevant in this geometry. Two horizontal tower positions were studied, centred ($a_9 = 0.4$) and offset ($a_{10} = 0.1$). Three different inlet conditions were also studied: natural convection and two cases of mixed-convection with Reynolds number of $Re_o = 100$ and $Re_o = 225$. Geometry 2 has 2.25 times more energy flowing into the domain relative to Geometry 1 (Gr = 2.25E+6). The decision was taken to also study cases of increased inlet mass flow rate by the same amount. Furthermore, different inlet and outlet port locations were studied; the results of maximum temperature are listed in Table 6.4. Later on Case 20 ($a_9 = 0.7$, $Re_o = 100$) was added to study the effect of moving the tower to the left hand side of the domain.

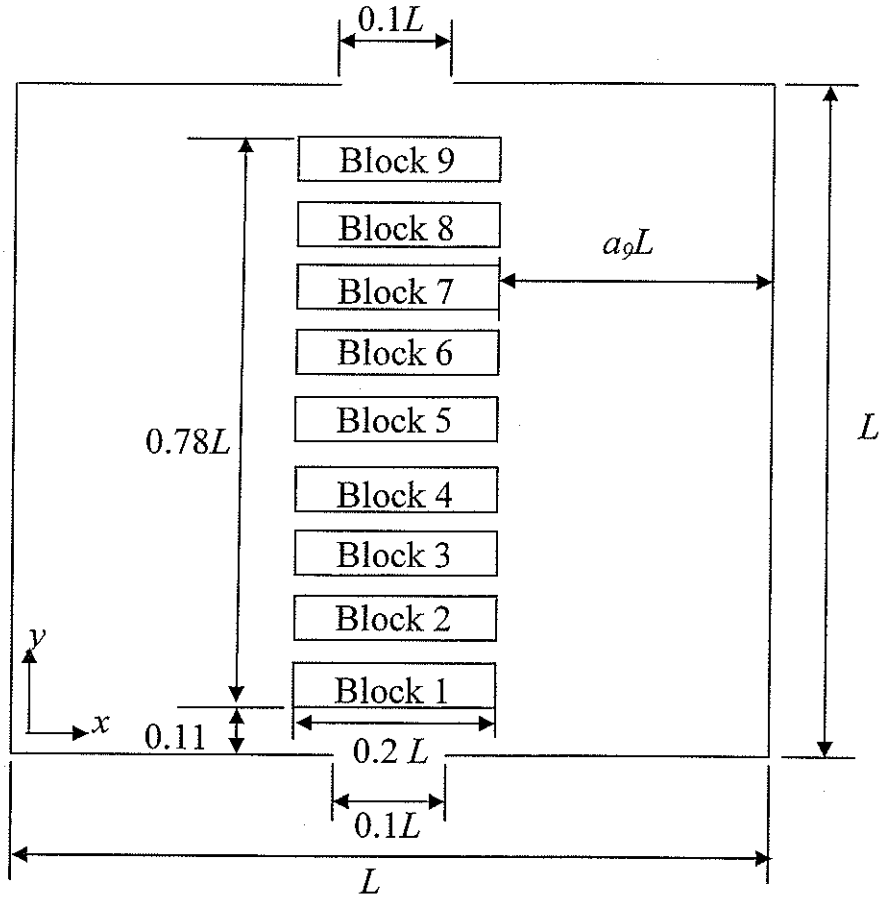

Figure 6.12: Geometry 2

Table 6.4: Results from Geometry 2

case	a_9	Re_o	Inlet	Outlet	θ_{max}	Location	θ_{avg}	% inlet mass flow
1	0.4	26.74	B – 0.5	T – 0.5	0.727	L9 – 0.500	0.466	0.00
2	0.4	25.84	L – 0.05	R – 0.95	0.736	L9 – 0.645	0.441	11.62
3	0.4	100	B – 0.5	T – 0.5	0.915	L6 – 0.500	0.569	0.00
4	0.4	100	L – 0.05	R – 0.95	0.609	L9 – 0.813	0.270	10.19
5	0.4	100	L – 0.5	R – 0.5	0.482	U8 – 0.833	0.161	21.51
6	0.4	225	B – 0.5	T – 0.5	0.775	L5 – 0.500	0.412	0.00
7	0.4	225	L – 0.05	R – 0.95	0.655	L9 – 0.500	0.245	7.20
8	0.1	28.82	B – 0.5	T – 0.5	0.794	L9 – 0.517	0.425	7.58
9	0.1	12.78	L – 0.05	R – 0.5	1.854	L9 – 0.683	0.985	42.36
10	0.1	20.85	L – 0.05	R – 0.95	0.709	L9 – 0.633	0.420	16.67
11	0.1	100	B – 0.5	T – 0.5	0.819	L9 – 0.617	0.416	4.61
12	0.1	100	L – 0.05	R – 0.05	1.577	L9 – 0.700	0.651	14.78
13	0.1	100	L – 0.5	R – 0.5	0.284	U8 – 0.783	0.103	31.36
14	0.1	100	L – 0.05	R – 0.5	0.281	U8 – 0.800	0.116	24.30
15	0.1	100	L – 0.05	R – 0.95	0.365	L6 – 0.750	0.172	14.73
16	0.1	225	B – 0.5	T – 0.5	0.735	U2 – 0.250	0.540	-1.20
17	0.1	225	L – 0.05	R – 0.95	0.212	L6 – 0.800	0.093	20.58
18	0.1	225	L – 0.05	R – 0.5	0.140	U7 – 0.917	0.057	28.86
19	0.1	225	L – 0.5	R – 0.5	0.212	U8 – 0.850	0.063	39.47
20	0.7	100	L – 0.5	R – 0.5	0.373	L3 – 0.833	0.164	21.80

6.3.1 Effect of the Tower Location Within the Domain

From the results obtained in Table 6.4 the following observations can be made regarding the effect of the tower location within the domain with the same inlet and outlet locations. When the inlet and outlet locations are at B – 0.5 and T – 0.5 and for the two possible tower locations [centred (a_9 = 0.4) and offset (a_9 = 0.1)], there is a small difference between the maximum temperature values. For mixed convection at Re_o = 100, the two cases compared were case 3 (a_9 = 0.4) and case 11 (a_9 = 0.1). For case 3, the maximum temperature was 0.914 where the maximum temperature for case 11 was 0.819. The velocity vector plots for case 3 and case 11 are shown in Figures 6.13 and 6.14, respectively.

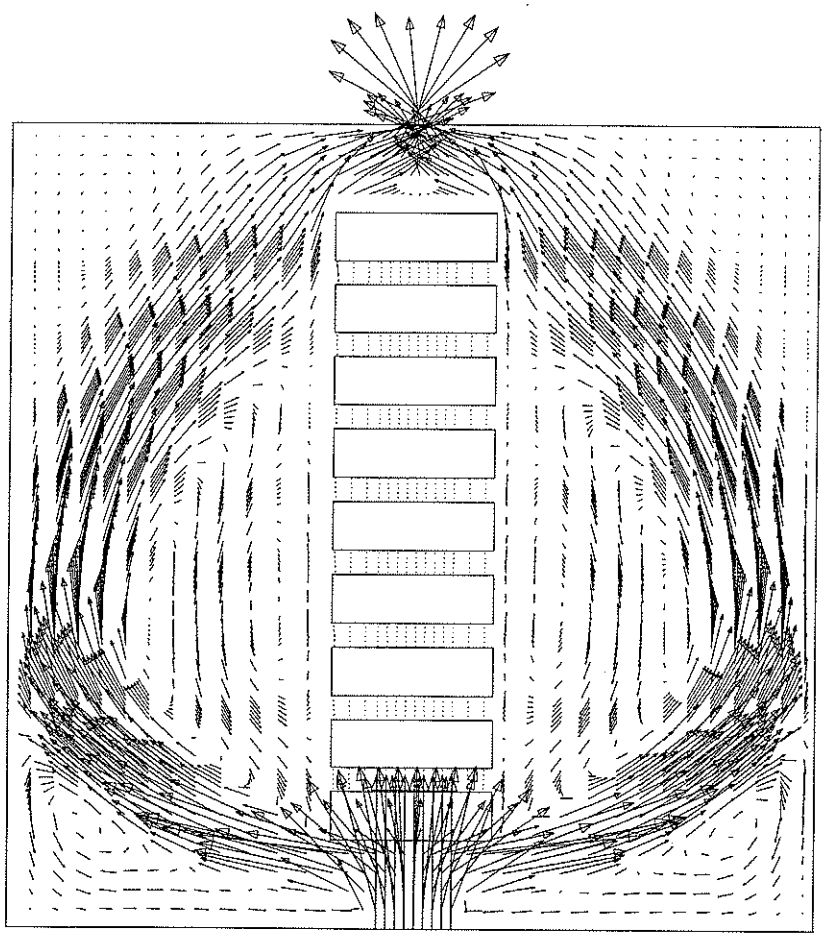

Figure 6.13: Case 3, mixed convection cooling (Re_o = 100), a_9 = 0.4, inlet B – 0. 5, and outlet T – 0. 5

From Figure 6.13, the incoming air is diverted around the tower once impacting the lower face of block 1 and it rejoins to exit the domain, also note that the flow is symmetric about $X = 0.5$. There are numerous recirculation zones within the domain. There are two small clockwise recirculation zones in the upper and lower corners on the right hand side of the domain. The opposite is seen in the left hand side of the domain, two counter-clockwise recirculation zones appear in the two corners. The flow directly beside the tower on both sides of the domain is very complex and includes many recirculation zones. Due to symmetry, the percentage of inlet flow between the blocks is 0 %.

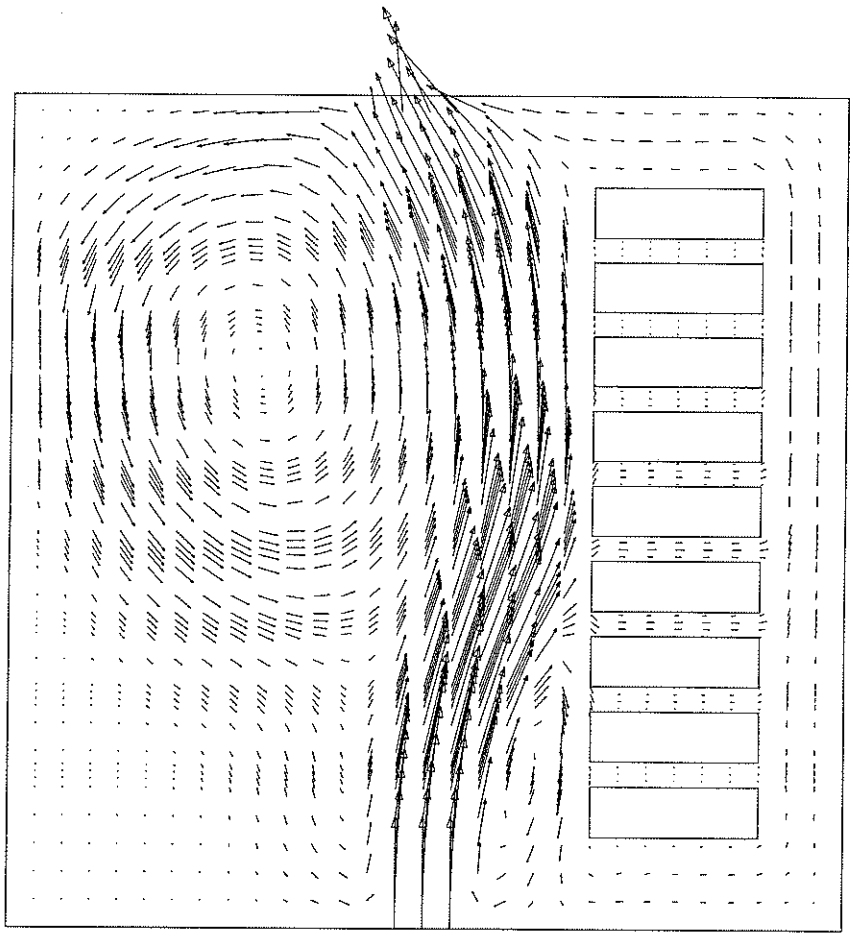

Figure 6.14: Case 11, mixed convection cooling ($Re_o = 100$), $a_9 = 0.1$, inlet B – 0. 5, and outlet T – 0. 5

Figure 6.14 shows more interaction between the flow and the tower. There is a large counterclockwise recirculation zone in the upper left hand side of the domain. The percent of inlet mass flow between the blocks is 4.61%, and there is a small clockwise recirculation zone between the inlet jet and block one.

Temperature contours or temperature isotherms are lines of constant temperatures in the domain. The closer the temperature isotherms are to each other the faster the temperature change in the domain. Figures 6.15 and 6.16 show the temperature contours of cases 3 and 11. All temperature contour plots presented have 20 contours, the value of θ for the contour is shown in the scale labeled "theta" on the right hand side of the plot. The domain is the square inside the larger rectangle and the blocks are visible in all the temperature contour plots. Every second temperature contour is labeled in the plot and the number is visible in the domain. Examining Figure 6.15, it can be seen that the temperature contours are symmetric about $X = 0.5$ and the maximum temperature occurs by contour # 19 in the fifth channel. We can clearly see the "bubble" of warm air that is enclosed by contour # 2. The temperature contours for case 11, shown in Figure 6.16 are very different from those in Figure 6.15 over the majority of the domain. On the left of contour # 2 is at a very low θ value of 4.31E-02. The immediate area around the blocks is where the temperature increases most rapidly. The maximum temperature occurs in channel 8 and is demonstrated by the area enclosed by contour # 19. Recalling that the percentage of inlet mass flow rate for case 11 is 4.61%, θ drops accordingly from 0.915 for case 3 to 0.819 for case 11.

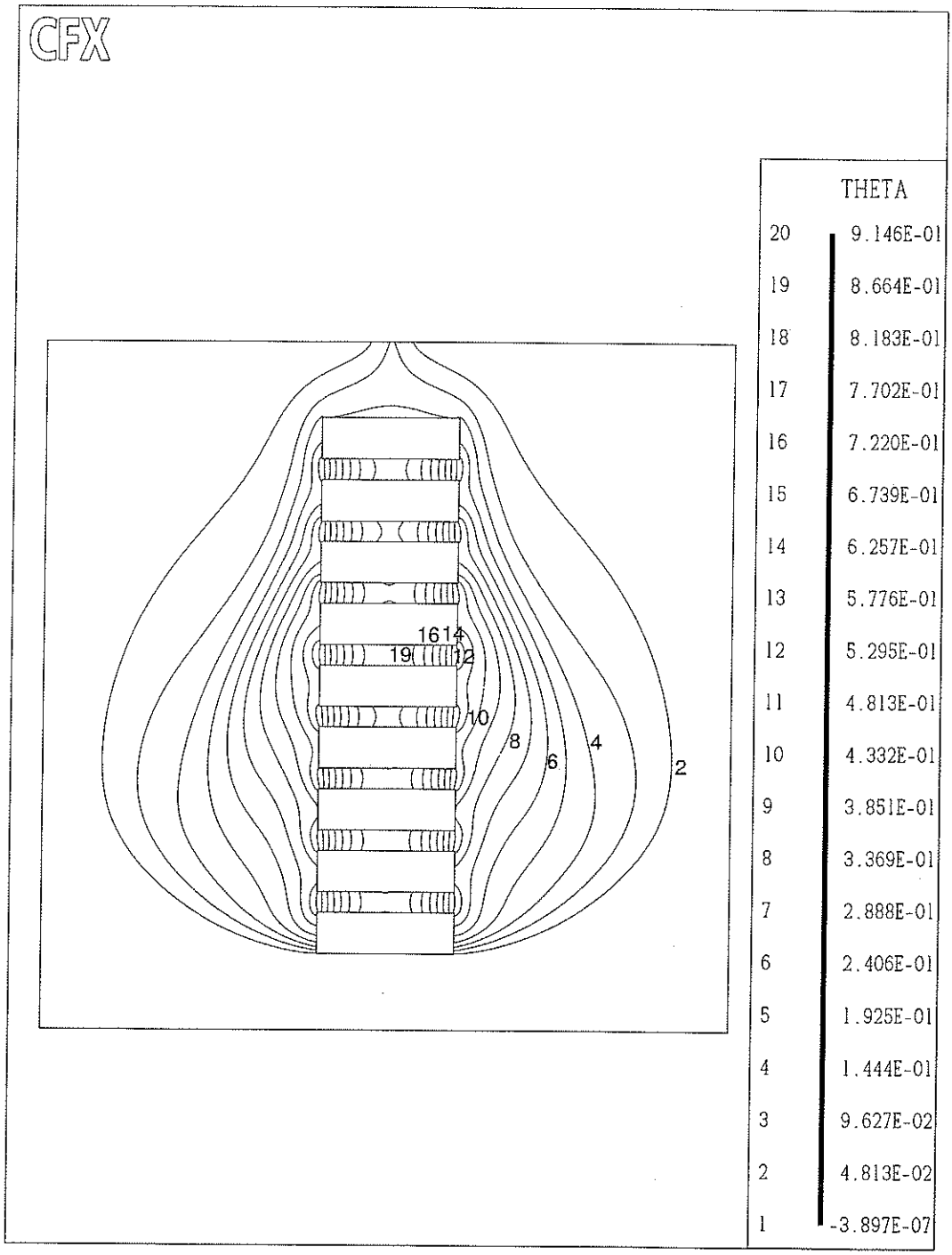

Figure 6.15: Temperature contours for case 3, mixed convection ($Re_o = 100$), inlet B-0.5, and outlet T-0.5

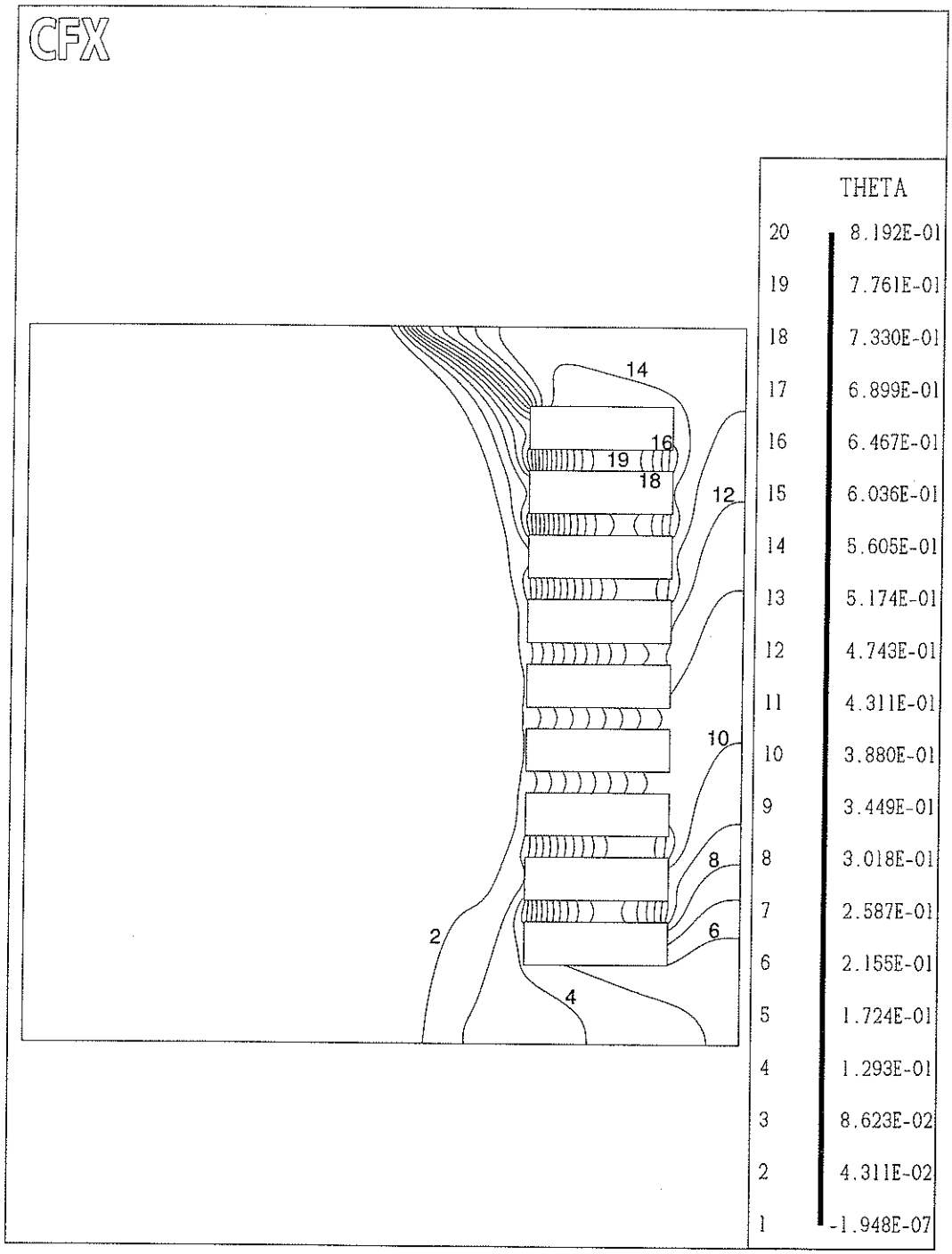

Figure 6.16: Temperature contour for case 11, mixed convection (Re_o=100), inlet B-0.5, and outlet T-0.5

The results were compared for mixed convection at $Re_o = 225$, where case 6 ($a_9 = 0.4$) had a maximum temperature of 0.775 and case 16 ($a_9 = 0.1$) had a maximum temperature of 0.735. The velocity vectors for cases 6 and 16 are shown in Figures 6.17 and 6.18, respectively.

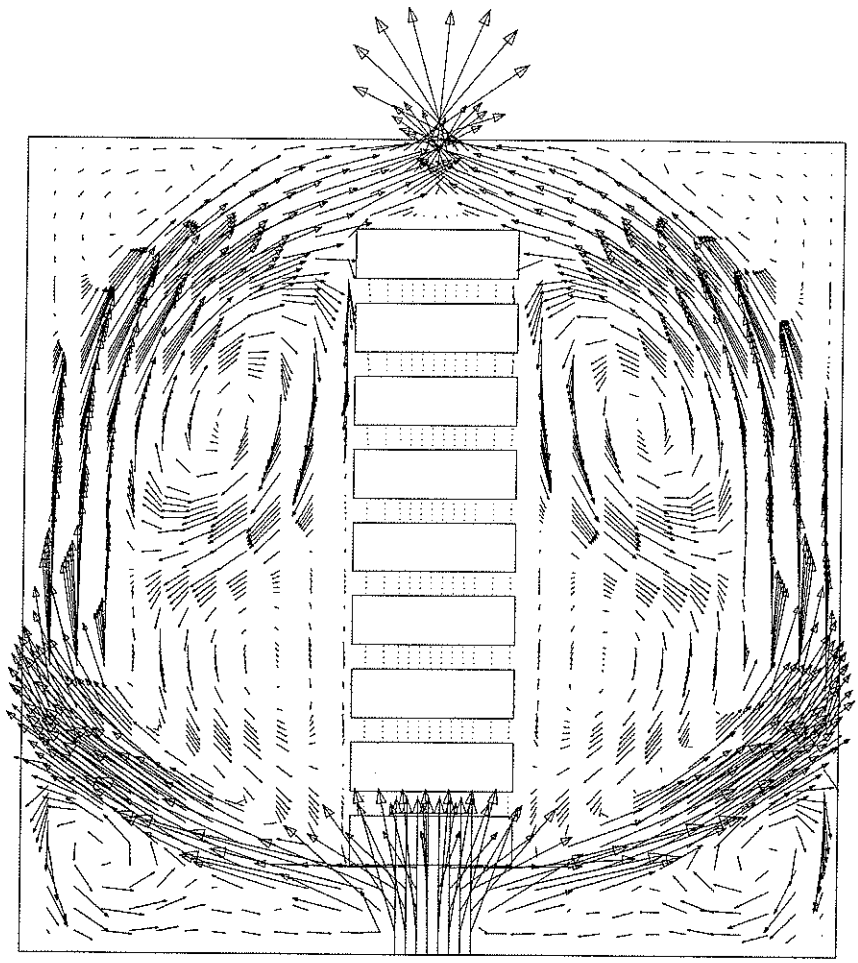

Figure 6.17: Case 6, mixed convection cooling ($Re_o = 225$) for $a_9 = 0.4$, inlet B-0.5 and outlet T-0.5

From Figure 6.17 it is seen that the flow is very complex and still symmetric about $X = 0.5$. The incoming air impacts the lower surface of block 1 and travels up the side walls. There are two pronounced recirculation zones on both sides of the upper part of the tower and smaller recirculation near the bottom of the tower. There are also recirculation zones in each corner of the domain. The percentage of the inlet mass flow rate through the gaps

between the blocks is 0%. In the case of an offset tower, shown in Figure 6.18, we see that the air flows more directly from the inlet and the outlet. There is a large recirculation zone in the upper left hand side of the domain. The flow in the region between the right hand side of the tower and the right side is different from what might have been expected. In this region, the air flows downward so that there is an overall clockwise circulation of flow around the tower. Air does flow through the channels formed by the blocks, the percentage of the inlet mass flow rate through the channels is -1.20%, the negative means the air flows from right to left through the channels.

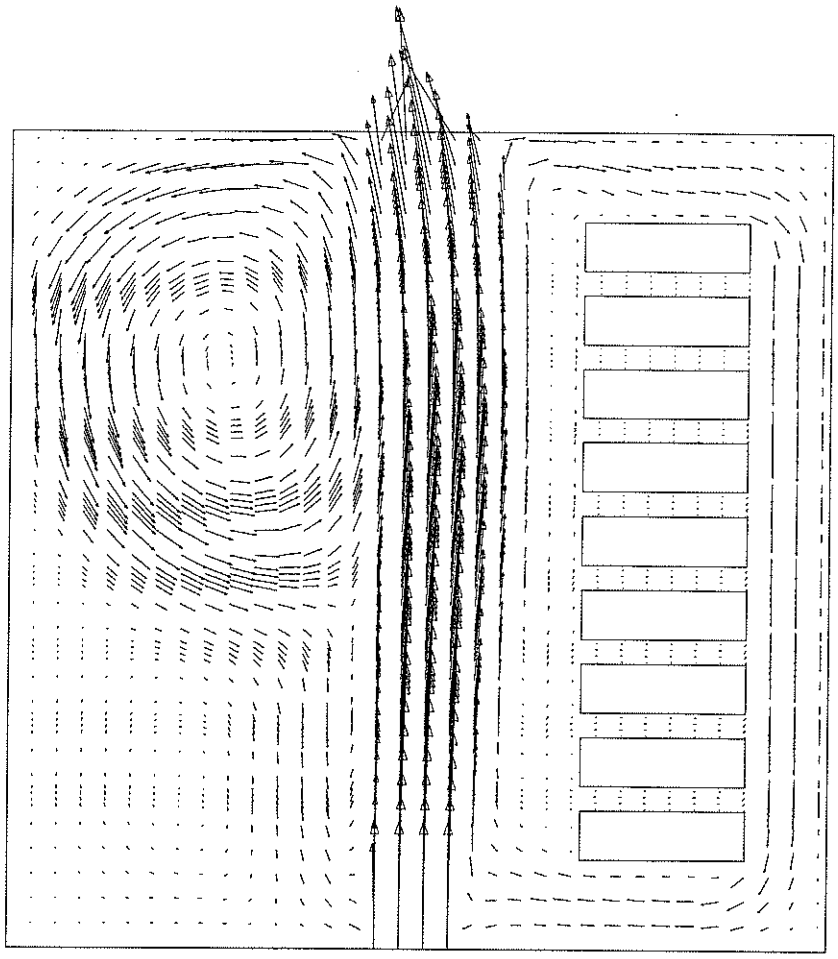

Figure 6.18: Case 16, mixed convection cooling ($Re_o = 225$) for $a_9 = 0.1$, inlet B-0.5 and outlet T-0.5

The temperature contours of the cases 6 and 16 are presented in Figures 6.19 and 6.20, respectively. Figure 6.19 again demonstrates that the incoming air once impacting the lower block flows around the domain forming a "bubble" around the tower. Because the flow is at a higher velocity the larger recirculation zones near the top of the tower pull more cool air and hence the top of the tower is at a lower temperature. The maximum temperature for case 6 is $\theta_{max} = 0.775$, and it occurs in the fourth channel formed by the blocks. Figure 6.20 is very different from Figure 6.16. The incoming air at a higher velocity creates a curtain of cold air demonstrated by contour #2, the temperature then increases in the tower region and the mode of heating is similar to conduction of heat through the air. The maximum temperature for case 16 is $\theta_{max} = 0.735$ and it occurs in the second channel. What is interesting to note from Table 6.4 is that although the maximum temperature is slightly lower for case 16 compared to case 6, the average temperature in the stack is higher in case 16 ($\theta_{avg} = 0.539$) when compared to case 6 ($\theta_{avg} = 0.412$).

The effect of the tower position was compared for the case of inlet L – 0.05 and outlet R – 0.95. The two mixed-convection inlet Reynolds numbers (Re_o = 100, 225) were investigated. When comparing case 4 ($a_9 = 0.4$) to case 15 ($a_9 = 0.1$), with $Re_o = 100$, inlet L – 0.05 and outlet R – 0.95, the maximum temperature of case 4 was $\theta_{max} = 0.609$ and the maximum temperature for case 15 dropped to $\theta_{max} = 0.365$. The velocity vector plots and the temperature contours will help explain why the temperature drops by moving the tower from the centered ($a_9 = 0.4$) position to the offset position ($a_9 = 0.1$). The velocity vector plot for case 4 is shown in Figure 6.21 and case 15 in Figure 6.22.

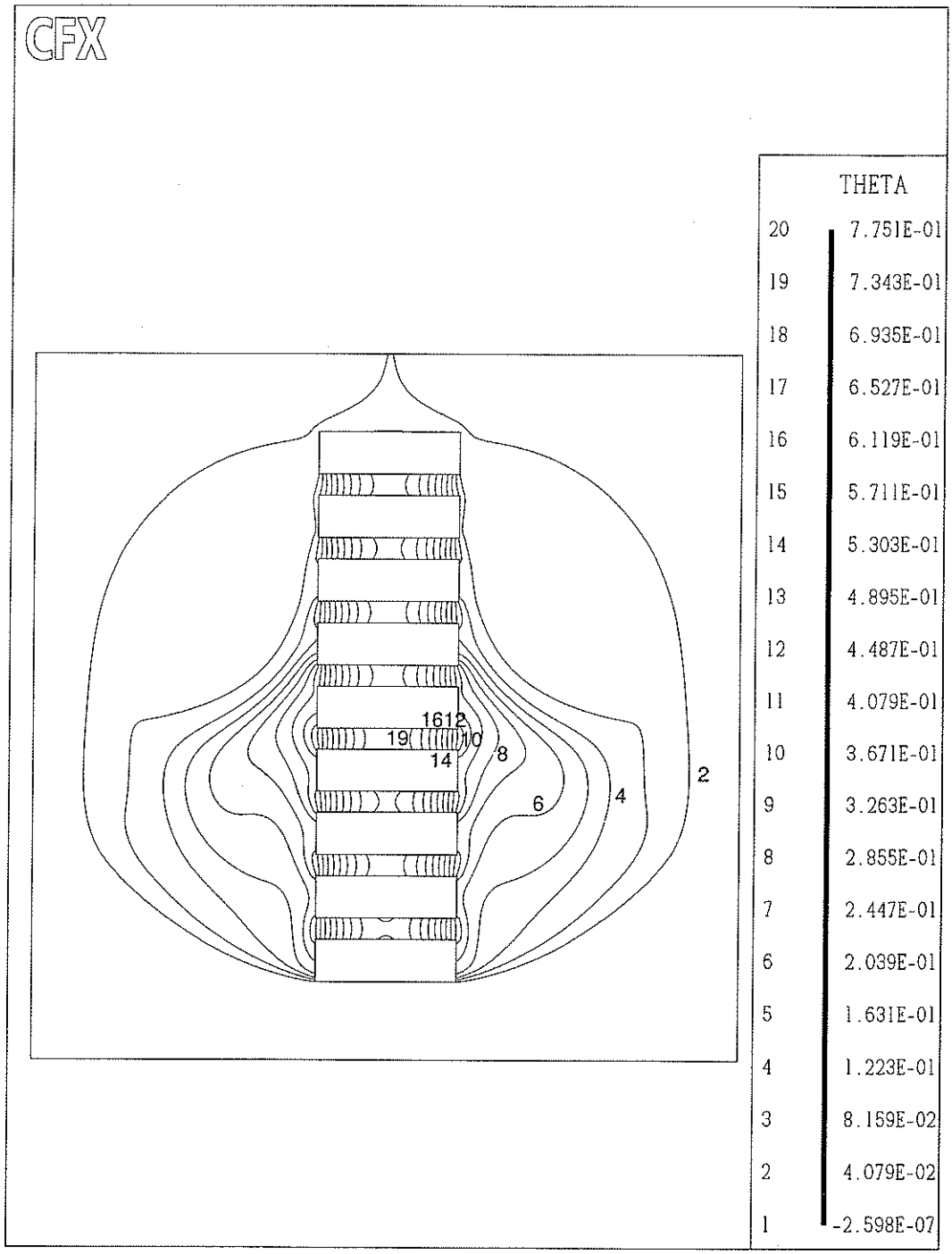

Figure 6.19: Temperature contours for case 6, mixed convection ($Re_o = 225$), inlet B-0.5 and outlet T – 0.5

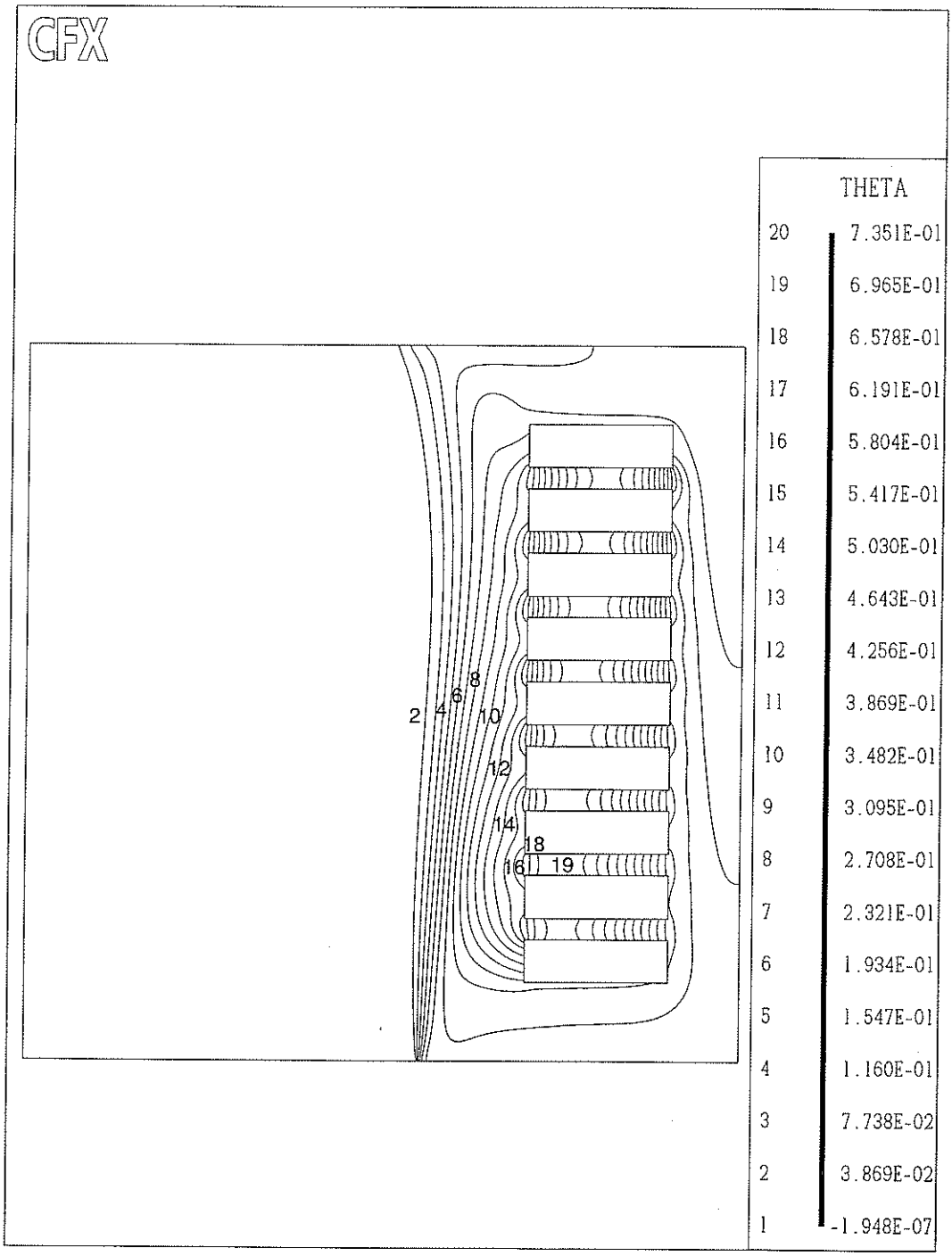

Figure 6.20: Temperature contours for case 16, mixed convection ($Re_o = 225$), inlet B – 0.5 and outlet T -0.5

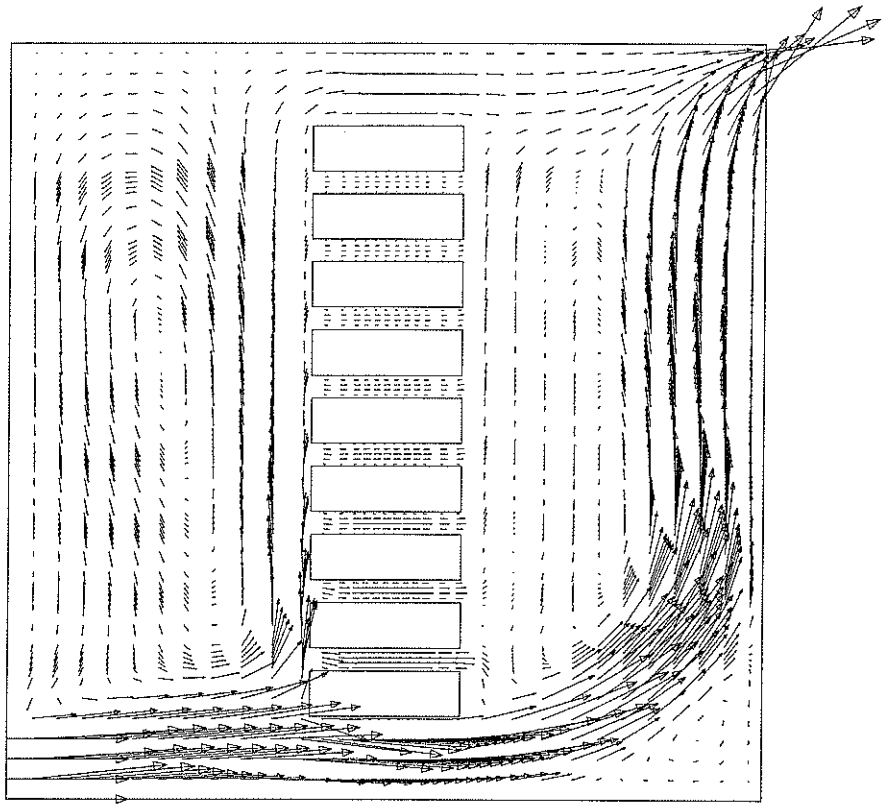

Figure 6.21: Case 4, mixed convection cooling ($Re_o = 100$) for $a_9 = 0.4$, inlet L – 0.05 and outlet R – 0.95

The majority of the incoming air of case 4 (Figure 6.21) flows underneath the tower. The flow through the channels decreases as we go up the tower. There is one large recirculation zone to the left of the tower. There is another small recirculation zone in the bottom right corner of the domain. There are numerous small recirculation zones to the right of the tower. The percentage of inlet mass flow rate that flows through the tower is 10.19%.

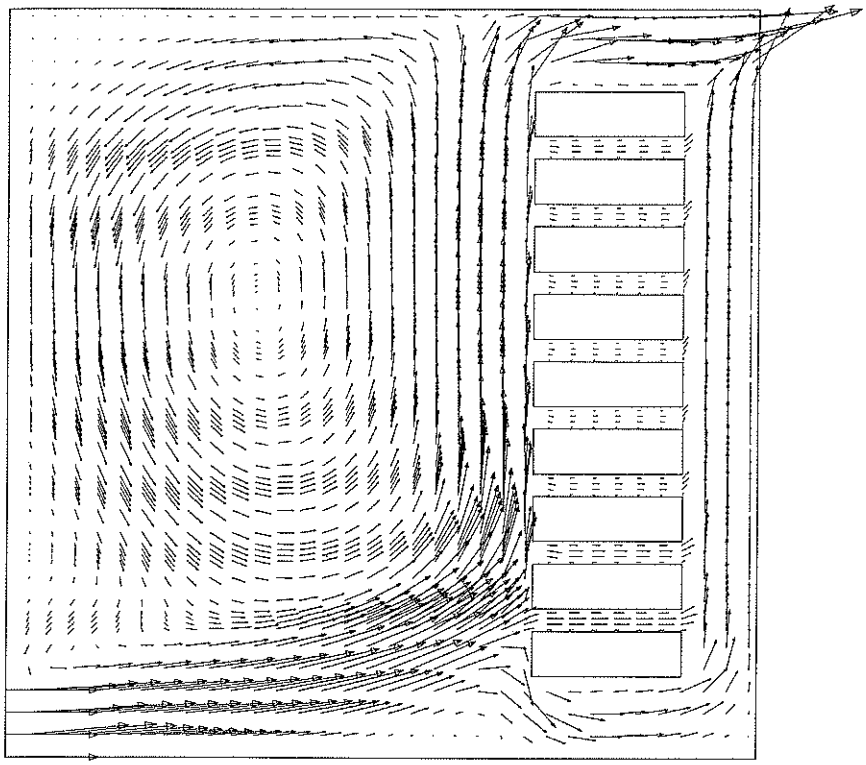

Figure 6.22: Case 15, mixed convection cooling ($Re_o = 100$) for $a_9 = 0.1$, inlet L-0.05 and outlet R-0.95

Figure 6.22 demonstrates a significant increase in the interaction between the air and the tower. There is a large counter-clockwise recirculation on the left hand side of the tower. The flow travels upwards on both sides of the tower. The vectors in the channels indicate that there is more flow traveling through the channels compared to the centered tower case. The total percentage of the inlet mass flow rate through the towers increased from 10.19% in case 4 to 14.73% in case 15. Figure 6.23 is a graph of the percentage of the incoming air going through the channels for cases 4 and 15. From Figure 6.23, it can be seen that for case 4 (hashed bars) the percentage of inlet mass flow rate decreases from a maximum of about 3.3% in the bottom channel as we move up the tower; leading to the maximum temperature in the top channel. For case 15 (black bars), the percentage of inlet mass flow rate decreases from channel one (3.6%) to channel four (1.01%) and increases again from 1.01% to 1.89% as we move up the tower. This leads to the

maximum temperature in channel 5. The flow rate through all channels is higher for case 15 than for case 4, except for channel 4.

The significant increase in the total flow rate through the channels in case 15 compared to case 4 resulted in a significant drop in θ_{max}. Figures 6.24 and 6.25 are the temperature contours for cases 4 and 15, respectively. Figure 6.24 shows that the left hand side of the domain is at a low temperature and the maximum temperature occurs in the highest channel in the tower ($\theta_{max} = 0.609$). In Figure 6.25, the greater part of the domain is at a low temperature as seen by contour #2 enclosing the tower. The maximum temperature occurs in the fifth channel ($\theta_{max} = 0.365$).

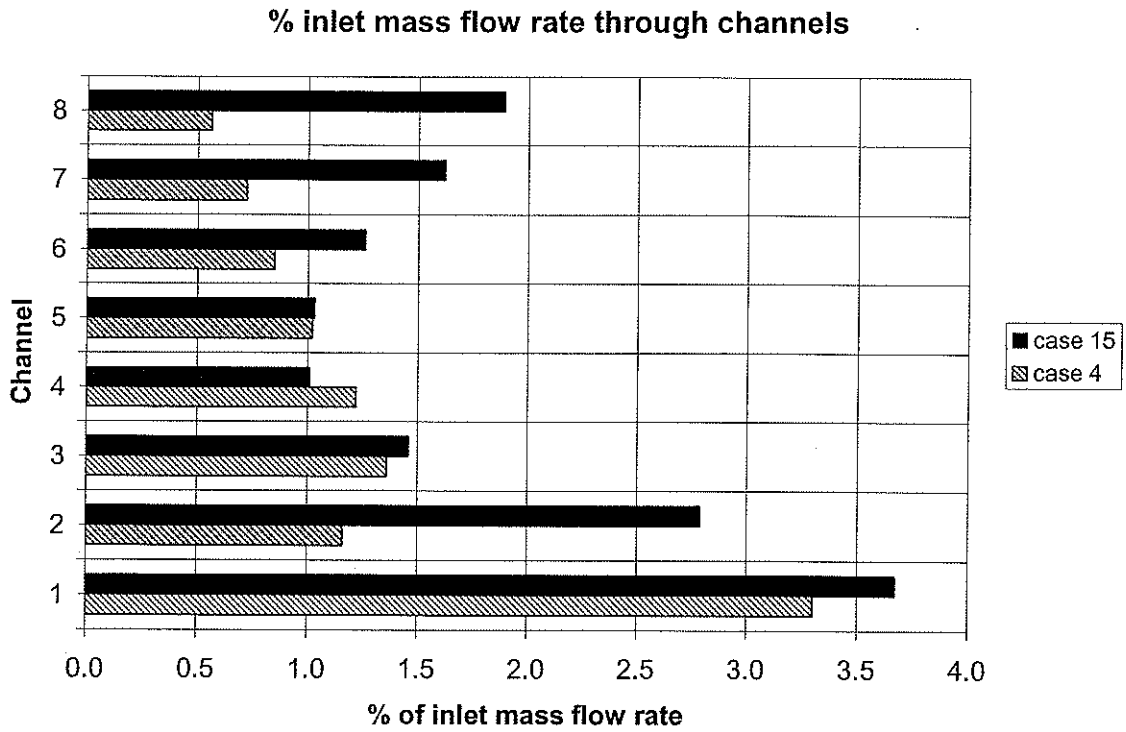

Figure 6.23: Percentage of inlet mass flow rate flowing through each channel for case 4 and case 15

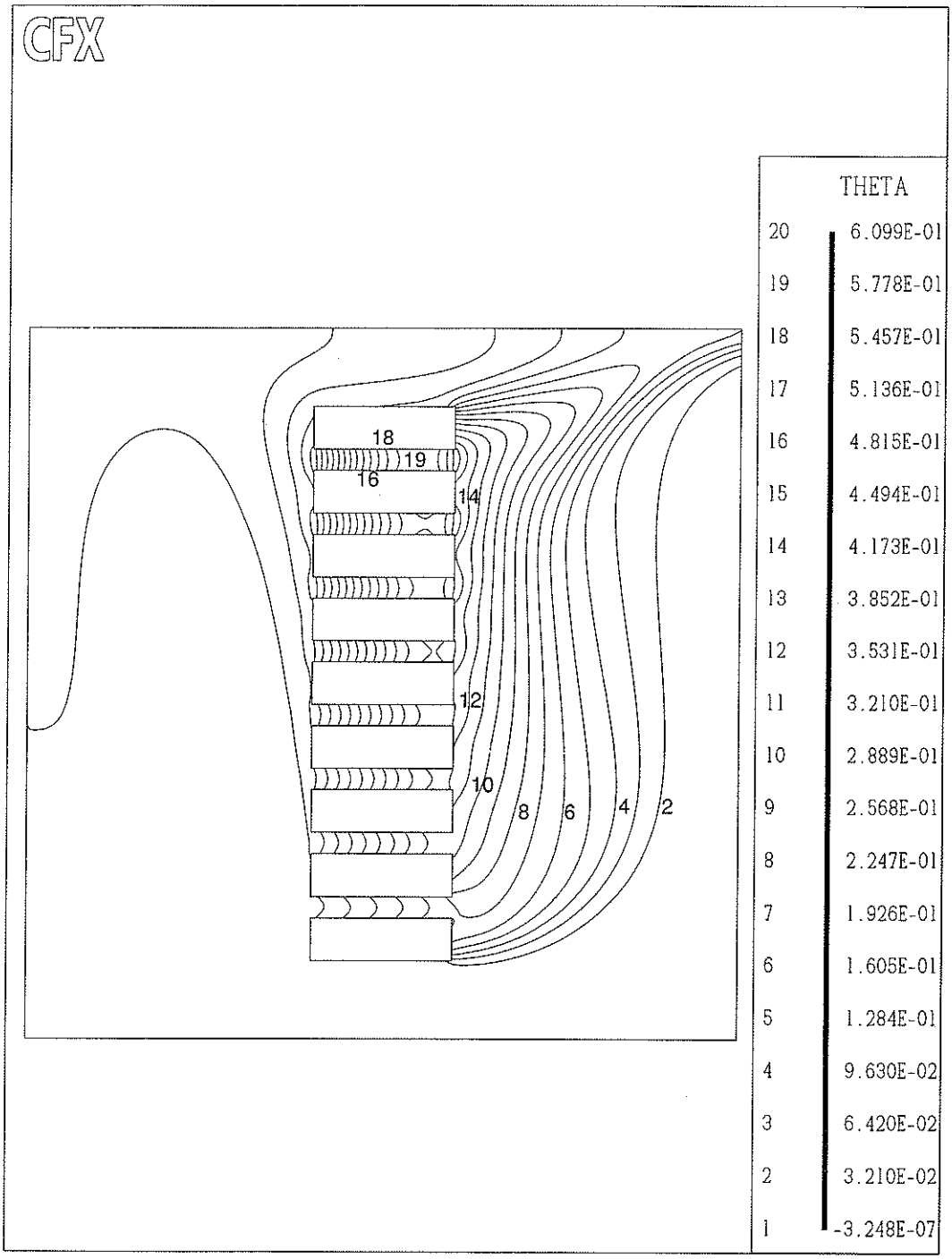

Figure 6.24: Temperature contours for case 4, mixed convection (Re_o = 100), inlet L-0.05 and outlet R -0.95

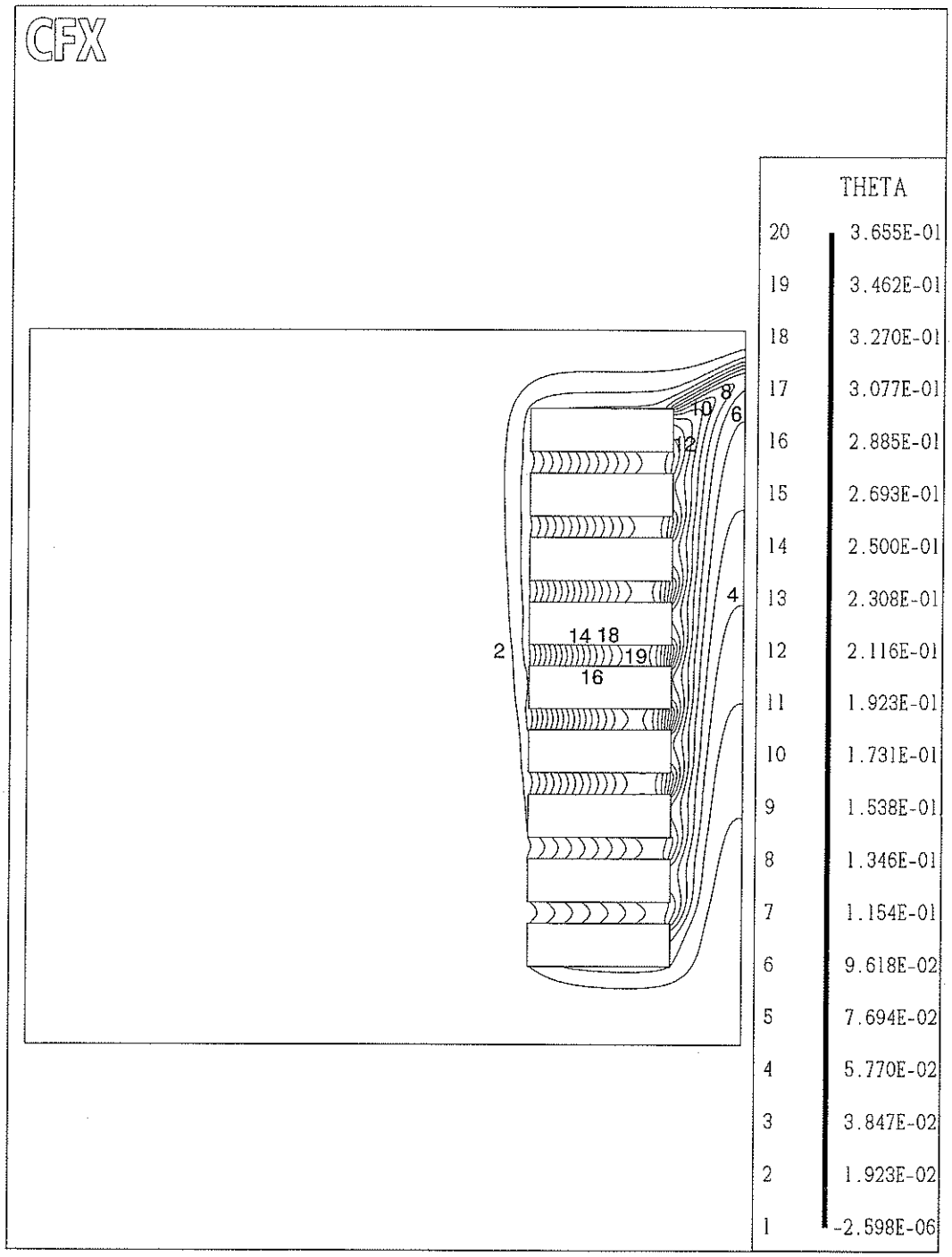

Figure 6.25: Temperature contours for case 15, mixed convection ($Re_o = 100$), inlet L-0.05 and outlet R-0.95

When comparing case 7 (a_9 = 0.4) to case 17 (a_9 = 0.1), Re_o = 225, inlet L – 0.05 and outlet R – 0.95. The maximum temperature of case 7 was 0.655 and the maximum temperature for case 17 dropped to 0.262. Again, the velocity vector plots and the temperature contours will help to explain why the temperature drops by moving the tower from the centered (a_9 = 0.4) position to the offset position (a_9 = 0.1). The velocity vector plot for case 7 is shown in Figure 6.26 and case 17 in Figure 6.27.

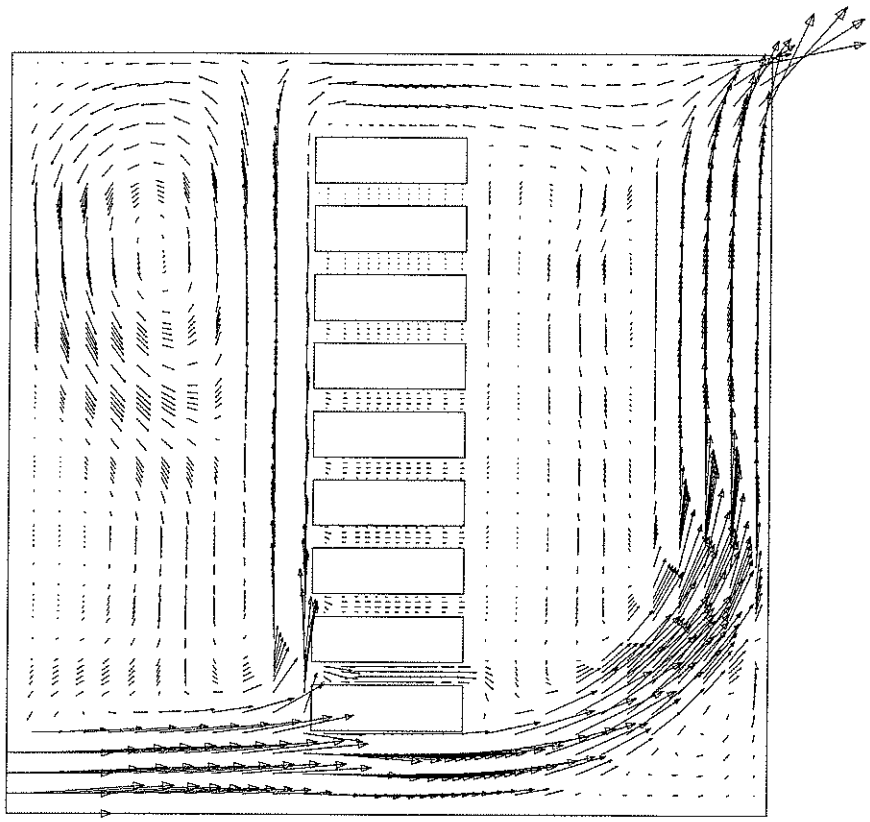

Figure 6.26: Case 7, mixed convection cooling (Re_o = 225) for a_9 = 0.4, inlet L-0.05 and outlet R-0.95

The flow for case 7 is similar to case 4 (Figure 6.21). The majority of the air flows underneath the tower, and there is a large counter-clockwise recirculation zone on the left hand side of the tower. There is a small recirculation zone in the lower right corner and

case 7 has numerous small recirculation zones to the right of the tower. The percentage of inlet mass flow rate flowing through the channels is 7.20%.

Figure 6.27 shows that there is again more interaction between the flow and the tower and there is a large recirculation zone to the left of the tower. The flow is upward on both sides of the tower and the percentage of inlet mass flow rate that flows through the channels is 20.58%.

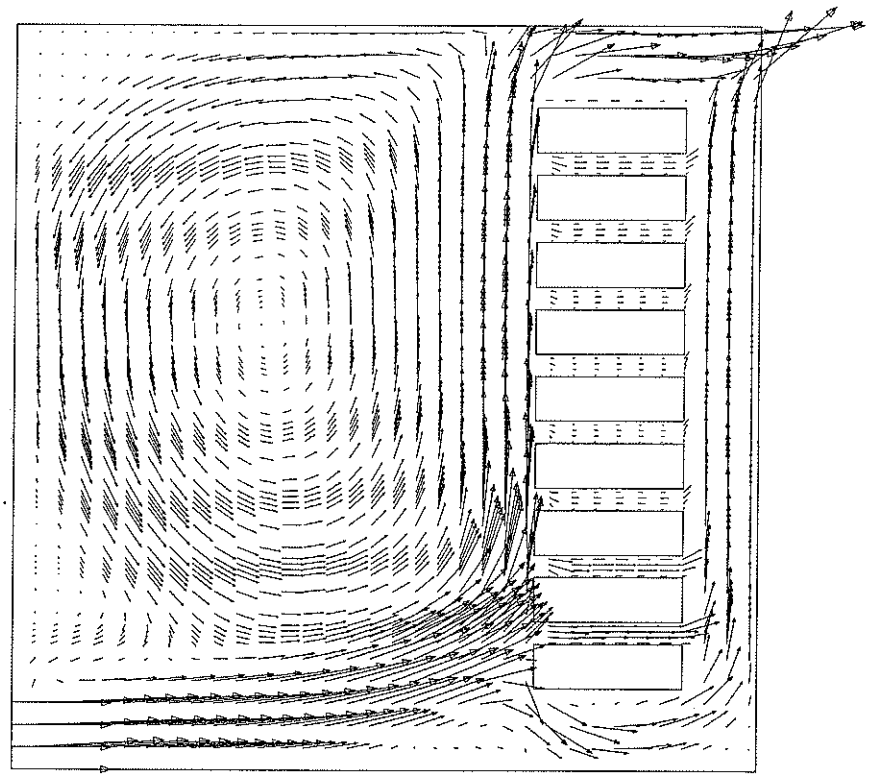

Figure 6.27: Case 17, mixed convection cooling ($Re_o = 225$) for $a_9 = 0.1$, inlet L-0.05 and outlet R-0.95

Figures 6.28 and 6.29 show the temperature contour plots for cases 7 and 17, respectively. Figure 6.28 shows the percentage of mass flow rate through the channels for cases 7 and 17. The results of Figure 6.28 are similar to those of Figure 6.23. For

case 7, the percentage of mass flow rate through the channels decreases as we go up the tower from 3.65% in channel 1 to 0% in channel 8. For case 17, the flow decreases from a maximum of 8.09% down to 0.73% in channel five and back up to 2.51% in channel nine.

Looking at Figure 6.29, contour #2 passes on the bottom of block one and on the left hand side of blocks 1 through 5. The temperature on the left side on the tower is low and the maximum temperature occurs in the last channel of the tower with $\theta_{max} = 0.655$. For case 17 (Figure 6.30), the maximum temperature occurs in channel 5 with $\theta_{max} = 0.262$, similar to case 15.

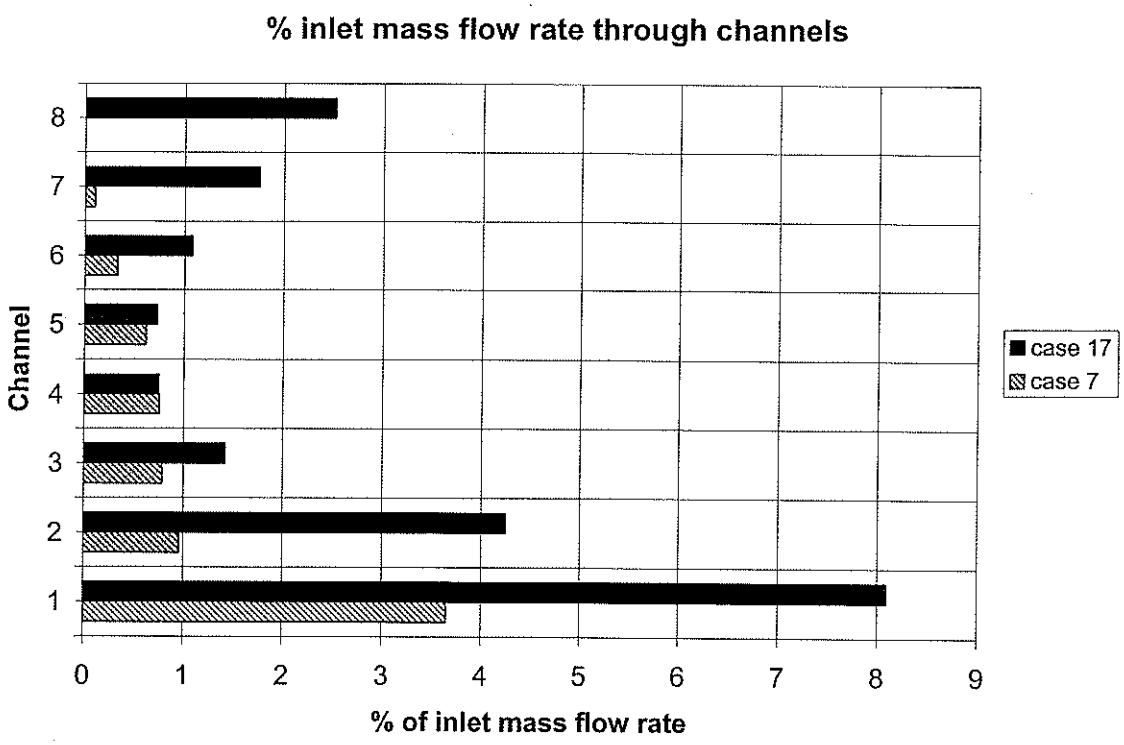

Figure 6.28: Percentage of inlet mass flow rate flowing through each channel for case 7 and case 17

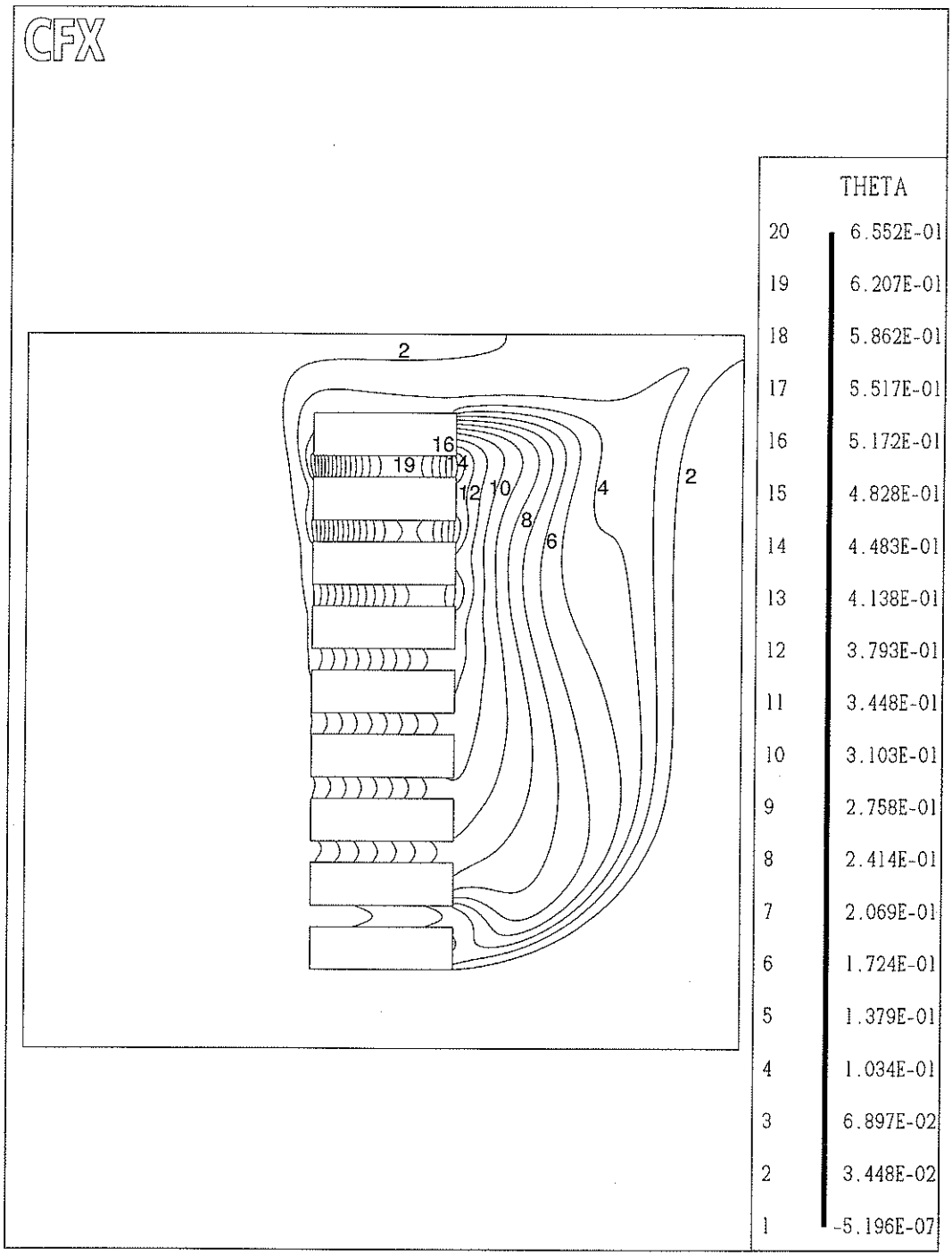

Figure 6.29: Temperature contours for case 7, mixed convection ($Re_o = 225$), inlet L-0.05 and outlet R-0.95

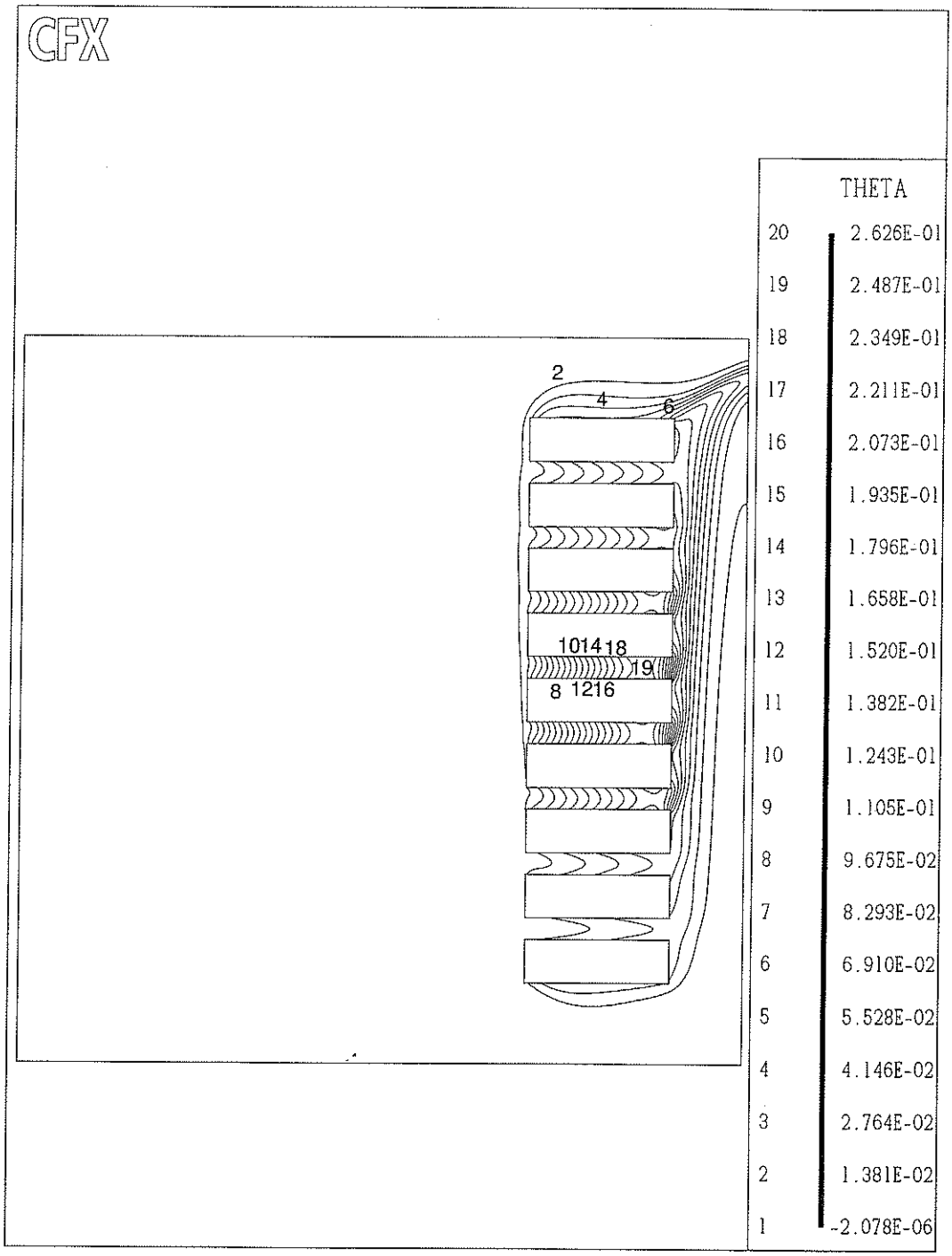

Figure 6.30: Temperature contours for case 17 mixed convection ($Re_o = 225$), inlet L-0.05 and outlet R-0.95

The final comparison of the effect of tower position was done for the cases of the inlet and outlet positioned at L – 0.5 and R – 0.5, respectively. From the previous comparisons it appeared that the best position for the tower is at a_9 = 0.1. This was investigated again with the inlet Reynold's number equal to 100; case 5 (a_9 = 0.4) and case 13 (a_9 = 0.1). Also, the tower was moved to the left hand side of the domain in case 20 (a_9 = 0.7) to see the effect that this would have on the velocity and temperature distribution.

Figures 6.31, 6.32 and 6.33 show the velocity vectors for cases 5, 13 and 20, respectively.

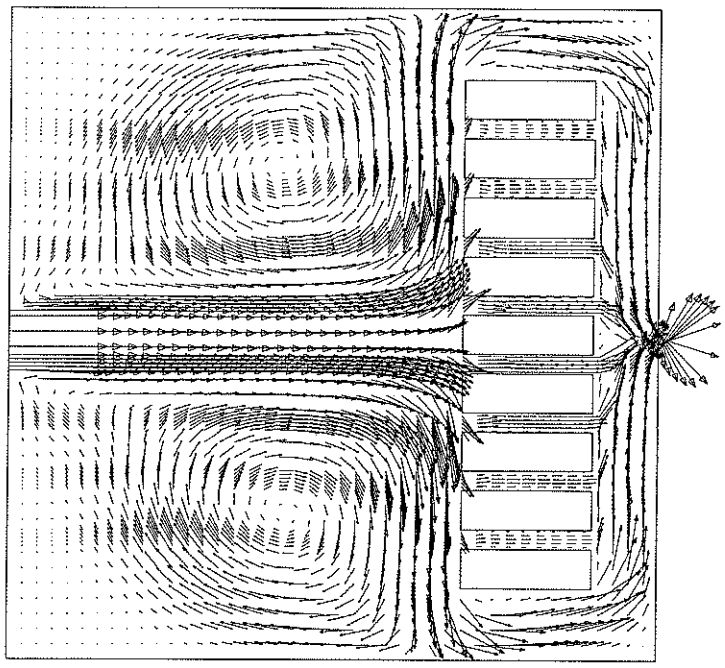

Figure 6.31: Case 5, mixed convection cooling (Re_o = 100) for a_9 = 0.4, inlet at L-0.5 and outlet at R-0.5

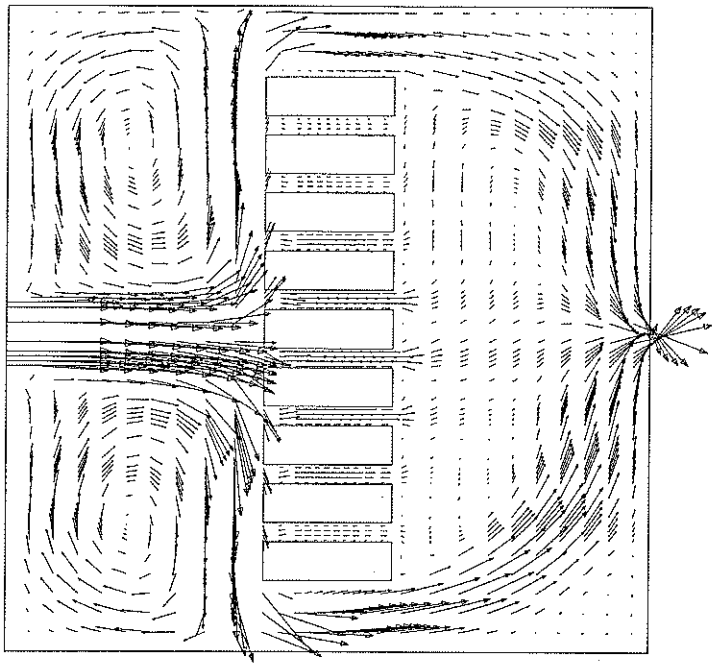

Figure 6.32: Case 13, mixed convection cooling ($Re_o = 100$) for $a_9 = 0.1$, inlet at L-0.5 and outlet at R-0.5

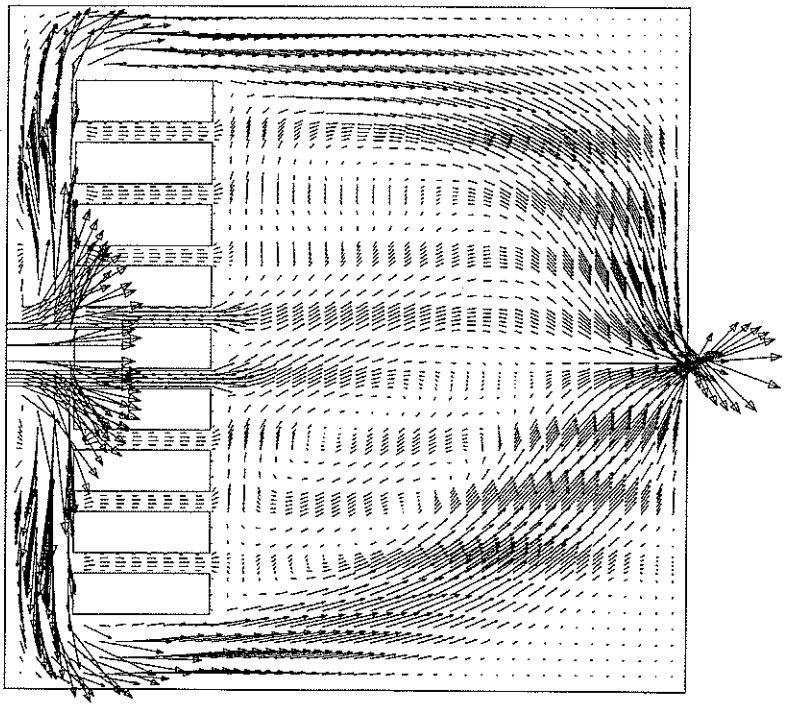

Figure 6.33: Case 20, mixed convection cooling ($Re_o = 100$) for $a_9 = 0.7$, inlet L-0.5 and outlet R – 0.5

All three cases have a high interaction between the incoming air and the tower; however, they all have different temperature distributions and maximum temperature values. For case 5 ($a_9 = 0.4$) the maximum temperature is 0.482, for case 13 ($a_9 = 0.1$) the maximum temperature is 0.284 and for case 20 ($a_9 = 0.7$) the maximum temperature is 0.373. Cases 5 and 20 have very similar tower average temperatures, $\theta_{avg} = 0.161$ for case 5, and $\theta_{avg} = 0.164$ for case 20. The tower average temperature for case 13 was $\theta_{avg} = 0.103$.

In Case 5 (Figure 6.31) the air coming in at $Y = 0.5$ encounters the tower and divides so much of it flows around the tower. The bulk of the flow goes around the bottom and the top of the tower, while the remainder flows through the channels. This action forms two pronounced recirculation zones in the left hand side of the domain, the top recirculation zone flows counter-clockwise and the bottom recirculation zone flows clockwise. There are smaller recirculation zones to the right of the tower. The total percentage of mass flow rate that flows through the tower is 21.51%, with more air flowing through the bottom 4 channels than the top four channels.

Figure 6.32 shows the flow encountering the tower and again the bulk of the air flowing above and below the tower, with the remainder flows through the tower and joining near the outlet. Again, there are two large recirculation zones in the domain. The total percentage of inlet mass flow rate to flow through the towers is 31.36% and the flow for case 13 is higher in all the channels when compared to cases 5 and 20.

When locating the tower near the inlet in case 20 (Figure 6.33), we are forcing the air to flow through the channels of the tower. The velocity vector plot indicates that the air flows above, below the tower, and through the channels of the tower. When looking at the percentage of inlet mass flow rate through the channels we see that the flow in channels 4 and 5 are at high values of 7.13% and 6.24%, respectively, while the airflow in the other channels does not increase past 1.6%. of the inlet flow

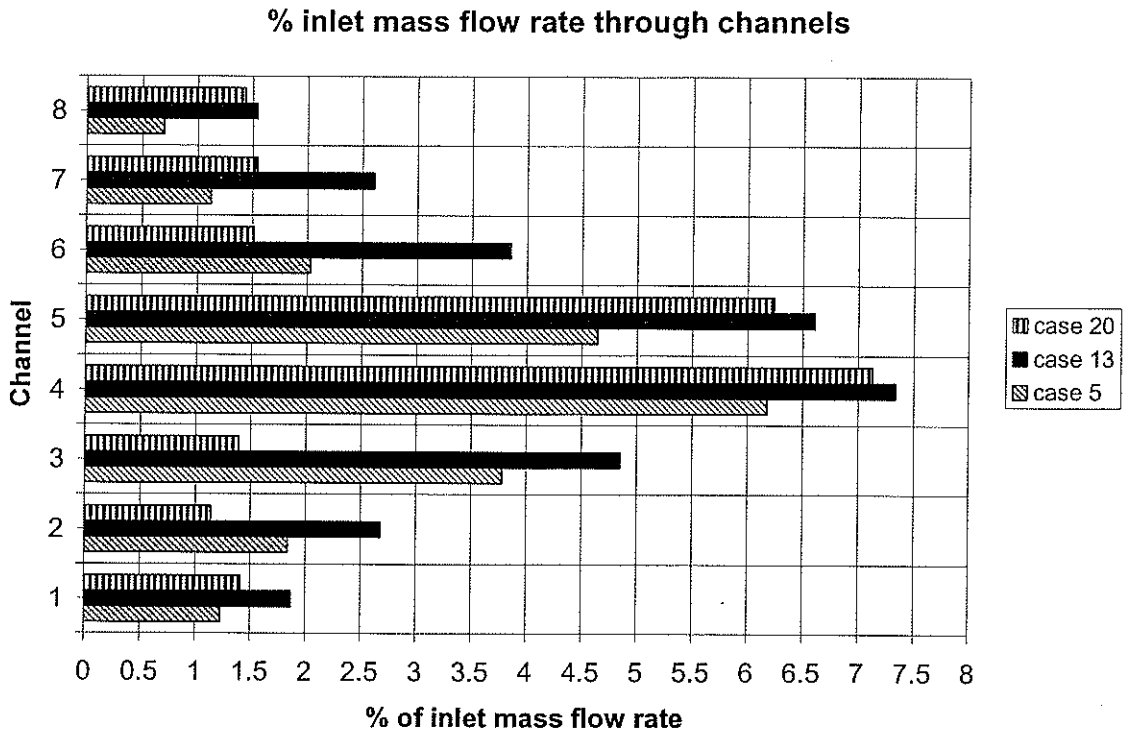

Figure 6.34: Percentage of inlet mass flow rate flowing through each channel for cases 5, 13 and 20

Figure 6.34 is a graph of the percentage of the mass flow rate through the channels. As demonstrated before, the case with the lowest maximum temperature had the highest percentage of inlet mass flow rate flowing through the channels. In addition, the position of the tower that takes advantage of the flow is the cases where $a_9 = 0.1$.

The temperature contour plots are shown in Figures 6.35, 6.36 and 6.37 for cases 5, 13 and 20, respectively. The maximum temperature for cases 5 and 13 occur in a similar spot, the upper surface of block 8. From Figure 6.34, channel 8 is the channel with the lowest value of percentage of inlet mass flow rate compared to the other channels. Similarly for case 20 the maximum temperature occurs on the lower face of block 3, and channel two is the channel with the lowest percentage of inlet mass flow rate when compared to the other channels. Since the flow rates through the different channels is not symmetric about $Y = 0.5$, the temperatures in the domain will not be symmetric about $Y = 0.5$ and is demonstrated in the Figures.

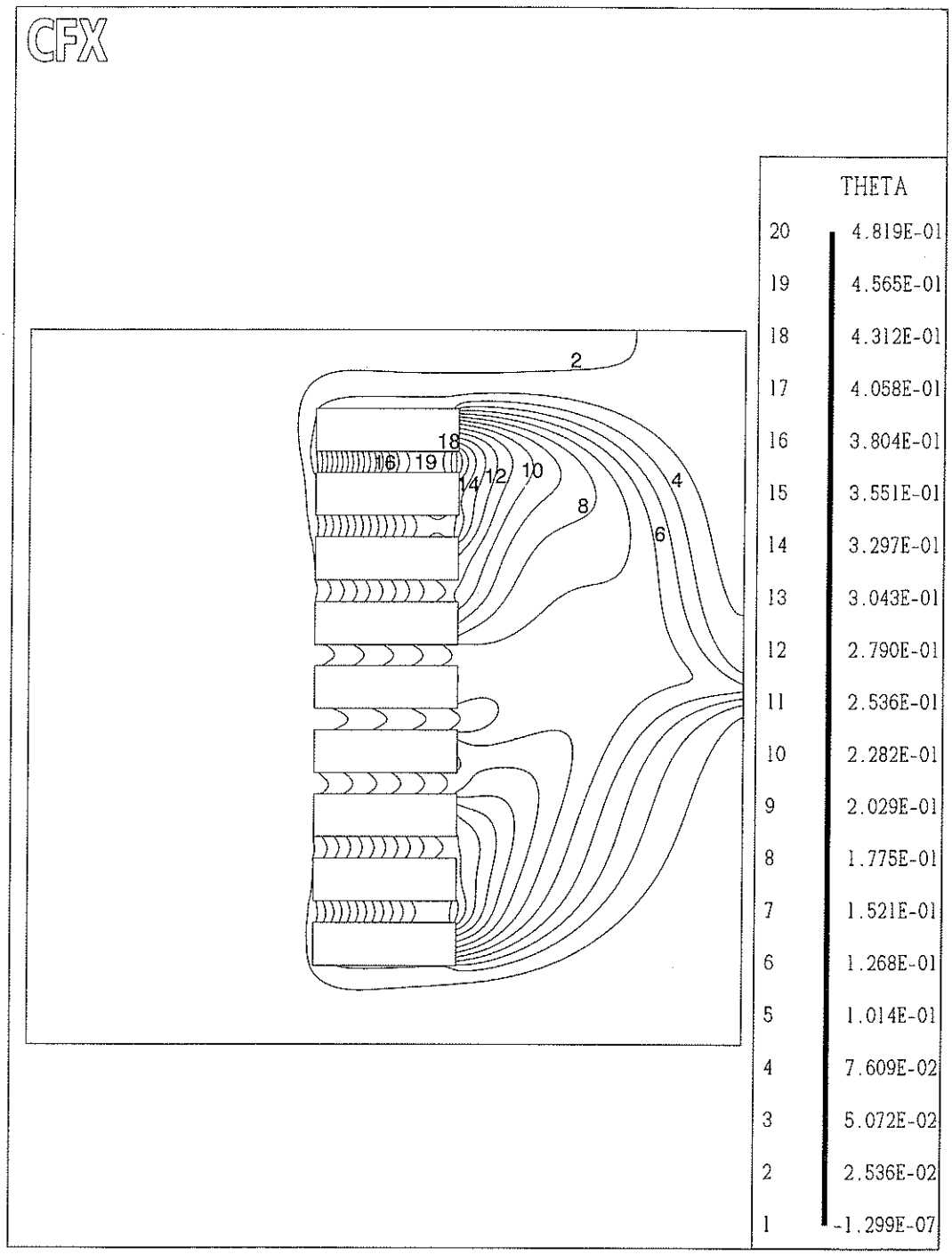

Figure 6.35: Temperature contours for case 5, mixed convection ($Re_o = 100$), inlet L-0.5 and outlet R-0.5

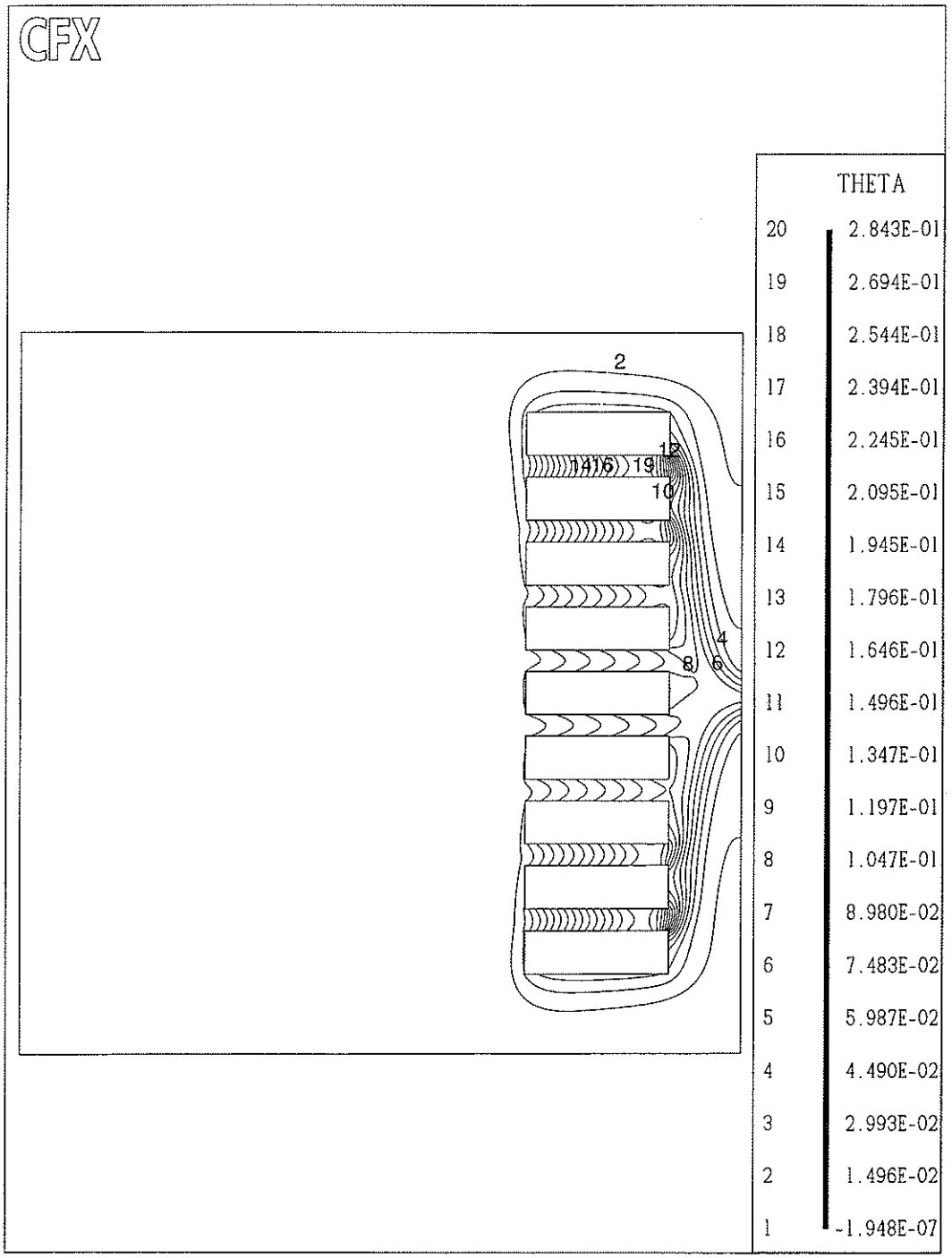

Figure 6.36: Temperature contours for case 13, mixed convection (Re_o =100), inlet L-0.5 and outlet R-0.5

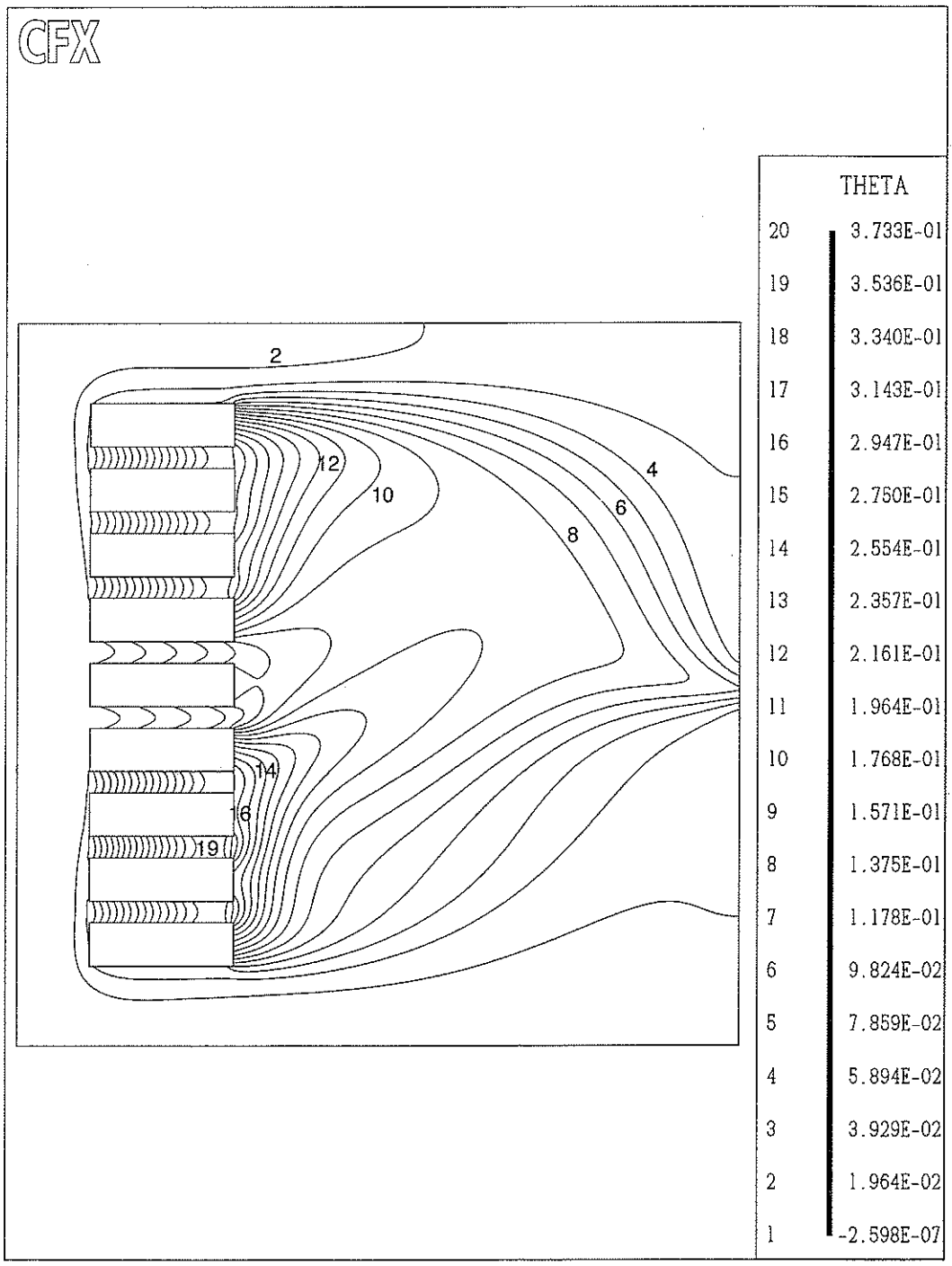

Figure 6.37: Temperature contours for case 20, mixed convection (Re_o = 100), inlet L-0.5 and outlet R-0.5

6.3.2 Passive Versus Mixed Convection Cooling

Passive versus mixed convection results for Geometry 2 were compared. From Table 6.4, cases 9 (Re_o = 12.78), 14 (Re_o = 100) and 18 (Re_o = 225) were selected since increasing the inlet mass flow rate significantly decreases the maximum temperature. All three cases had the same tower position a_9 = 0.1 and inlet and outlet positions [inlet, L – 0.05; outlet, R – 0.5]. Figures 6.38, 6.39 and 6.40 show the velocity vector plots for cases 9, 14 and 18, respectively.

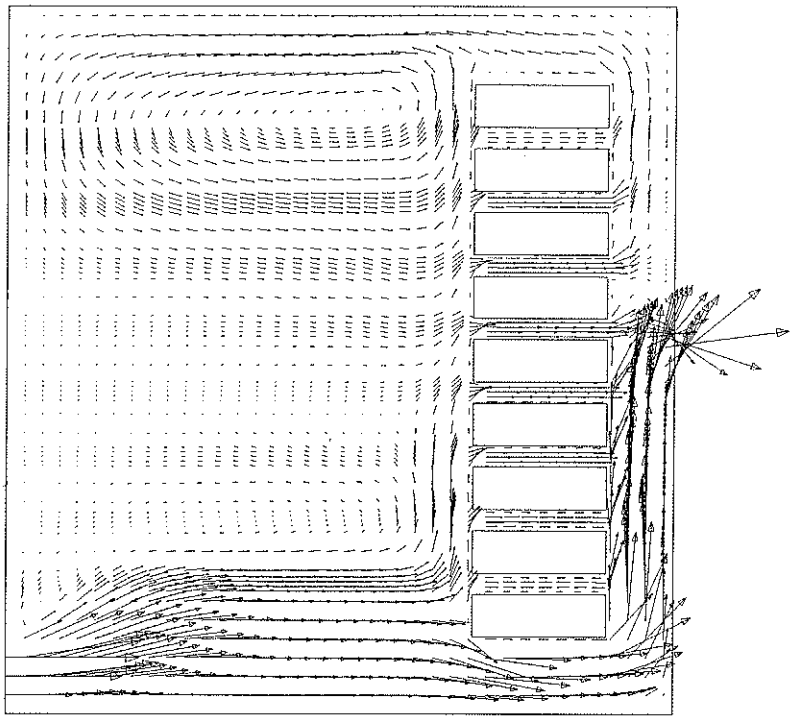

Figure 6.38: Case 9, passive cooling (Re_o = 12.78) for a_9 = 0.1, inlet L-0.05 and outlet R-0.5

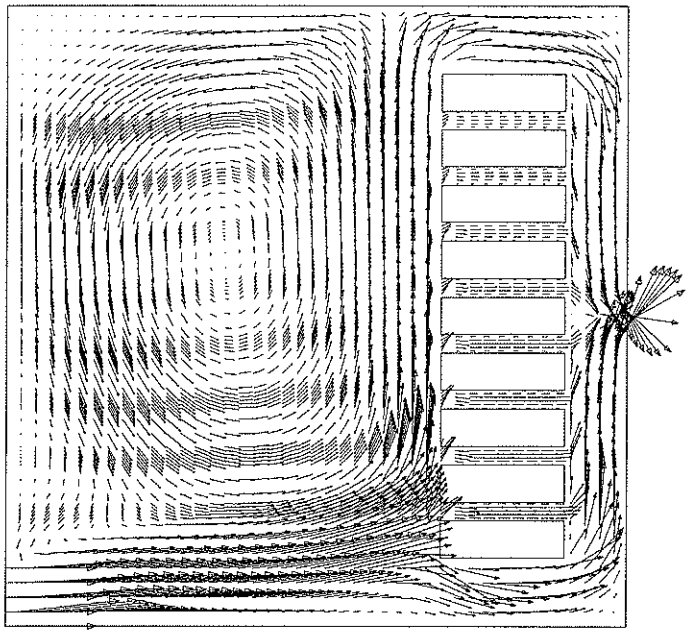

Figure 6.39: Case 14, mixed convection cooling ($Re_o = 100$) for $a_9 = 0.1$, inlet L-0.05 and outlet R-0.5

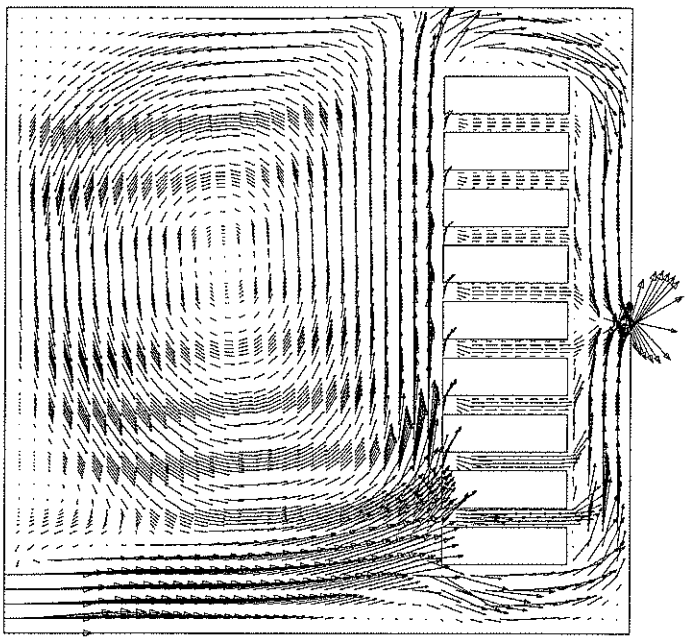

Figure 6.40: Case 18, mixed convection cooling ($Re_o = 225$) for $a_9 = 0.1$, inlet L-0.05 and outlet R-0.5

When comparing the three velocity vector plots it is seen that for passive cooling, the air movement in the domain is minimal; whereas the mixed convection velocity vector plots are very similar and would be indistinguishable without labels. The difference between the plots is the magnitude of the vectors in the plots.

This difference in magnitudes leads to the different temperature contours in the domains. For case 9 (Re_o = 12.78), the maximum temperature is 1.854, case 14 (Re_o = 100) has a maximum temperature of 0.282 and case 18 (Re_o = 225) has a maximum temperature of 0.140. Figures 6.41, 6.42 and 6.43 show the temperature contours for cases 9, 14 and 18, respectively. In Figure 6.41, temperature stratification is clearly demonstrated on the left-hand side, where the temperature increases as we move up along the domain. The highest temperatures are found in the upper right hand corner of the domain between the 8^{th} and 9^{th} block.

The temperature distributions of cases 14 and 18 are similar but the temperatures in case 18 are lower. Figure 6.44 shows the percentage of mass flow through the channels of cases 9, 14 and 18. Cases 14 and 18 demonstrate similar patterns with high percentage of mass flow rate through the first channel and then decreasing as we move up the tower. The total percentage of inlet mass flow rate through the channels for case 9 was 42.36%, case 14 was 31.36%, and for case 18 was 28.86%. For Geometry 2, the combination of a_9 = 0.1, inlet L-0.05, and outlet R-0.5 produced the lowest values of θ_{max} for forced-convection cooling (θ_{max} = 0.281 at Re_o = 100 and θ_{max} = 0.140 at Re_o = 225). For passive cooling, the combination that gave the most effective cooling was a_9 = 0.1, inlet L-0.05, and outlet R-0.95. It must be noted that the combination that was most effective in forced-convective cooling turned out to be the least effective for passive cooling.

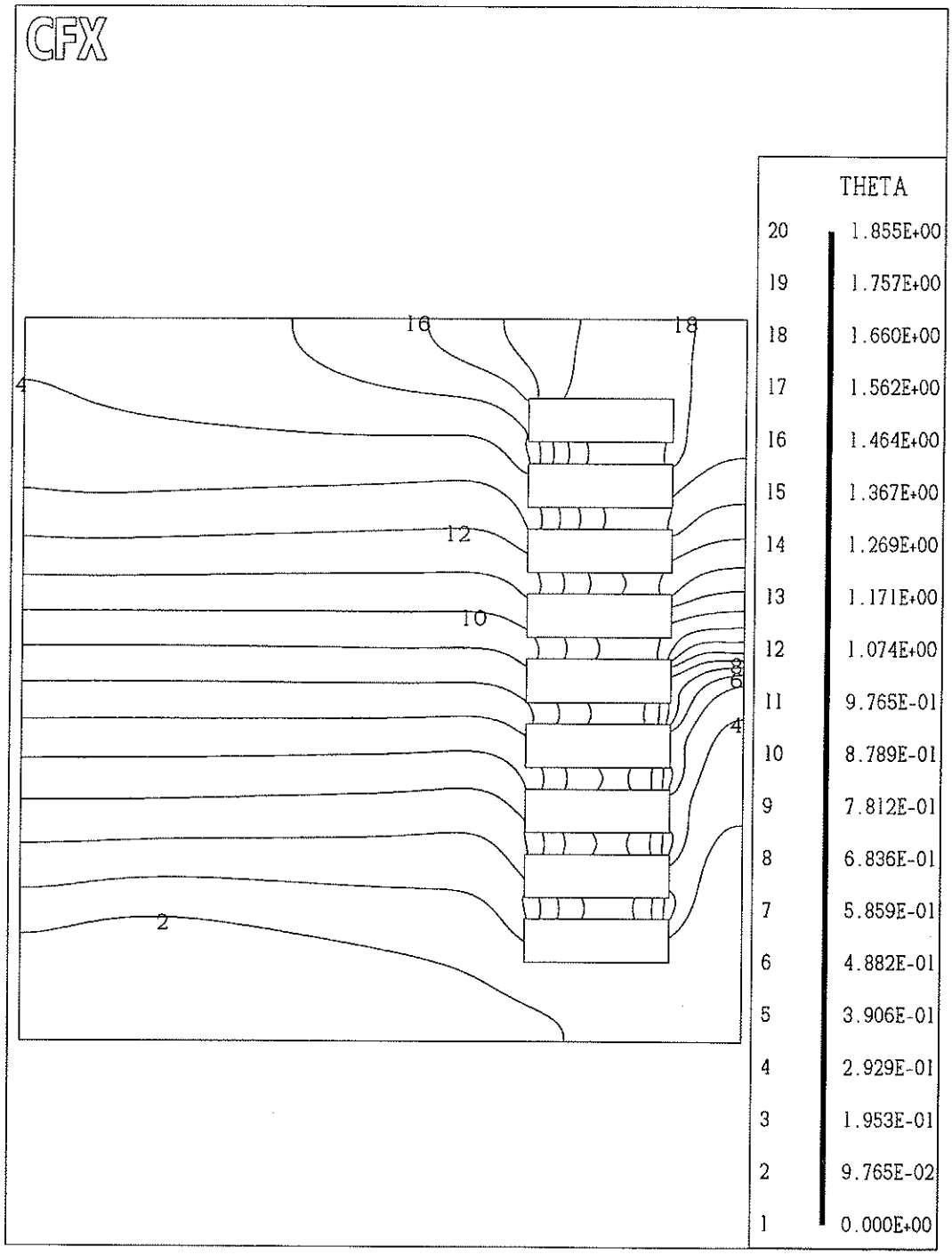

Figure 6.41: Temperature contours for case 9, passive cooling (Re_o = 12.78), inlet L-0.05 and outlet R-0.5

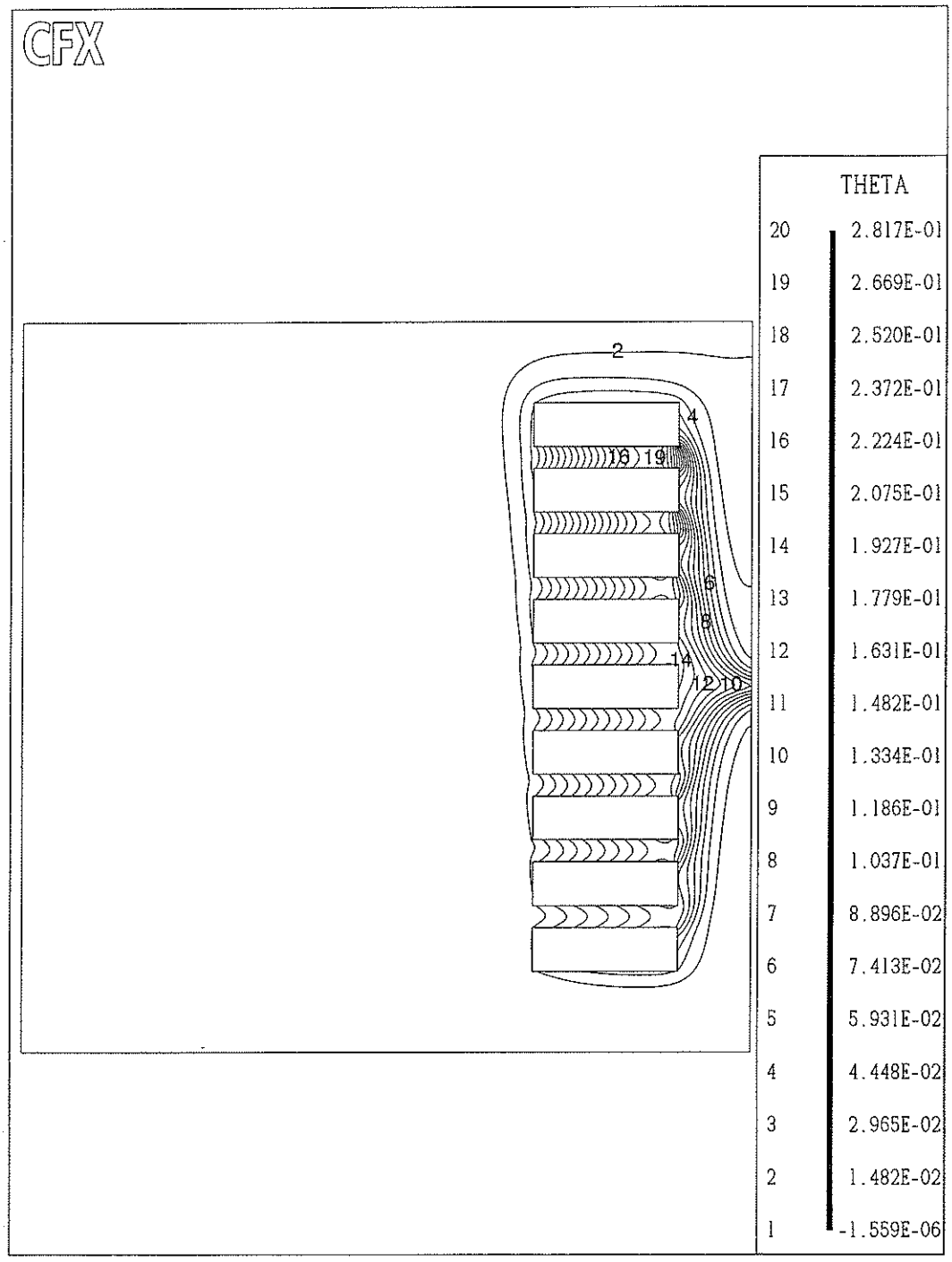

Figure 6.42: Temperature contours for case 14, mixed convection (Re_o = 100), inlet L-0.05 and outlet R-0.5

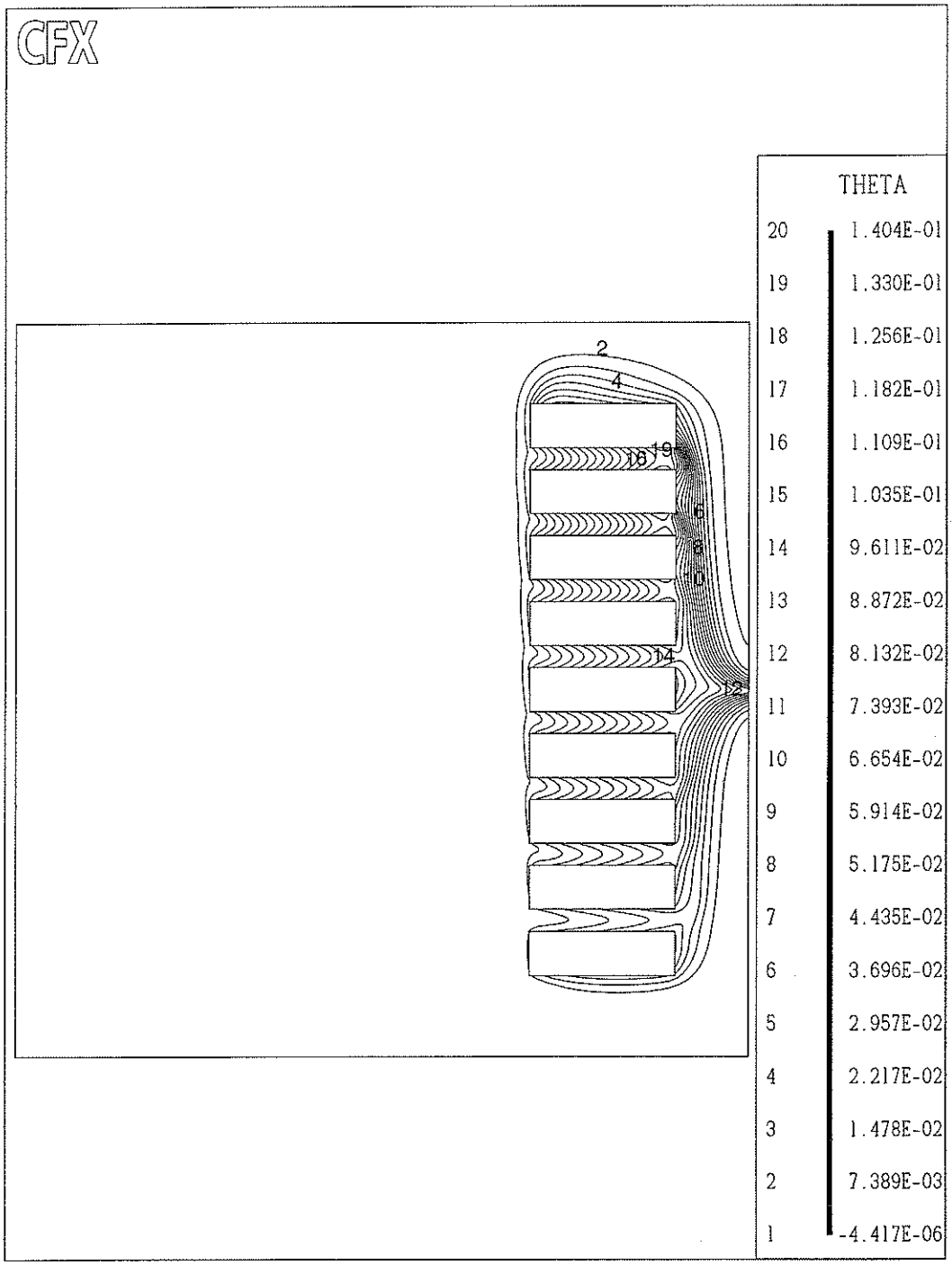

Figure 6.43: Temperature contours for case 18, mixed convection ($Re_o = 225$), inlet L-0.05 and outlet R-0.5

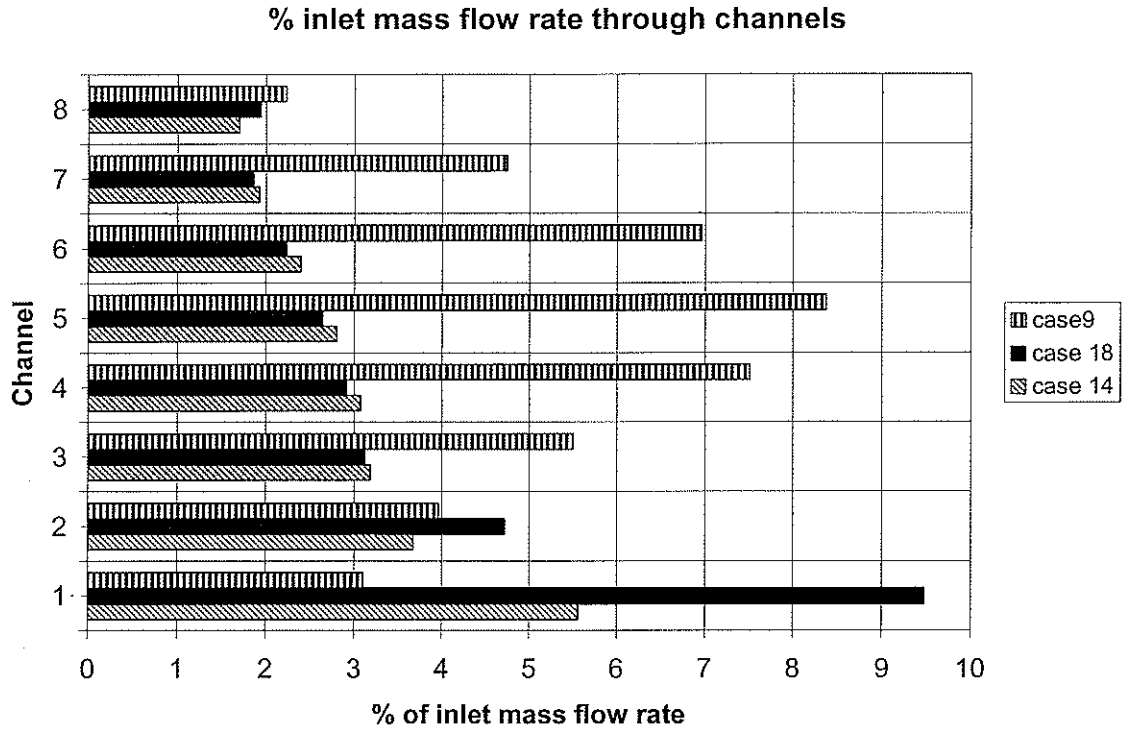

Figure 6.44: Percentage of mass flow rate flowing through each channel for cases 9, 14 and 18

6.3.3 Effect of the Location of Inlet and Outlet Ports

As seen earlier for Geometry 1, the locations of the inlet and outlet have a significant impact on the velocity in the domain and hence an impact on the temperature distribution. Two previously presented cases will be compared in this section. Case 17 [inlet L – 0.05, outlet R – 0.95, Re_o = 225, a_9 = 0.1] had a maximum temperature of 0.262 and case 18 [inlet L – 0.05, outlet R – 0.5, Re_o = 225, a_9 = 0.1] had a maximum temperature of 0.140. By lowering the outlet from a height of 0.95 to 0.5 on the right hand side it decreased the temperature significantly. The velocity vector graphs and temperature contours are presented in Figures 6.22 and 6.24 for case 15 and Figures 6.40 and 6.43 for case 18. The inlet and outlet positions that produced the lowest temperatures in the stack were L – 0.05 and R – 0.5, as demonstrated in this section. This can also be confirmed by comparing the temperatures among cases 11, 14 and 15.

6.4 Geometry 3

For Geometry 3 seen in Figure 6.45, it was decided to obtain results for a geometry that is closer to the original problem in the valve hall. Referring to Figure 3.1, Geometry 3 corresponds to $a_1 = a_3 = 0.1$, $a_5 = 0.1$, $a_6 = 0.06$, $a_7 = 0.1$, $a_8 = 0.03$, $a_9 = 0.1$, $a_{10} = 0.11$, M = 3, Gr = 6.75E+6 and N = 9. Three towers were positioned inside the domain and the only variables were the inlet mass flow rate and the positions of the inlet and outlets ports. When looking at Figure 6.45, the tower on the left hand side is referred to as T1, the center tower is referred to as T2, and the tower to the right is referred to as T3.

There is only one case of passive cooling to determine if passive conditions would have an impact on the velocity and temperature distributions. The locations of the inlet and outlet ports that were examined can be found in the Table 6.5. Cases 3 and 7 were for inlet and outlet conditions that did not provide a converged solution and were not included in the report. Also, for case 6 the location of the inlet was placed on the bottom of the left hand side and the outlet was placed on the bottom of the right hand side, this is an unrealistic placement of an outlet and therefore caused a very stratified flow and very high temperatures in the domain.

Run 5, the case of Re_o = 100, Inlet L – 0.05, Outlet R – 0.95, resulted in the lowest maximum temperature of 0.629. The vector plot can be seen in Figure 6.46 and the temperature contour plot can be seen in Figure 6.47

Table 6.5: Results from Geometry 3

						θ_{avg}			% inlet mass flow rate		
case	**Re_o**	**Inlet**	**Outlet**	**θ_{max}**	**Location**	**T1**	**T2**	**T3**	**T1**	**T2**	**T3**
1	37.68	B - 0.5	T - 0.5	0.931	L9 - 0.5, T2	0.531	0.536	0.506	4.13	-1.18	-4.20
2	100	B - 0.5	T - 0.5	0.637	L9 - 0.5, T2	0.314	0.381	0.314	4.73	0.00	-4.73
4	100	L - 0.05	R - 0.5	0.791	L9 - 0.675, T2	0.356	0.429	0.288	5.94	6.33	21.00
5	100	L - 0.05	R - 0.95	0.629	L9 - 0.675, T1	0.350	0.374	0.283	4.44	5.15	8.81
6	100	L - 0.05	R - 0.05	10.04	L9 - 0.5, T2	6.306	6.382	6.707	4.10	3.60	2.04
8	100	L - 0.5	R - 0.5	0.735	U8 - 0.775, T3	0.167	0.381	0.426	21.23	14.29	22.01

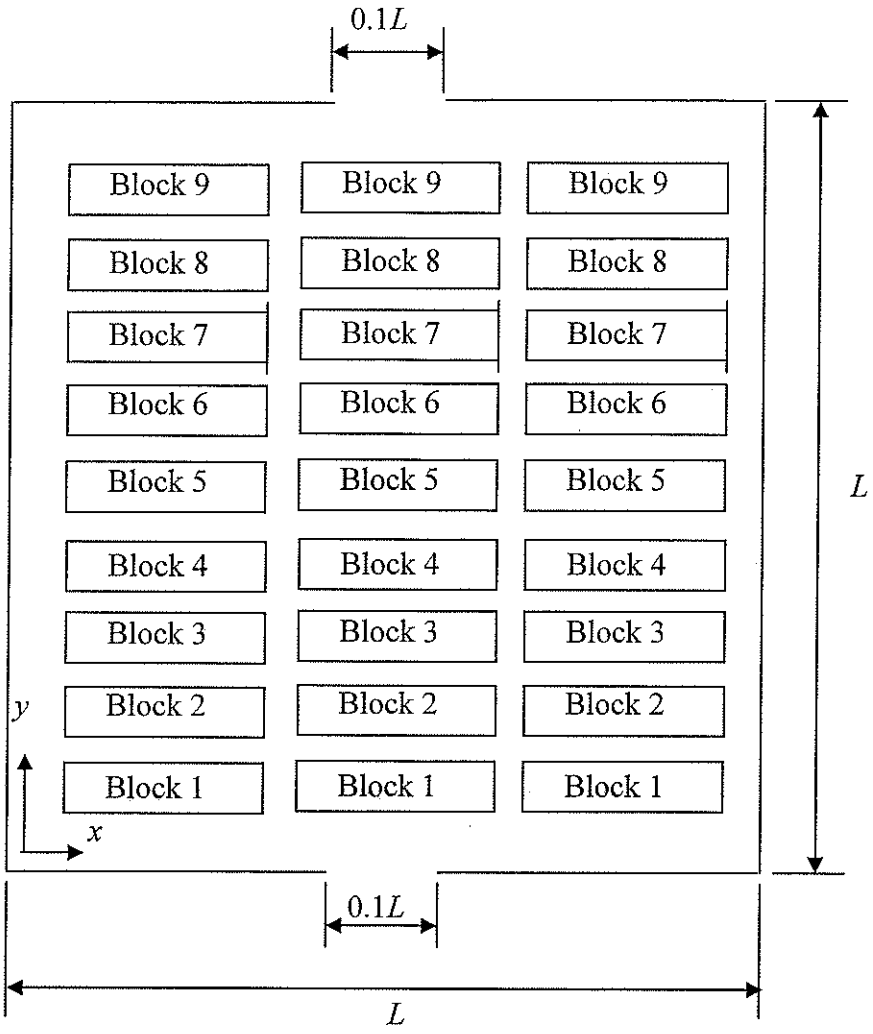

Figure 6.45: Geometry 3

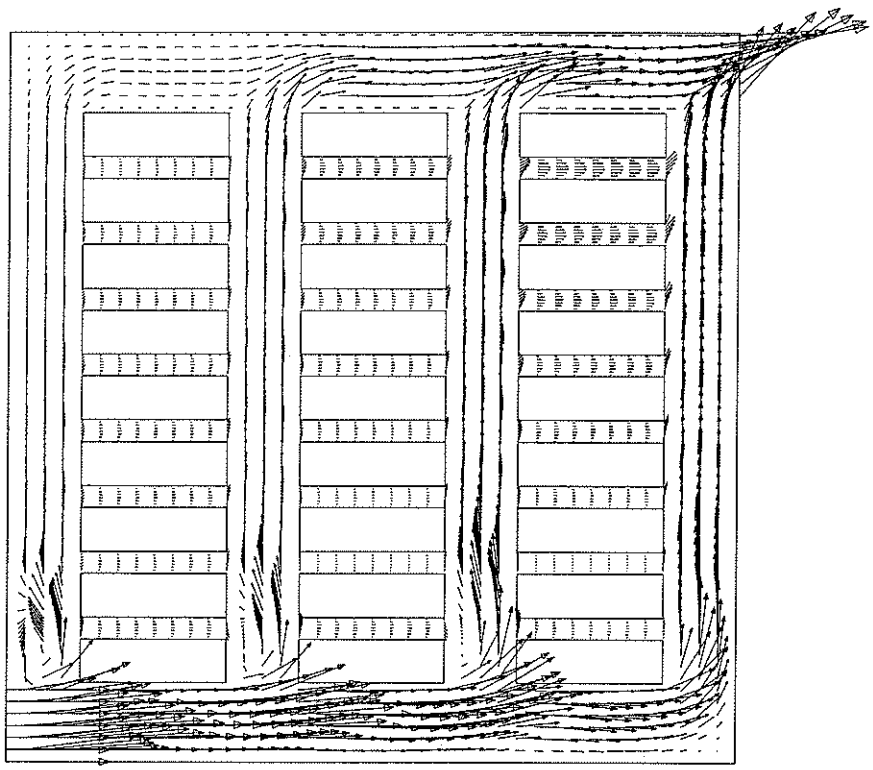

Figure 6.46: Case 5, mixed convection cooling ($Re_o = 100$), inlet L-0.05 and outlet R-0.95

The velocity vectors in Figure 6.46 show incoming air being introduced into the domain from the bottom left corner and the air flows upward in the vertical spaces formed by the three towers. The air then rejoins and flows through the outlet.

The temperature contours shown in Figure 6.47 demonstrate that the velocity contours shown in Figure 6.46 have most of the domain at a low temperature. For example temperature contour # 10 ($\theta = 0.298$) is near the top of the domain on the right hand side of tower one. The temperature contours demonstrate that the maximum temperature occurs in the channel formed by blocks 8 and 9 in tower 1.

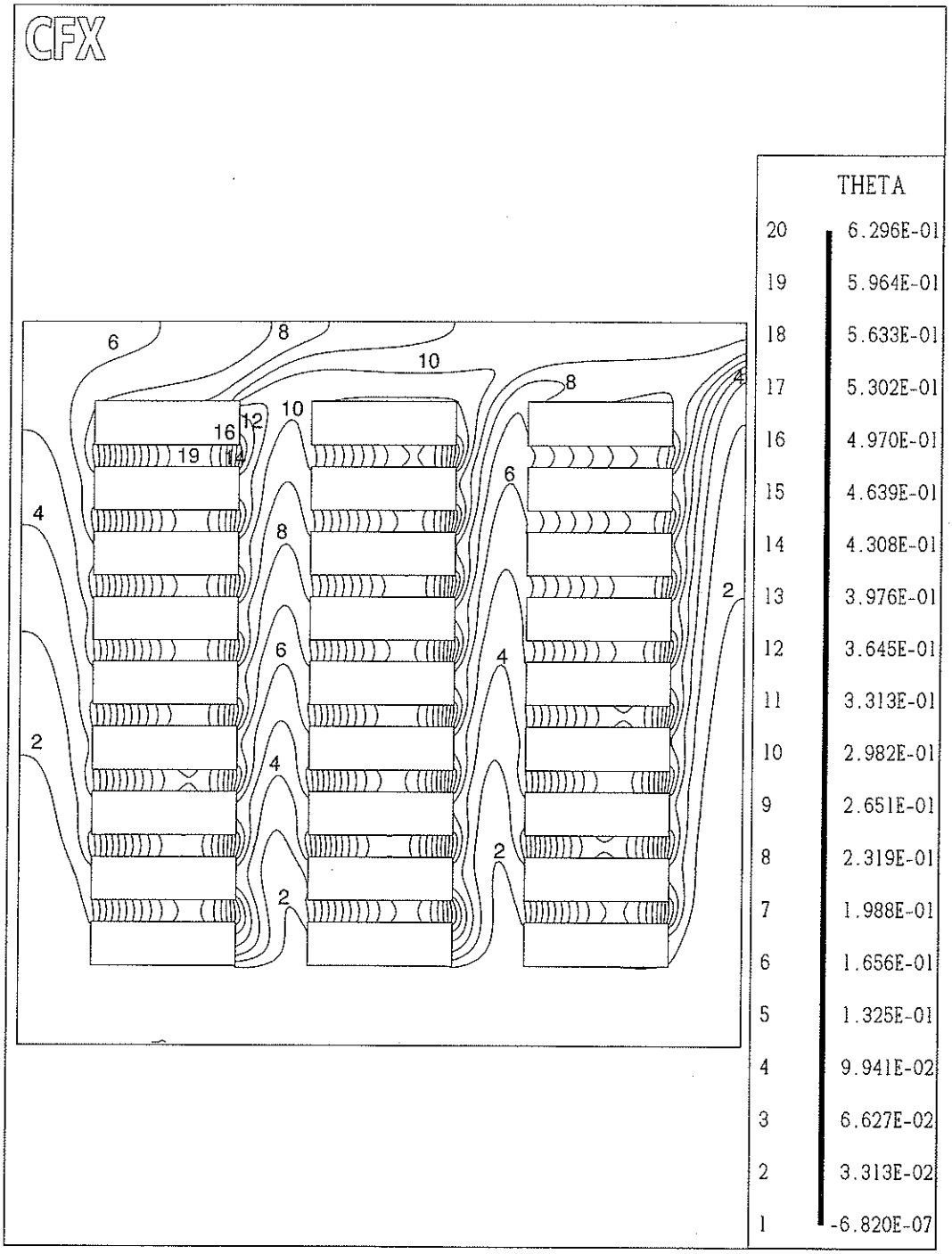

Figure 6.47: Temperature contours for case 5, mixed convection (Re_o = 100), inlet L-0.05 and outlet R-0.95

The second lowest maximum temperature occurred in case 2 [Re_o = 100, inlet B – 0.5, outlet T – 0.5], where the maximum temperature was 0.637. The velocity plot for run 2 is shown in Figure 6.47.

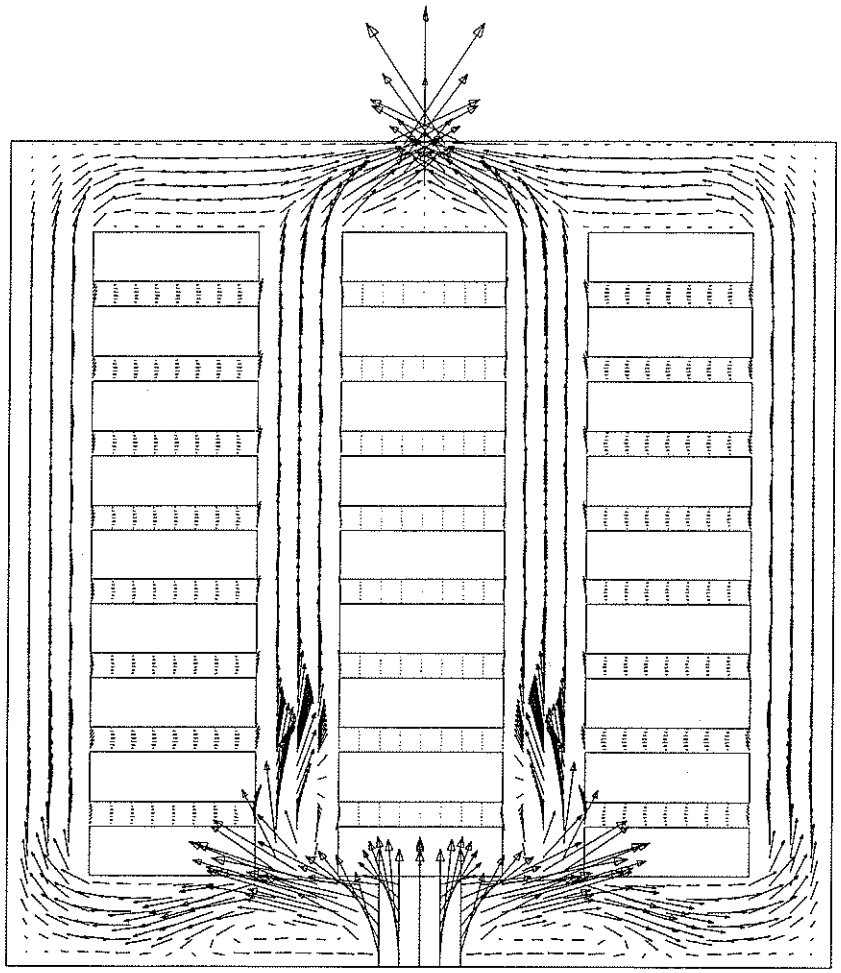

Figure 6.48: Case 2, mixed convection cooling (Re_o =100), inlet B-0.5 and outlet T-0.5

The incoming air shown in Figure 6.48 impacts the lower surface of block 1 in the middle tower and then the flow continues upward in each of the vertical spaces formed by the towers. The temperature contours are shown in Figure 6.49.

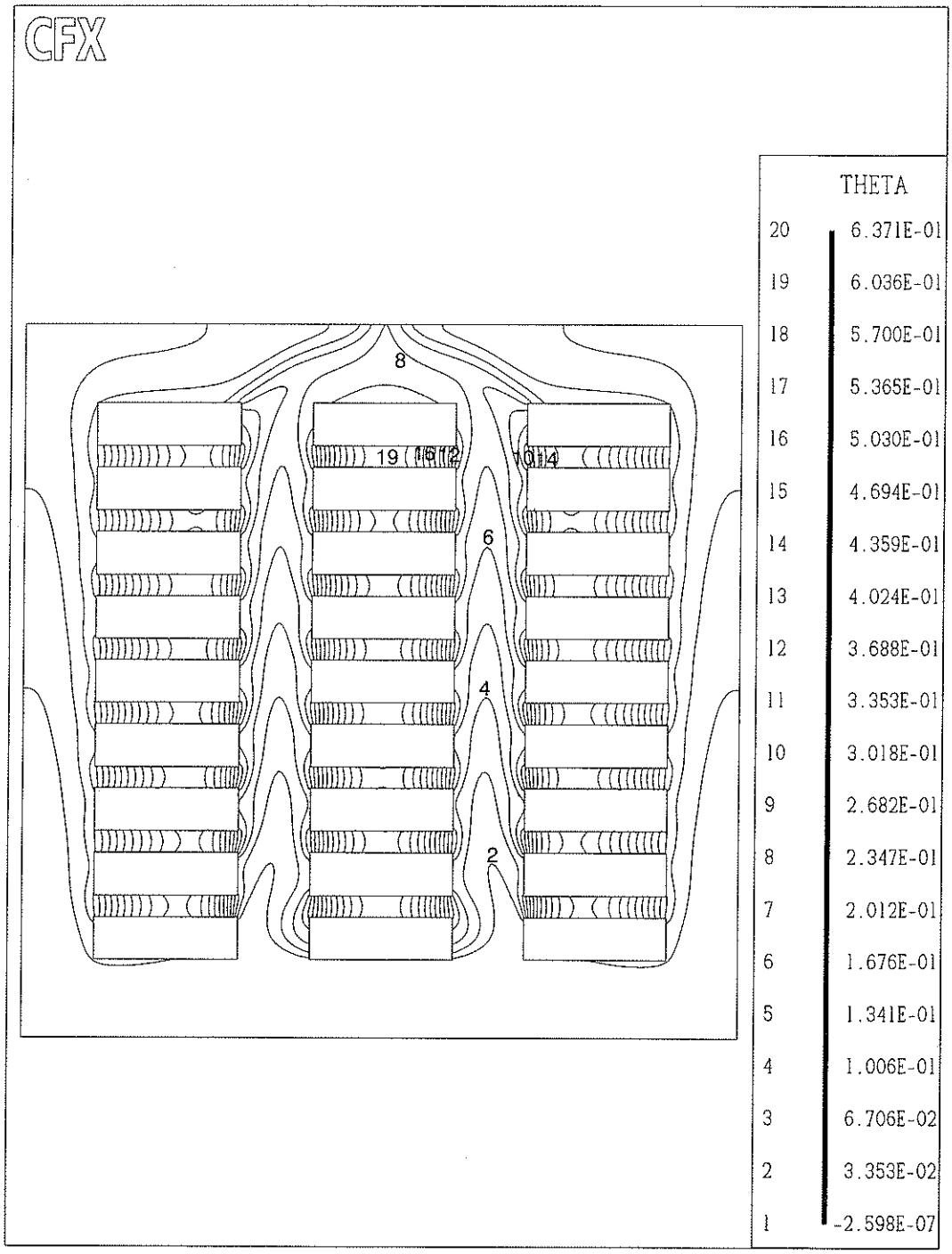

Figure 6.49: Temperature contours for case 2, mixed convection (Re_o=100), inlet B-0.5 and outlet T-0.5

When comparing the temperature distributions of the two cases, the observation would be that both have similar distributions of temperature. The temperature surrounding the towers in the domain is around contours # 8 ($\theta \approx 0.23$) to # 10 ($\theta \approx 0.30$), and where the towers are the temperature rises accordingly and especially in the channels between the blocks. The maximum temperatures occur in different places, for run 5 the maximum temperature occurs in the last channel formed by the blocks of tower one and for run 2 the maximum temperature occurs in the last channel formed by the blocks of tower 2.

For Geometry 2 the location of inlet and outlet that was most effective in cooling the tower was L – 0.05 and R – 0.5. This did not continue for Geometry 3. The velocity vector plot and the temperature contour plots are shown in Figures 6.50 and 6.51, respectively.

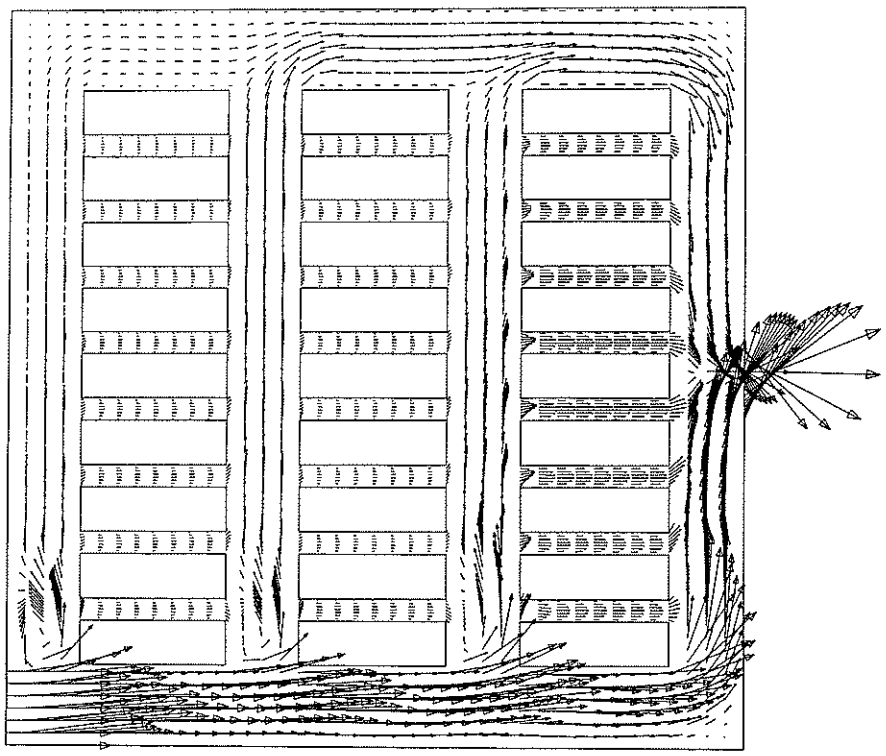

Figure 6.50: Case 4, mixed convection cooling (Re_o =100), inlet L-0.05 and outlet R-0.5

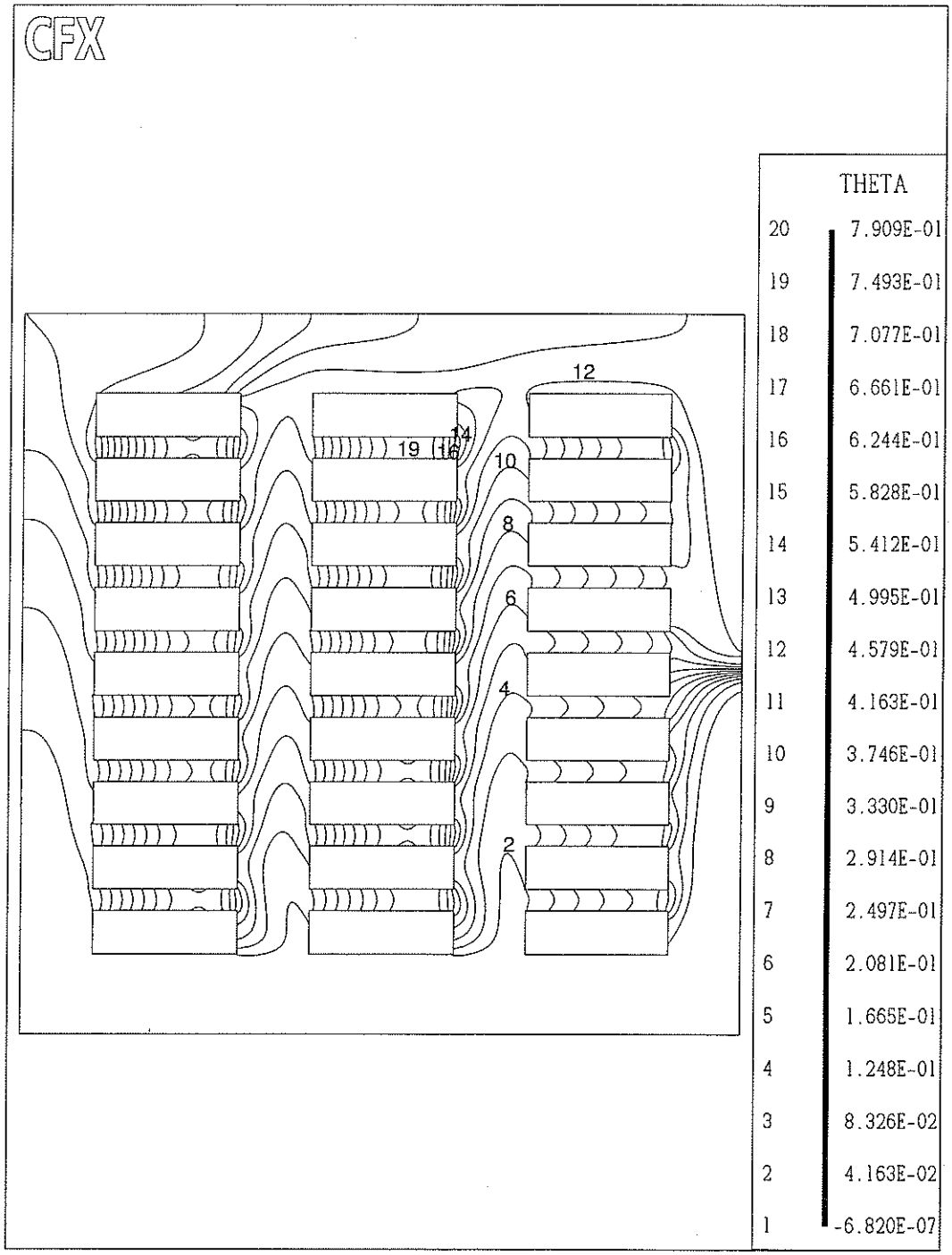

Figure 6.51: Temperature contours for case 4, mixed convection (Re_o=100), inlet L-0.05 and outlet R-0.5

From Figure 6.50, the velocity vector plot shows the incoming air mostly bypassing the first two towers. From Table 6.5, The percentage of inlet mass flow rate to flow through the towers increases for each tower, from 5.94% in tower 1, 6.33% in tower 2 and up to 21.0% in tower 3. However the maximum temperature occurs in tower 2 and has a value of $\theta_{max} = 0.791$. The average θ values in the three towers varies, $\theta_{avg} = 0.356$ for tower 1, $\theta_{avg} = 0.429$ for tower 2, and $\theta_{avg} = 0.288$ for tower 3. The higher average values lie in tower 2 and therefore has the value of maximum temperature.

Case 8 where the inlet and outlet were at L – 0.5 and R – 0.5, respectively, was also studied. The velocity vector plot is seen in Figure 6.52 and the temperature contour plots is seen in Figure 6.53.

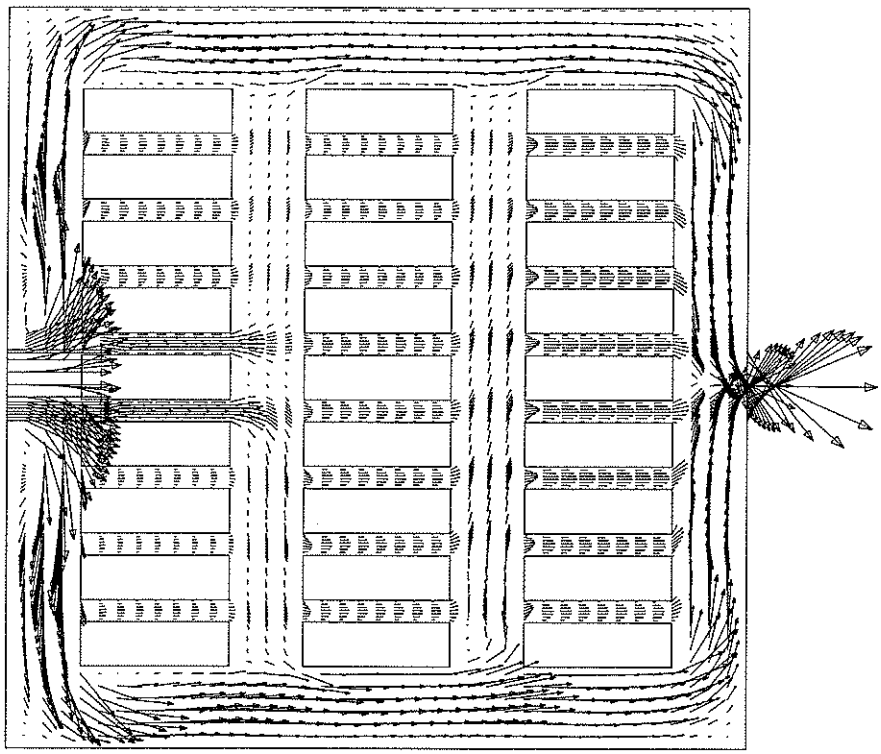

Figure 6.52: Case 8, mixed convection cooling (Re_o =100), inlet L-0. 5 and outlet R-0.5

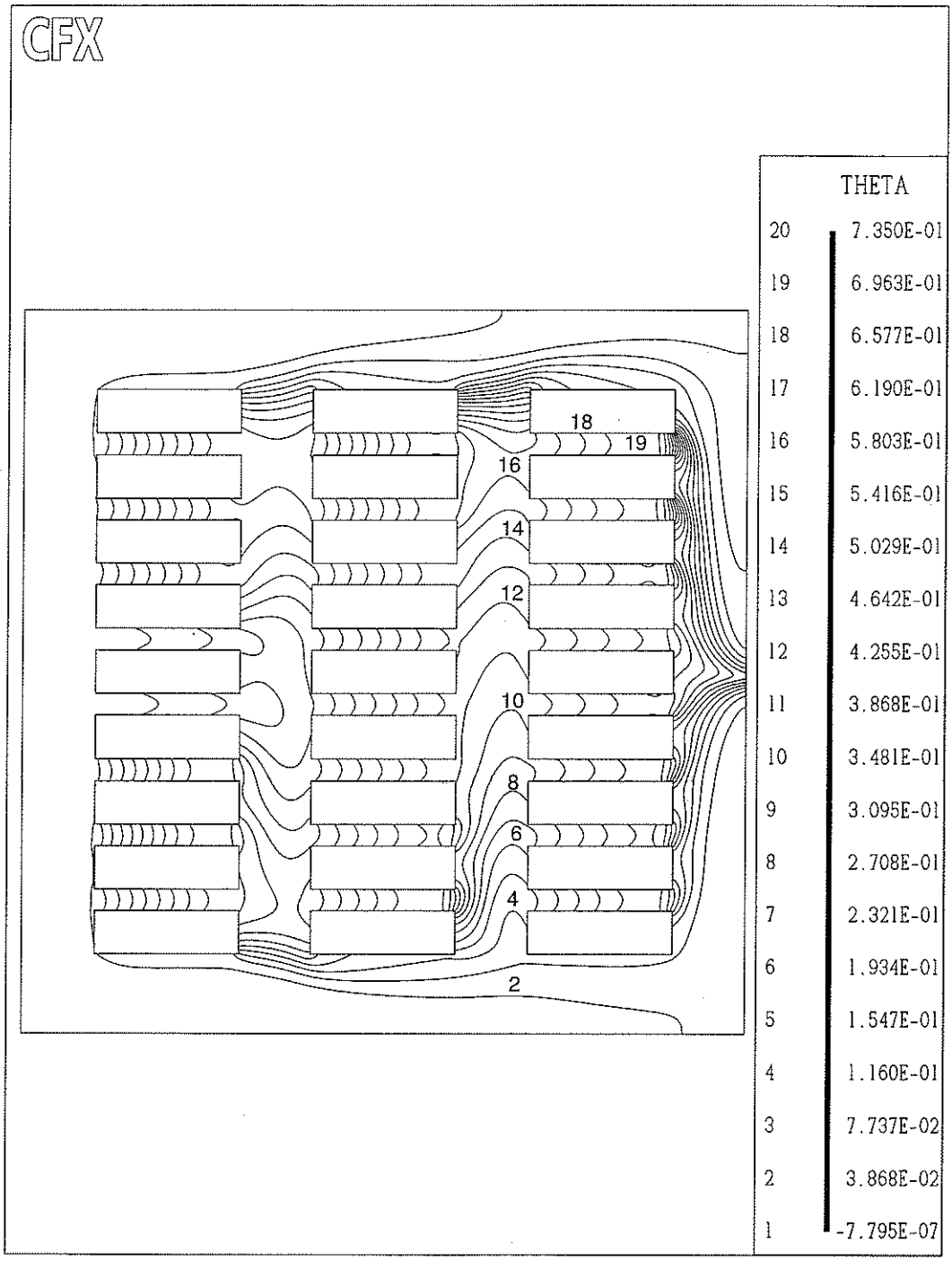

Figure 6.53: Temperature contours for case 8, mixed convection (Re_o=100), inlet L-0.5 and outlet R-0.5

From Figure 6.52, it can be seen that the flow comes in at $Y = 0.5$ and the flow is forced to flow through the channels of the three towers. From Table 6.5, the percentage of inlet mass flow rate that flows through the channels was 21.23% for tower 1, 14.29% for tower 2 and 22.01 for tower 3. The average temperature increases from tower 1 to tower 3, $\theta_{avg} = 0.167$ for tower 1, $\theta_{avg} = 0.381$ for tower 2 and $\theta_{avg} = 0.426$ for tower 3.

From the comparisons of the cases listed in Table 6.5, the case that had the lowest maximum temperature was case 5 ($\theta_{max} = 0.629$). However, the second lowest maximum temperature was obtained with case 2 ($\theta_{max} = 0.637$). Case 2 has inlet and outlet positions at B – 0.5 and T – 0.5 and these positions had high maximum temperatures in Geometries 1 and 2.

Chapter 7

SUMMARY, CONCLUSIONS AND RECOMMENDATIONS

7.1 Summary

A numerical investigation was conducted on a two dimensional cavity with an inlet and outlet openings enclosing heat generating bodies. The effect on the velocity and temperature distributions caused by the number of towers, position of the tower, size of tower, inlet mass flow rate, and the location of inlet and outlet was studied. Three different geometries were studied based on the generic description (Figure 3.1). Geometry 1 was a single tower formed by four blocks (Figure 6.1); geometry 2, a single tower formed by nine blocks (Figure 6.12) and geometry 3 was three towers each formed by nine blocks (Figure 6.45). Air was used as the coolant and was introduced at three different velocities. For geometry 1 the location of tower, inlet mass flow rate, and location of inlet and outlet were studied. The location of tower, inlet mass flow rate and location of inlet and outlet were studied for geometry 2. For geometry 3 the inlet mass flow rate and the location of inlet and outlet were studied. The thesis presents the results of these studies and serves as the basis for a three dimensional numerical study of the valve halls of the Dorsey converter station currently underway.

7.2 Conclusions

The following conclusions were extracted from the results of the three geometries.

7.2.1 Geometry 1

1. Tower location within the domain keeping the inlet mass flow rate and inlet and outlet positions constant had a significant impact on the velocity and temperature distribution as discussed in section 6.1.1. Results were obtained for six different stack positions with mixed convection (Re_o =100), inlet at B-0.5 and outlet T-0.5. The direct result of moving the tower is the air movement near and through the stack. To maximize the cooling effectiveness, the tower has to be positioned so that there is increased flow through the channels formed by the stack and flowing near the stack.

2. In most applications increased flow rates result in higher velocities, higher heat transfer coefficients and consequently, improved cooling characteristics. Passive versus mixed convection cooling was investigated for Geometry 1. It was found that when comparing results of passive and mixed-convection cooling for the same stack position and the same inlet and outlet position the increased flow rate improved the heat transfer which led to lower temperatures. However, the results also demonstrate that a higher velocity does not necessarily provide higher cooling rates. The case where passive cooling provided a lower maximum temperature was discussed in detail.

3. Cases having the same inlet mass flow rate and the tower position, the effect of the location of inlet and outlet ports was investigated. The importance of the location of the inlet and outlet ports is demonstrated as the same amount of mass flow rate can significantly reduce the average and maximum temperatures when the mass flow is introduced into the domain at different locations.

7.2.2 Geometry 2

4. The effect of the tower position was studied for Geometry 2 and stated previously the position of the tower had to maximize the flow flowing near and through the tower. Several cases were compared and the optimal position for the single tower with nine blocks was closest to the left hand side of the domain ($a_9 = 0.1$).

5. The results for a particular set if inlet and outlet conditions were compared and the inlet mass flow rate corresponding to $Re_o = 225$ was best suited to cool the tower. The air around and through the tower was maximized resulting in lower tower temperatures.

6. For Geometry 2 the inlet location did not have a significant impact on the temperature distribution. However, the outlet location did have an impact on the temperature distribution. Lowering the outlet from a height of 0.95 to 0.5 on the right

hand side it decreased the temperature significantly. The results are discussed in section 6.2.3

7.2.3 Geometry 3

7. The cases discussed for Geometry 3 did not produce a satisfactory answer to the best possible location of inlet and outlet. The second lowest temperature was obtained for a B-0.5 to T-0.5 flow which is contradictory to the results of the other geometries. In addition the inlet and outlet location that provided the lowest maximum temperature were located at L-0.05 and R-0.95.

7.3 Recommendations

Recommendations for future work with heat generating blocks in a square cavity with inlet and outlet openings would be to extend the domain in three dimensions to make the domain closer to the valve halls at the Dorsey converter station and to study the impact of the inlet and outlet openings for Geometry 3.

REFERENCES

Bejan, A., Kim, S.J., Morega, Al.M., and Lee, S.W., 1995, Cooling of Plates Shielded by Porous Screens, *International Journal of Heat and Fluid Flow* 16, pp. 16-24.

Dooher, B.P., and Mills, A.F., 2000, Natural-Convection Thermosyphon Heat Transfer from a Stack of Horizontal Plates, *Experimental Heat Transfer* 13, pp. 125-136.

Dubovsky, V., Ziskind, G., Weiss, Y., Aharon, J., Katz, M., and Letan, R., 2002, Passive Coolin of Cylindrical Bodies in an Enclosed Space with Openings, *Proceedings of the 12th International Heat Transfer Conference*, Vol. 2, pp. 717-722.

Fowler, A.J., Ledezma, G.A., and Bejan, A., 1997, Optimal Geometric Arrangement of Staggered Plates in Forced Convection, *International Journal of Heat and Mass Transfer* 40, pp. 1795-1805.

Hung, T.C., 2001, A Conceptual Design of Thermal Modeling for Efficiently Cooling an Array of Heated Devices Under Low Reynolds Numbers, *Numerical Heat Transfer, Part A*, 39, pp. 361-382.

Mufuta, J.-M., and Van den Bulck, E., 2001, Modelling of the Mass Flow Distribution Around an Array of Rectangular Blocks In-Line Arranged and Simulating the Cross Section of a Winding Disc-Type Transformer, *Applied Thermal Engineering* 21, pp. 731-749.

Patankar, S.V.,1980, Numerical Heat Transfer and Fluid Flow, Hemisphere Publishing Corporation, New York.

Shuja, S.Z., Yilbas, B.S., and Budair, M.O., 2000, Natural Convection in a Square Cavity with a Heat Generating Body: Entropy Consideration, *Heat and Mass Transfer* 36, pp. 343-350.

Shuja, S.Z., Iqbal, M.O., and Yilbas, B.S., 2001, Natural Convection in a Square Cavity Due to a Protruding Body – Aspect Ratio Consideration, *Heat and Mass Transfer* 37, pp. 361-369.

Young, T.J., and Vafai, K., 1999, Experimental and Numerical Investigation of Forced Convective Characteristics of Arrays of Channel Mounted Obstacles, *Journal of Heat Transfer* 121, pp. 32-42.